DYNAMIC CORONARY ARTERY PHANTOM TEST SYSTEM EMULATING CARDIAC AND RESPIRATORY MOTION

By

JORGE ALBERTO GUTIERREZ VALENZUELA

Department of Mechanical Engineering

McGill University, Montreal

NOVEMBER 2022

A thesis submitted to McGill University in partial fulfillment of the requirements of the degree of Master of Engineering

©Jorge Alberto Gutierrez Valenzuela, 2022

Abstract

The continuous innovation and development of cardiovascular disease diagnosis and treatment devices entail the need for proper validation testbeds, such as the anatomically and bio-mechanically correct testing platforms commonly referred to as “Phantoms.” Besides validation, Phantoms are a very effective tool used to perform simulations and fine-tune medical devices where sometimes motion is also needed for a more accurate simulation. Computer-aided design and 3D printing technologies are cost-effective tools to develope controlled motion systems.

In this work, a Dynamic Phantom Test System was designed, prototyped, and tested to emulate the impact of Cardiac and Respiratory Motion on the coronary artery. A stenotic coronary artery phantom was developed in three different versions: PVA-C, 3D printed material (TangoPlus) and composite material (TangoPlus & VeroWhite). A hemodynamic circuit representing the circulatory system was developed and attached to the phantom and a pulsatile pump. Finally, a cam mechanism was incorporated to generate the movement of the coronary artery in the superior-inferior direction, with the capacity to exchange movement profiles such as heartbeat, respiration and their combination. The results showed an impact on the pressure curve. However, the FFR and dPR readings during a pressure guidewire angiogram showed no discrepancies between the static and moving hemodynamic circuit.

Resume

L'innovation et le développement continus des dispositifs de diagnostic et de traitement des maladies cardiovasculaires impliquent la nécessité de bancs d'essai de validation appropriés, tels que les plates-formes de test anatomique et bio-mécaniquement correctes, communément appelées "Phantoms". Outre la validation, les fantômes sont également un outil très efficace utilisé pour effectuer des simulations et affiner les dispositifs médicaux où parfois le mouvement est également nécessaire pour une simulation plus précise. La conception assistée par ordinateur et les technologies d'impression 3D sont des outils utiles pour développer un système de mouvement contrôlé. Dans ce travail, un système de test fantôme dynamique a été conçu, prototypé et testé pour émuler l'impact des mouvements cardiaques et respiratoires sur l'artère coronaire. Un fantôme d'artère coronaire sténosé a été développé en trois versions différentes : PVA-C, matériau imprimé en 3D (TangoPlus) et matériau composite (TangoPlus & VeroWhite). Un circuit hémodynamique représentant le système circulatoire a été développé et attaché au fantôme et à une pompe pulsatile. Enfin, un mécanisme à came a été incorporé pour générer le mouvement de l'artère coronaire dans le sens supérieur-inférieur, avec la capacité d'échanger des profils de mouvement tels que le rythme cardiaque, la respiration et combiné. Les résultats ont montré un impact sur la courbe de pression. Cependant, les lectures de FFR et de dPR au cours d'une angiographie par fil-guide de pression n'ont montré aucune différence entre le circuit hémodynamique statique et mobile.

Acknowledgments

I would like to greatly appreciate the constant financial and emotional support from my supervisor, Professor Rosaire Mongrain; his positive attitude and vast knowledge form an essential pillar in this research. Thank you for allowing me to show what I am capable of.

Thanks to Dr. Ramses Galaz for his support, advice and friendship.

Thanks to my fiancé, Yessica, this adventure would have been impossible without her support, courage, creativity, patience and love.

I appreciate the love, guidance and sacrifice of my parents, who have given everything for their son and daughters and have instilled in them values and a spirit of improvement. Thank you for teaching us that there is no better gift and inheritance than education, knowledge and preparation.

To my sisters, Cindy and Wendy, thank you for always watching my back; your good wishes, comments, and actions have been solid supports for as long as I can remember.

To my uncles Martha Silvia and Arthur for their advice, encouragement, and always being there for me.

Thanks also to my fellow lab partners, teachers and staff whom I had the opportunity and luck to meet during this research at McGill University. A special thanks to Carlos Gil, a fellow lab mate, for facing the challenges of this project with me and for your help, advice, and great friendship.

Last but not least, I would like to thank my friends, those geographically distant and those close, with whom I speak daily and with whom I do not need to speak to feel their support; thank you all, especially: Leonardo, Luis Antonio, Adriana, Miguel, Raul, Arnoldo, Gabriel and Lorena.

Thank you all for your help and inspiration.

Contributors

This research was possible thanks to the financial support of the Mexican institution CONACYT (Consejo Nacional de Ciencia y Tecnología), the financial support of the Mexican institution FER (Fundación Esposos Rodríguez) and the financial support of the Natural Sciences and Engineering Research Council of Canada (NSERC)

Table of Contents

List of Figures

List of Tables

List of Terms and Abbreviations

3D	Three Dimensional
AV	Atrioventricular
CAD	Coronary Artery Disease
CAD	Computer Aided Design
CAM	Computer Aided Manufacturing
Cath Lab	Cardiac Catheterization Lab
CHD	Coronary Heart Disease
Coronary CTA	Coronary Computed Tomography Angiography
CT Scan	Computer Tomography Scan
Cx	Circumflex Artery
dPR	Diastolic Pressure Ratio
FFR	Fractional Flow Reserve
IHD	Ischemic Heart Disease
LAD	Left Anterior Descending
LCA	Left Coronary Artery
LMCA	Left Main Coronary Artery
MRI	Magnetic Resonance Imaging
OTS	Off the Shelf
Pa	Aortic Pressure
PCI	Percutaneous Coronary Intervention
Pd	Distal Pressure
PVA	Poly Vinyl Alcohol
PVA-C	Poly Vinyl Alcohol Cryogel
SA	Sinoatrial
WHO	World Health Organization

Chapter 1: Introduction

1.1 Introduction and Rationale

It is estimated that around 126 million individuals (1.72% of the world population) die annually from ischemic heart disease [1], which positions this pathology as the number one cause of death worldwide[2].

Given these data, it is only logical that numerous investigations around this topic are developed, specifically those related to the precise diagnosis of this pathology, for the appropriate treatment selection.

There are different methods for the diagnosis of cardiovascular diseases. Usually, a non-invasive method is used to evaluate the possibility of a coronary artery disease (CAD). If the physician considers the results abnormal, an invasive test such as coronary angiography may be performed, which consists of injecting contrast agent (ionized solution) in the area of interest and performing a CT scan, which will result in a 2D image of the vessel. The main shortcoming of coronary angiography is that it depends entirely on the physician's judgment. The technique considered the gold standard used today is the pressure guidewire technique [3], which consists of using a catheter with a tip pressure sensor (pressure guidewire) during coronary angiography to measure the difference of blood pressure in the area of interest before and after stenosis. This technology allows the physician to obtain physiological measurements like Fractional Flow Reserve (FFR), and Diastolic Pressure Ratio (dPR), that are necessary for the classification of severity and the choice of the necessary treatment.

Companies dedicated to improving the diagnosis and treatment of cardiovascular diseases, require advanced anatomically and biomechanically correct vascular testing beds, capable of simulating physiological conditions to test technologies and tune equipment under controlled and repeatable conditions. Tools like these can also be used for educational and training purposes.

1.2 Thesis Research Specific Objectives

The specific objectives of this research are:

1. To design, develop and build a dynamic phantom test system of different severities of a stenotic coronary artery, with anatomically correct mechanical properties and the capability to simulate respiratory and cardiac motion. This testbed consists of the following sub-systems:

    a. The model of a coronary artery with a feasible manufacturing process and an accessible material that emulates the anatomically correct and mechanical properties of a coronary artery.

    b. A hemodynamic circuit that simulates blood flow and pressure in the coronary artery area resulting in a physiologically correct pressure curve.

2. To develop in vitro testing methodologies for verification and validation to evaluate FFR and dPR readings in a hemodynamic circuit and the resemblance to the readings on an angiogram of a patient.

Chapter 2: Literature and Background

2.1 The Heart

Developing energy-efficient mechanisms for the proper functioning of our body has always been the goal of human evolution. These adaptive mechanisms have been carried out to maintain a balance between external factors that affect our internal environment. This process of balance is known as homeostasis. Variables such as temperature, oxygen concentration, pH, osmolarity, and many others are closely controlled. The cardiovascular system aids in maintaining homeostasis due to an elaborate transport material network that consists of the exchange of solutes through diffusion and convection along vessels that start and end at the heart[4].

The heart is located in the center of the thoracic cavity, it has the size of a fist, and it works as a double-pressure pump that adapts to supply blood to our entire body. The right heart pump provides the energy to carry blood through the pulmonary vessels, and the energy to move blood through the systemic organs is provided by the left heart pump[4].

The right side of the heart receives oxygen-deficient blood, also known as venous blood, from the body through the superior vena cava into the right atrium. Then the right atrium contracts and pushes the blood through the tricuspid valve into the right ventricle. Then the right ventricle contracts and opens the pulmonic valve to send the blood into the pulmonary circulation via the pulmonary arteries so it can be “reoxygenated” by exposure to oxygen-rich inspired air. Then, the oxygenated pulmonary venous blood flows in pulmonary veins to return to the heart into the left atrium. The left atrium contracts and blood passes to the left ventricle through the mitral valve.

From there, blood is pumped through the aortic valve into the aorta to be distributed to the systemic organs[4].

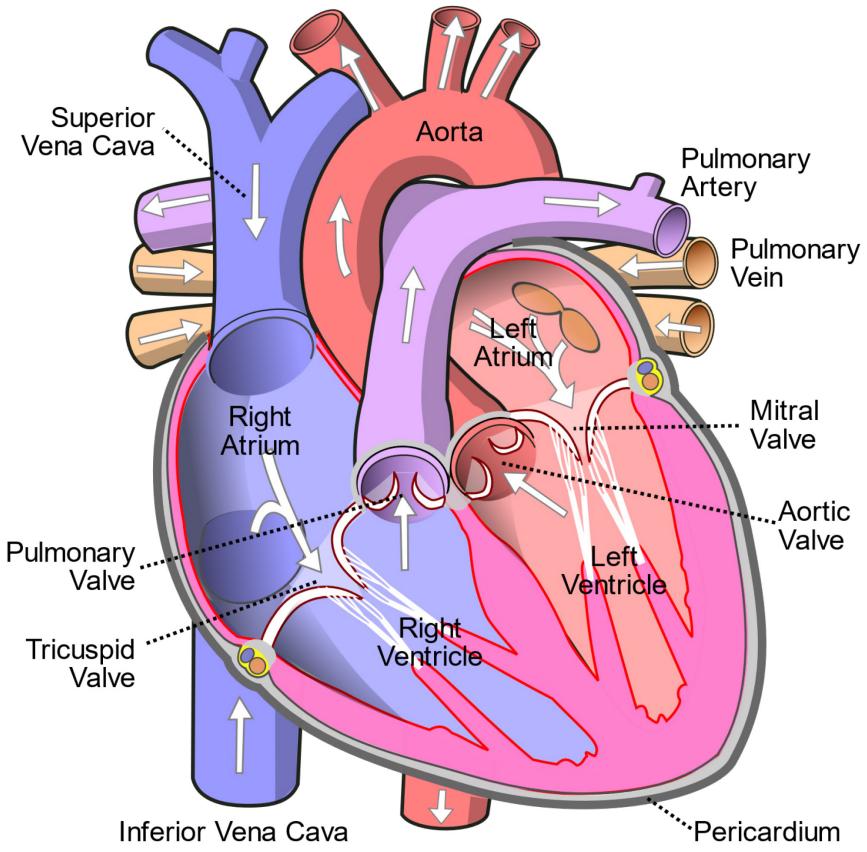

Figure 2-1 Diagram of the human heart, showing the location and names of the ventricles, valves, and vessels. Licensed under the Creative Commons Attribution-Share Alike 3.0 Unported license.

The right and left heart pumps have the same pumping principles. Thanks to the valves, a ventricle is a closed chamber that contracts during each pump. These valves allow flow in only one direction. Differences in pressure in the chambers open and close the valves allowing blood flow through in a rhythmic and synchronized contraction and relaxation cycle of the cardiac muscle. The systole is the cardiac cycle phase during which the ventricular muscle cells contract.

Diastole is the cardiac cycle phase when the ventricular muscle cells relax, and the ventricle refills with blood so that systole can happen again.

Before returning to the right heart, blood that was ejected from the left heart into the aorta goes through different types of vessels. The major vessel classifications are arteries, arterioles, capillaries, venules, and veins[4]. These types of vessels differ among them in their physical dimensions, morphological characteristics, and function, but what these vessels have in common is that they are lined with a single contiguous layer of endothelial cells.

Arteries are thick-walled vessels, about 1mm to 2 mm. They contain a large amount of elastin and collagen fibres, allowing arteries to expand up to twice their unloaded length when pressure is increased to accept and temporarily store some of the blood ejected by the heart during systole. The largest artery is the aorta, which has an internal diameter of approximately 25 mm, the diameter decreases with each consecutive branching, and the smallest arteries have a diameter of approximately 0.1 mm[4].

2.1.1 Coronary Arteries

The right and left coronary arteries branch off the aorta and supply blood to the myocardium and the pericardium. These arteries emerge from their corresponding aortic sinuses in the proximal part of the ascending aorta, just above the aortic valve, and pass around opposite sides of the pulmonary artery.

The right coronary artery originates in the right aortic sinus of the ascending aorta and passes to the right side of the pulmonary artery. Near its origin, it divides, giving rise to a branch that irrigates de SA (sinoatrial) node. It then descends through the coronary sulcus and gives rise

to the right marginal branch that irrigates the right border of the heart as it courses toward the apex. Then it continues into the coronary sulcus to the posterior aspect of the heart to give rise to the atrioventricular (AV) node branch that irrigates the AV node. This artery irrigates the right atrium, most of the right ventricle, part of the left ventricle, part of the interventricular septum, the sinus node (in approximately 60% of the population), and the AV node (in approximately 80% of the population).

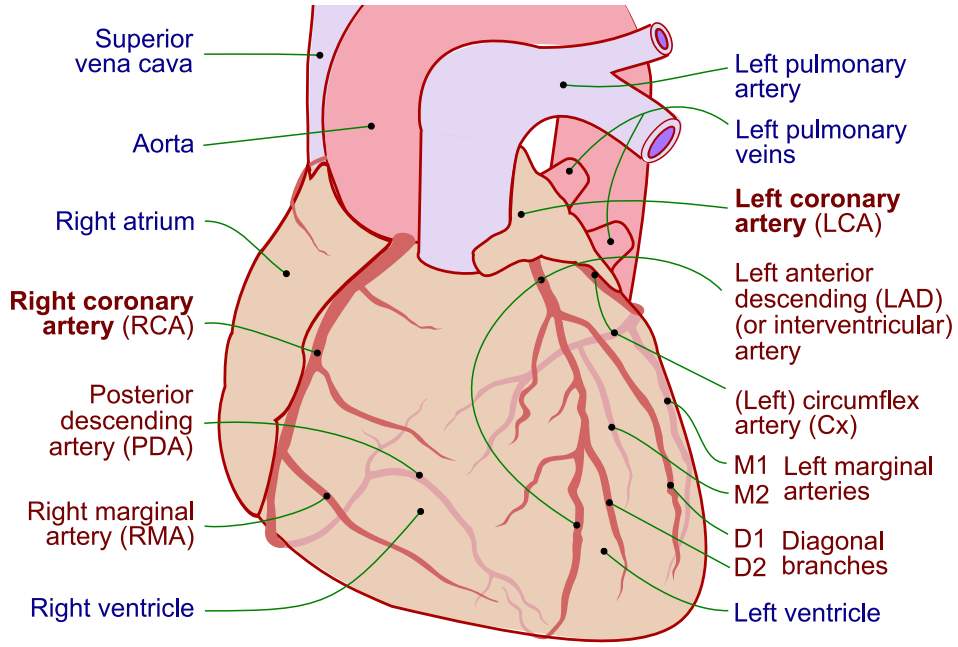

Figure 2-2 Coronary circulation, with coronary arteries labeled in red text and other landmarks in blue text. Licensed under the Creative Commons Attribution-Share Alike 3.0 Unported license.

The left coronary artery (LCA) originates in the left aortic sinus of the aorta. It passes to the left side of the pulmonary artery and runs through the coronary sulcus. In some people, the sinus node branch arises from the LCA's circumflex branch. After passing through the coronary sulcus, the LCA divides into two branches, the left anterior descending artery and the circumflex artery. The left anterior descending artery (LAD) irrigates adjacent portions of both ventricles and the anterior two-thirds of the intraventricular septum. The left marginal artery rises from the

circumflex artery (Cx) and irrigates the left ventricle. This artery irrigates the left atrium, most of the left ventricle, part of the right ventricle, most of the interventricular septum, and the sinus node.

The coronary arteries are composed of three layers: tunica intima, tunica media and tunica adventitia[5].

The tunica intima is the innermost layer of the coronary arteries and is composed of the endothelium, sub-endothelium, and internal elastic lamina. The subendothelial layer contains elastic fibres, type I collagen fibrils, fibroblasts and myointimal cells. Lipid deposits can form in this layer producing atherosclerotic plaques. The tunica media contains muscle cells, elastic fibres, and collagen. It is the middle layer of the vessels and has a hexagonal pattern arrangement of muscle cells to allow better contractility. The tunica adventitia is the outer coat of the vessels and is made up of connective tissue, nerves and vessel capillaries.

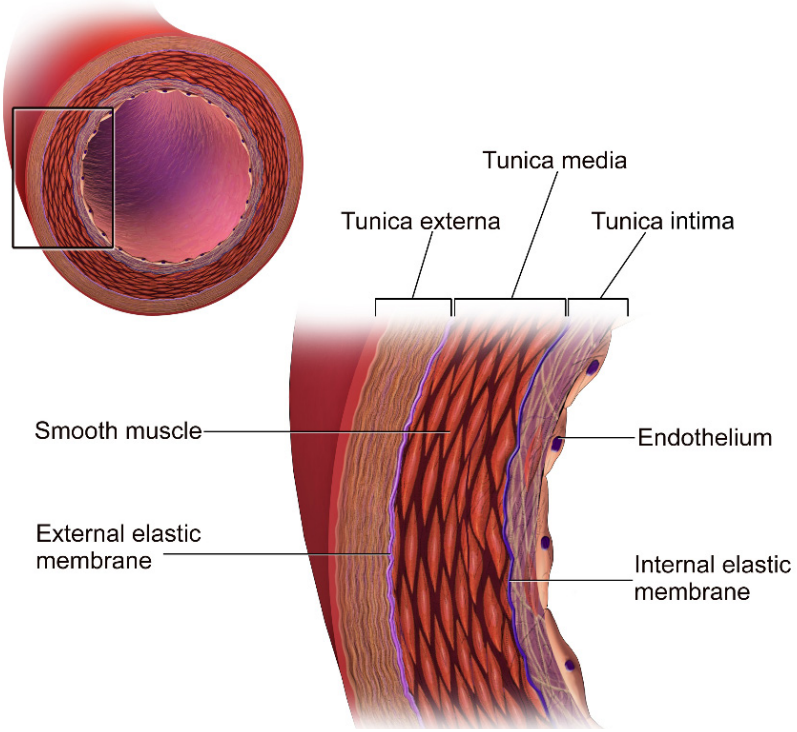

Figure 2-3 Structure of an Artery Wall. Licensed under the Creative Commons Attribution-Share Alike 3.0 Unported license.

2.2 Ischemic Heart Disease

There are situations where the maintenance of normal arterial pressure is threatened due to the malfunctioning of some components of the cardiovascular system. The myocardium is said to be ischemic when a malfunction impairs coronary blood flow, and the metabolic requirements of the heart are not satisfied. Ischemic heart disease (IHD), also referred to as coronary heart disease (CHD), or coronary artery disease (CAD), is a condition in which the epicardial coronary arteries are blocked, and the myocardium receives insufficient blood flow[6].

According to the World Health Organization (WHO), “ischemic heart disease” was the number one cause of death in 2019; almost one out of two and a half deaths result from cardiovascular disease.[2]

Most of these diseases are rooted in a pathology called “Atherosclerosis,” which is the gradual accumulation of fats, cholesterol crystals, cellular waste products, and calcium minerals in the walls of blood vessels. This chronic inflammatory response can cause the narrowing of the artery's lumen in various severities, causing ischemia and inadequate blood flow due to blockage. This narrowing manifestation is known as stenosis and can reduce the flow of oxygen and nutrients to the heart, which may lead to thrombosis, heart attack and possibly death.

Heart function can be endangered by coronary heart disease in several ways. Ischemic muscle cells are electrically irritable and unstable, which increases the risk of cardiac arrhythmias and fibrillation.

Myocardial ischemia may produce chest pain called angina pectoris, and in most situations, the patient visits the doctor for this symptom. The disease's severity must be determined to guide the treatment and establish a prognosis. Stress testing, cardiac imaging, and angiography can assess the extent and severity of the coronary disease. Stress testing is the most common method [6]. Specialized CT (Computer Tomography) scans or magnetic resonance imaging (MRI) are non-invasive imaging techniques that have also proven helpful in determining the extent of coronary artery disease.

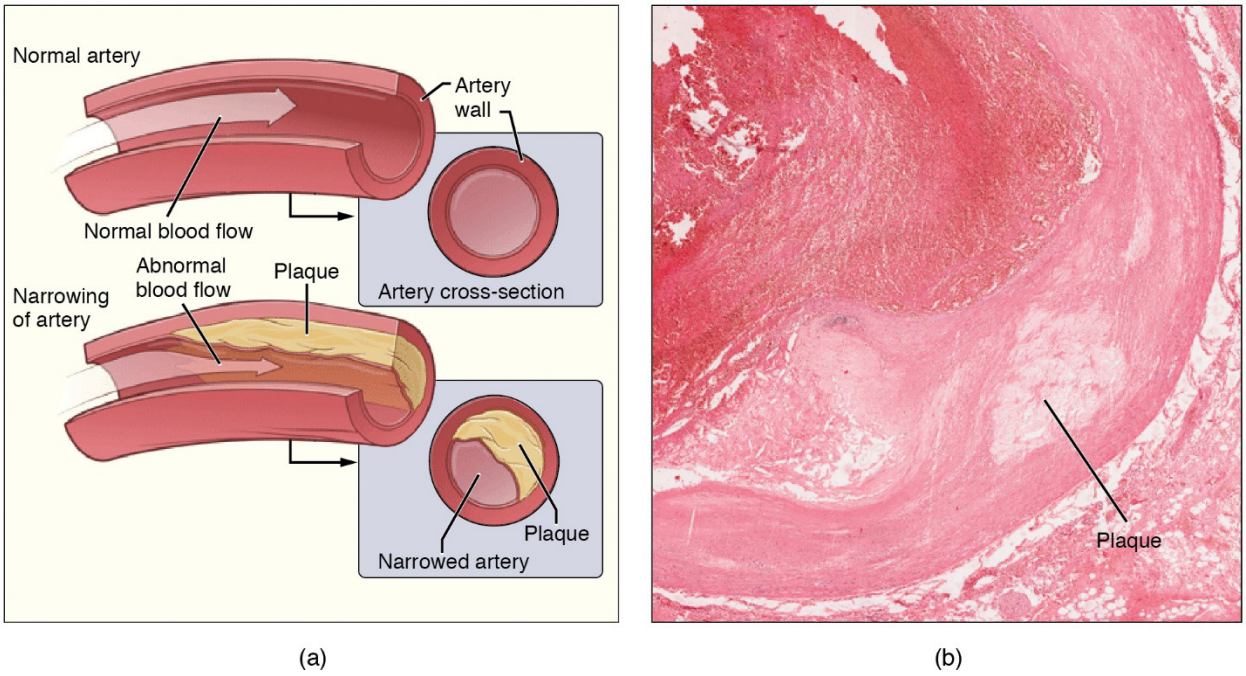

Figure 2-4 Atherosclerosis (a) Atherosclerosis can result from plaques formed by the buildup of fatty, calcified deposits in an artery. (b) Plaques can also take other forms, as shown in this micrograph of a coronary artery that has a buildup of connective tissue within the artery wall. LM × 40. (Micrograph provided by the Regents of University of Michigan Medical School © 2012). Reproduced with permission from [7]

2.3 Coronary Angiography

When a patient has atypical symptoms and ambiguous results from stress testing, an invasive coronary angiography may also be utilized to assess the severity of the disease. During the coronary angiography, the radial or femoral artery is cannulated with a sheath; after that, the LCA or RCA Ostia is engaged with a catheter. Through this catheter, a radiocontrast agent is injected under continuous fluoroscopy to delineate the coronary arterial anatomy (Figure 2-5). During radiocontrast injection, a rotating X-ray source enables several images for artery visualization in various planes. Also, a pressure wire may be used during coronary angiography to perform FFR readings.

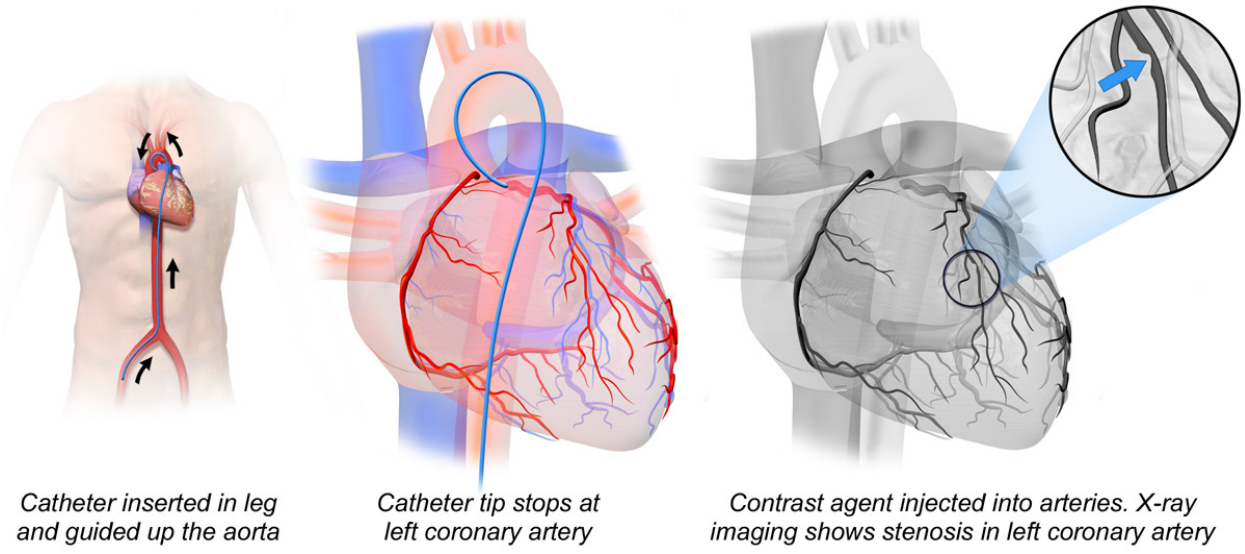

Figure 2-5 Coronary Angiography. Showing the route of the catheter to reach the coronary artery and the insertion of the contrast agent for x-ray imaging. Licensed under the Creative Commons Attribution-Share Alike 4.0 International license.

2.4 Fractional Flow Reserve (FFR)

The Fractional Flow Reserve (FFR) is the maximum blood flow through the myocardium in the presence of a stenosis in the coronary artery divided by the maximum theoretical flow. This ratio represents the fraction of the maximum myocardial flow possible with coronary stenosis [8]. Gould et al. first described this concept in 1974 in canine models[9], [10]. The FFR measurement has the complication of being extremely difficult when the patient is at rest as a result of the coronary flow auto-regulation. Yet, there is a linear correlation between perfusion pressure and blood flow during maximum hyperemia. The FFR value can be derived by the relation between the average pressure on the distal coronary artery and the average aortic pressure during maximum hyperemia (Figure 2-6) [9], [11]. The FFR ratio can be defined as:

$$\boldsymbol{FFR = \frac{Q_S^{max}}{Q_N^{max}}} \qquad \textit{2-1}$$

Where Q_S^{max} is the maximum blood flow in the stenotic artery, Q_N^{max} is the maximum normal coronary flow. Flow (Q) is also the ratio of pressure (P) difference across the coronary system divided by its resistance (R), Q can be substituted as following:

$$\boldsymbol{FFR = \frac{(P_d - P_v)/R_S^{max}}{(P_a - P_v)/R_N^{max}}} \qquad \textit{2-2}$$

Where P_d is distal pressure in relation with the lesion and P_a is the aortic pressure. As already mentioned, the measurements are made during maximum hyperemia, so the resistance is

considered minimal, so they can be cancelled. Finally, the Pv (venous pressure) is considered negligible, therefore:

$$\boldsymbol{FFR = \frac{(P_d - P_v)}{(P_a - P_v)} = \frac{Pd}{Pa}} \qquad \textit{2-3}$$

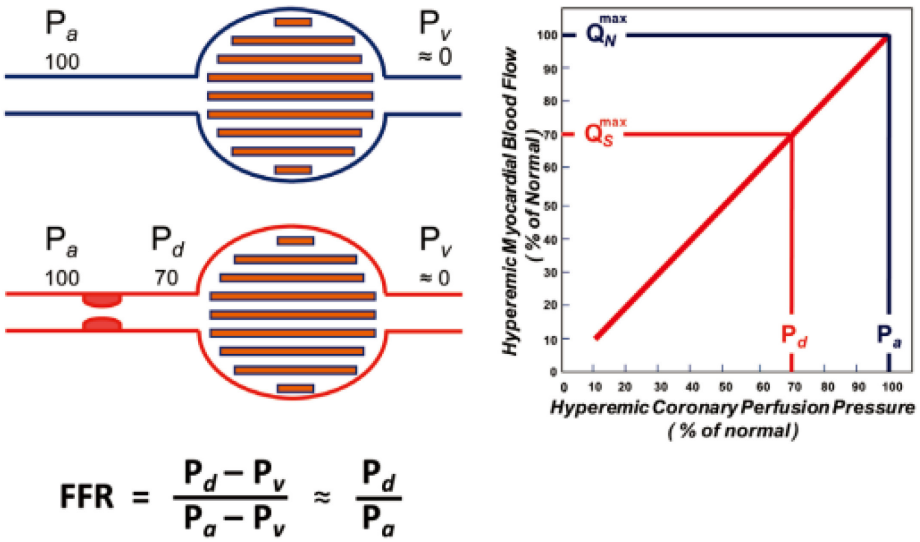

Figure 2-6 Concept of fractional flow reserve (FFR): if epicardial stenosis is not present (blue lines), the driving pressure Pa determines a normal (100%) maximal myocardial blood flow. In the case of stenosis responsible for a hyperemic pressure gradient of 30mmHg (red lines), the driving pressure will no longer be 100 mmHg, but instead will be 70mmHg (Pd). Because the relationship between driving pressure and myocardial blood flow is linear during maximal hyperemia, myocardial blood flow will only reach 70% of its normal value. This numerical example shows how a ratio of 2 pressures (Pd/Pa) corresponds to a ratio of 2 flows (QSmax/ QNmax). It also illustrates how important it is to induce maximal hyperemia. Pv=central venous pressure. Reproduced with permission from [12]

The FFR measurement on a healthy patient should be one. The value is not influenced by hemodynamic changes such as cardiac frequency, arterial pressure, or contractibility. In general, when the FFR measurement is ≤ 0.80, it indicates that the lesion is physiologically relevant, and

intervention should be evaluated.[13]. The FFR measurement is obtained during a diagnostic cardiac catheterization or coronary angiography using a pressure wire (Figure 2-7). This procedure must be done during maximal blood flow (maximal hyperemia). To achieve hyperemia, the physician administers a hyperemic stimulant, usually adenosine[14].

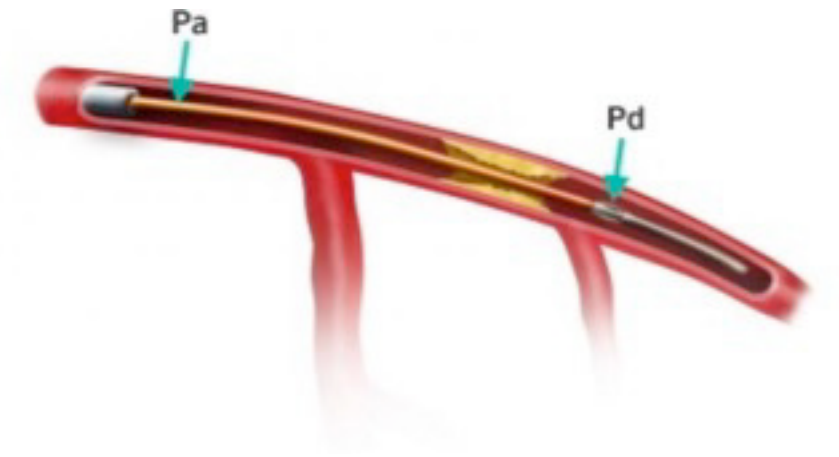

Figure 2-7 FFR measurement. The pressure wire sensor moves to the "Pd" position, which measures the distal pressure. A pressure transducer measures the "Pa" or aortic pressure. Using the Pa and Pd measurements, a monitor calculates the FFR. Licensed under a Creative Commons Attribution 4.0 International License.

2.4.1 Diastolic Pressure Ratio (dPR)

Numerous studies have been conducted since fractional flow reserve (FFR) was introduced more than 25 years ago to prove the benefit of FFR-guided treatment strategy, constantly looking for methods to improve the process to get better outcomes and to save significant resources. Determination of FFR requires pressure measurement by inserting a pressure wire distal to the stenosis in the condition of maximum dilation through the administration of adenosine.

Alternate methods that are adenosine-free, such as the instantaneous wave-free pressure ratio (iFR) and diastolic pressure ratio (dPR), have shown a non-inferior revascularization strategy to the FFR while using fewer resources and operating more effectively [15]. iFR and dPR are numerically identical in almost all cases [16]. An advantage to the dPR method is that the software to compute dPR is available on open source through the internet, without the proprietary restrictions of iFR.

Later in the cardiac cycle, coronary flow is often higher, which results in higher pressure gradients and lower pressure ratios. dPR includes areas below the average aortic pressure with a negative slope. In cases with a blunted or damped dicrotic notch, it can be challenging to determine the diastolic period from pressure recordings. For the purpose of locating a portion of the cardiac cycle that approximates diastole, dPR utilizes two simple criteria independent of the dicrotic notch. The first criterion includes portions of the tracing below the mean of the aortic pressure (Pa). The second criterion selects samples with a negative slope (each with a pressure lower than its predecessor) [17]. Only samples that satisfy both criteria are taken into account in the dPR computation, and these requirements only apply to the aortic pressure tracing. The algorithm averages the values from the aortic (Pa) and coronary (Pd) tracings over five consecutive cardiac cycles. The Pd/Pa ratio of these subset averages equals dPR.

2.5 Cam Mechanism

The cam mechanism consists of a disc or cylinder with a non-circular surface and a sliding piece, which, with their mechanical connection, transform rotary motion into linear motion [18]. It is a widespread mechanism estimated to have been used for over 10,000 years [19]. Today this mechanism can be found in almost all devices and machines, from agricultural machinery to the combustion mechanisms used in automobiles [19].

Due to its extensive history and the facilities that CAD/CAM (computer-aided design and computer-aided manufacturing) tools provide for its design, there is a great diversity of styles and configurations of this mechanism. For this research, the cam mechanism used is one called "Roller follower (Figure 2-8)," which consists of a disc (cam plate) and a rod that will make contact with the disc through a bearing (follower).

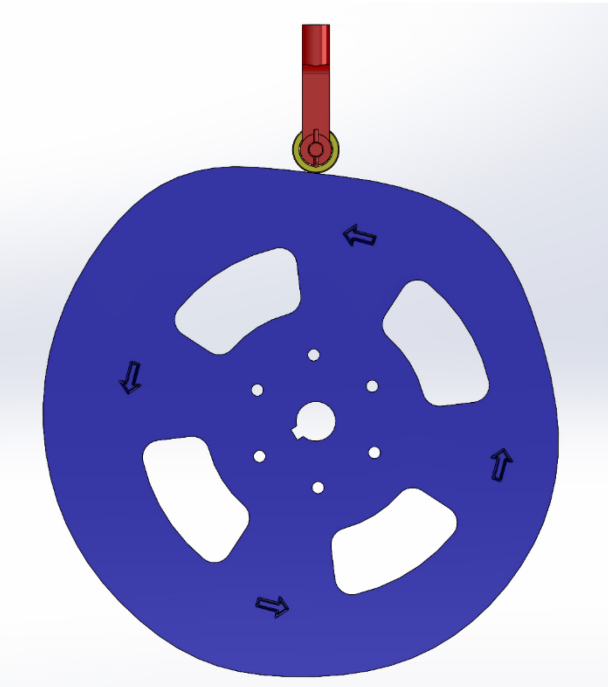

Figure 2-8 Roller-follower mechanism. In blue, the cam plate. In red is the stem of the follower, and in yellow is the bearing or tip of the follower.

For the cam plate design, it is necessary to have the desired displacement curve, a displacement-time graph. Since the cam consists of rotary motion, the time duration of the curve must be equivalent to one cycle of the desired motion. This displacement curve can be considered the surface of the disc or cam plate with which the follower will make contact and move linearly. There are libraries in CAD/CAM tools, such as the "Cams" library in SolidWorks, which facilitate the transformation of this displacement curve into a cam disk. However, this process can also be carried out manually, as will be demonstrated in this investigation.

Chapter 3: Materials and Methods

This chapter shows the methodologies developed for the experiments carried out in this investigation and the workflow implemented (Figure 3-1). The designed and purchased parts that make up the dynamic coronary artery phantom test bed are also described.

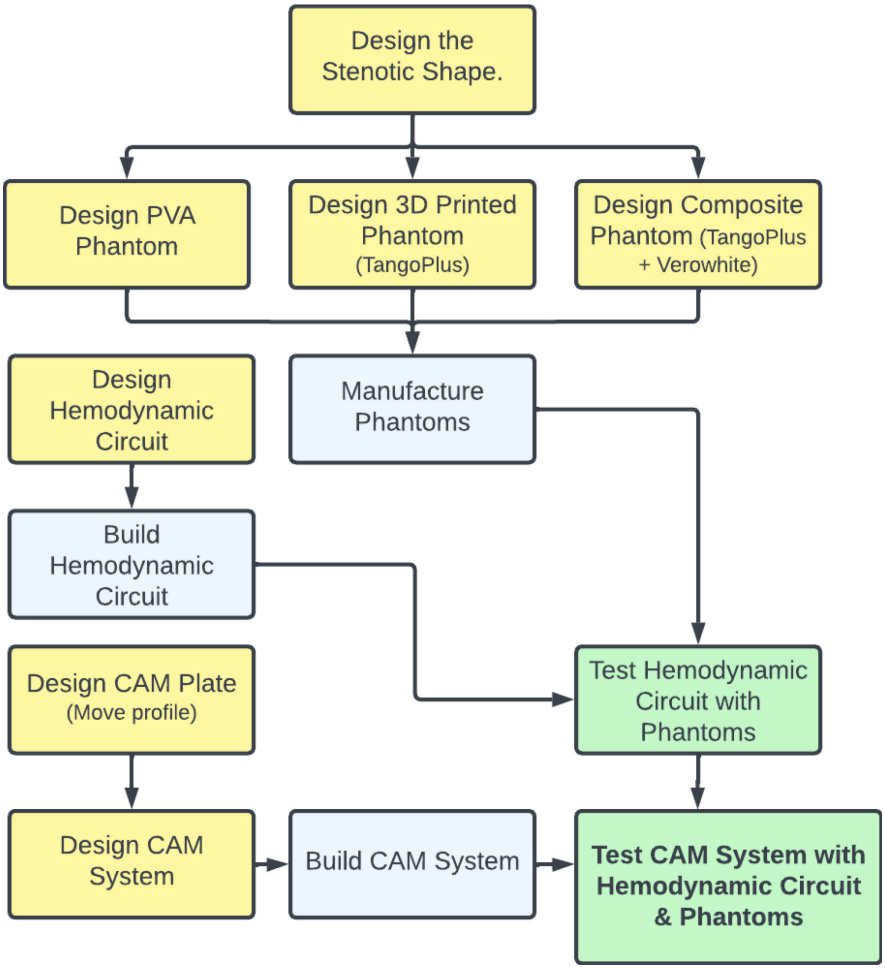

Figure 3-1 Diagram describes the planned workflow for developing the dynamic coronary artery phantom test bed that can simulate the movement caused by the heartbeat and breathing.

3.1 Phantom Design & Manufacturing

The dynamic coronary artery phantom test system began with the design of the stenotic coronary artery phantom. The objectives of this design were:

- To accurately represent the visual appearance of a stenotic coronary artery. The final phantom would undergo angiography to check the visual appearance and dimensions of the stenotic coronary artery.

- To accurately represent the mechanical behaviour of the blood vessel. For this, it will be necessary to consider selecting the most appropriate material and manufacturing process.

Other aspects that should also be considered are:

- Manufacturability: the design must be easy to manufacture, always complying with the previously stated objectives.

- Repeatability: the phantom must be simple enough to replicate for proper comparison between various phantoms.

- Versatility: the design must be easy to change and adapt to changes in dimensions or, in the case of composite material, changes in the structure and relationship between the two materials used.

- Finally, it should be considered that the phantom materials must be X-Ray compatible, since, as previously mentioned, they will be subjected to angiography.

Three phantom design proposals were made for three different materials to choose the one that performs the best and the one with the most potential in the future. The materials considered were:

- PVA-C: As previously explained, PVA-C is a material widely used in phantoms; it is a biocompatible material with mechanical properties similar to human tissue. The disadvantage of PVA-C is the complexity of its manufacturing in comparison to a 3D printing method. For the elaboration of a PVA-C Phantom, it is necessary to manufacture a mould, which needs to be filled with PVA in its liquid format, to subsequently be subjected to a cycle of freezing and thawing to achieve its final consistency[20], [21].

- Tango Plus: This material is selected due to its ease of manufacture and properties similar to rubber. TangoPlus is a high-precision 3D printing material which is essential given the dimensions of the coronary artery phantom.

- Composite (Tango Plus and Verowhite) - Since the TangoPlus material is very flexible, it is intended to make a composite material that allows us to vary the properties of the vessel wall to a certain degree. The material will consist of TangoPlus that will provide the hyperelastic properties of human tissue and Verowhite material, a more rigid and high-precision printed material, giving structure and strength to the phantom.

3.1.1 Geometry of Stenosed Coronary Artery

Patients' anatomical geometry of the coronary artery and stenosis vary. Therefore, a simplified synthetic geometry of an epicardial coronary artery was designed. The dimensions of this idealized geometry were taken from the work carried out by Galaz et al., a former member of this lab, where it is mentioned that the measurements used correspond to the proximal third portion of the major epicardial coronary arteries. This section is where statistically, the most significant cases of plate rupture occur [22].

The geometries shown in Figure 3-2 and Figure 3-3 corresponds to the vessel's lumen, not the vessel itself because it will be used to be later subtracted from the phantoms designs that will be discussed below.

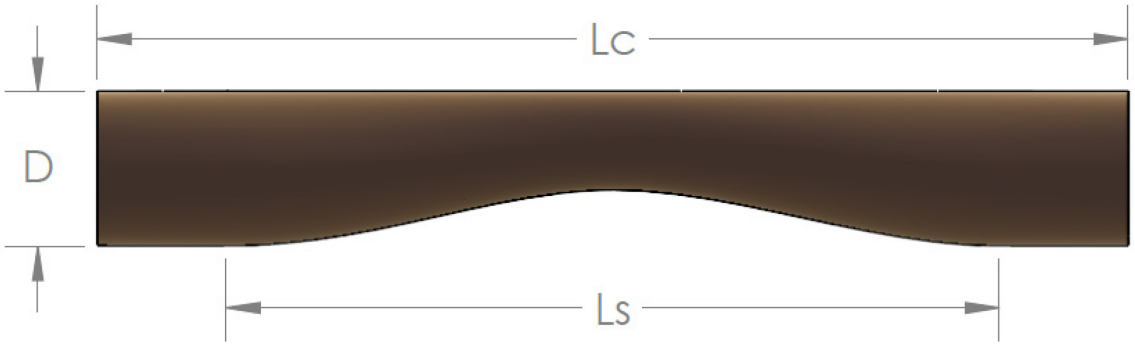

Figure 3-2 Stenotic coronary artery's lumen design

The internal diameter (D), i.e., the lumen of the designed vessel corresponding to this section, is 3 mm. the total length of the model (Lc) is 20mm.; however, the size of the affected area (Ls), i.e., the stenosis, is 15mm.

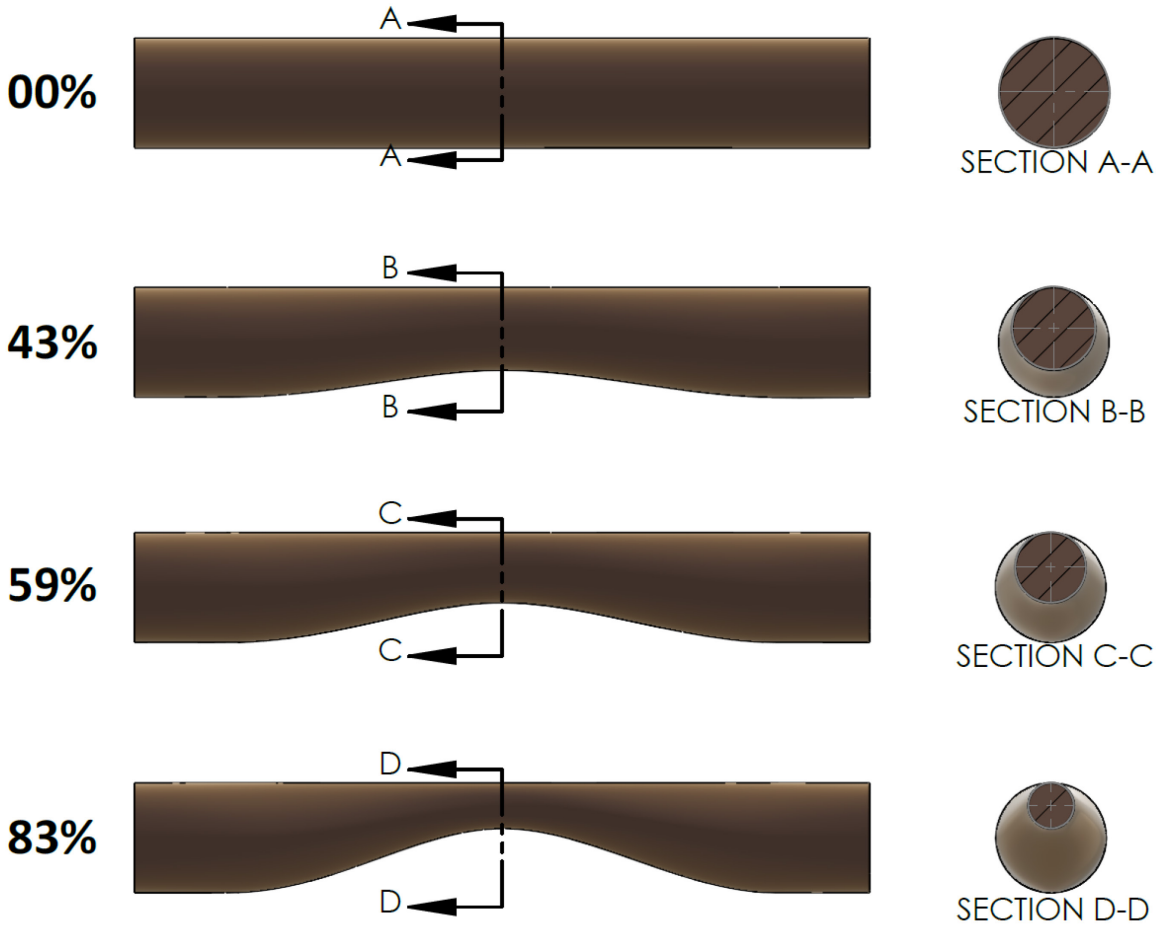

Figure 3-3 The four different stenosis severities used in this research. Longitudinal and cross-section view. Modeled using the percentage of cross-sectional area reduction.

3.1.2 PVA-C Phantom

The first phantom to be developed was the polyvinyl alcohol cryogel (PVA-C) phantom. This material is initially in a powder form; later, a liquid consistency is achieved by adding temperature mixed with the desired water ratio. It will then be subjected to several polymerization cycles of freezing and thawing, resulting in an aortic tissue-like consistency. Therefore, it can be concluded that casting is the process of making the phantom with this material. Casting is the manufacturing process that consists, in a nutshell, of pouring a fluid into a mould with a hollow cavity of the desired shape, which means this phantom needs a mould. The steps followed to achieve the PVA-C Phantom are shown in Figure 3-4.

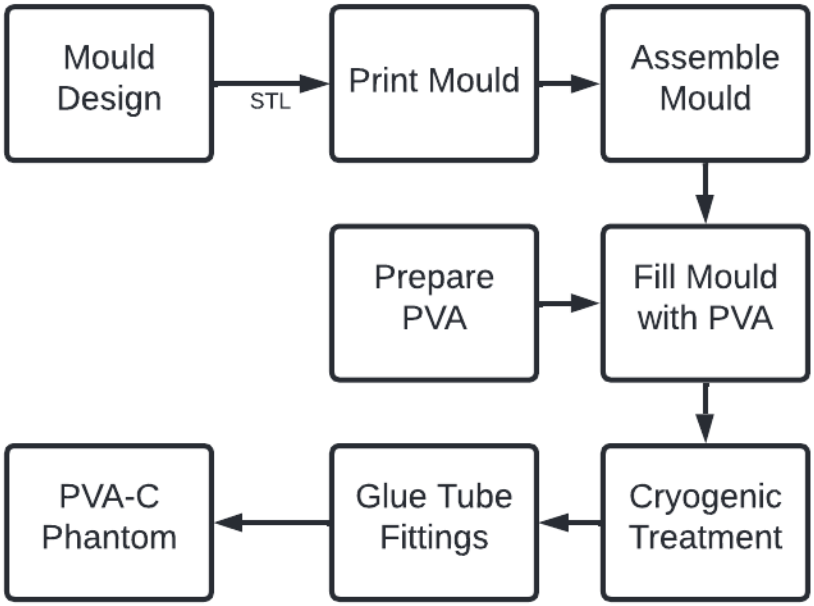

Figure 3-4 PVA-C Phantom workflow, Showing the steps taken to generate a PVA-C Phantom, from mould design and fabrication to injection, polymerization cycles and gluing of tube fittings.

Mould Design & Fabrication

For the designed mould, the following considerations were taken:

1. Hollow cavity and core: Due to the geometry of the desired phantom, the mould consists of the outer and inner walls of the phantom. This hollowed shape is achieved with a core or mould insert.

2. Injection point and air outlets: This design considered the way the mould would be filled with PVA and that it had enough air outlet points to avoid generating bubbles in the phantom.

3. Connection with the circuit: the resulting phantom had to have the appropriate adapters at the ends to allow a proper connection with the rest of the hemodynamic circuit. These adapters had to be added to the phantom once the PVA solidified and after the insert was removed.

These considerations resulted in the mould whose components are presented in Table 3-1. Once the parts were designed in SolidWorks (Figure 3-5), they were exported individually in STL format and finally sent to print in VeroWhite material with a CONNEX3 Object500 (Stratasys, MN, USA) printer.Figure 3-6 shows the final printed mould result.

No.	Qty	Name	Functions	Image
1	1	Top Shell	• Allows the injection of the material and allows the exit of air. • Hold anchors 1 and 2 in position. • Shape the top of the phantom. • Assemble with the bottom shell.	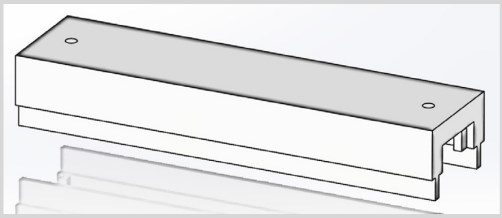
2	1	Bottom Shell	• Hold anchors 1 and 2 in position. • Shape the bottom of the phantom. • Assemble with the bottom shell.	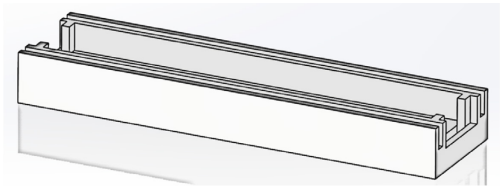
3	1	Core	• Shape the inner wall of the phantom.	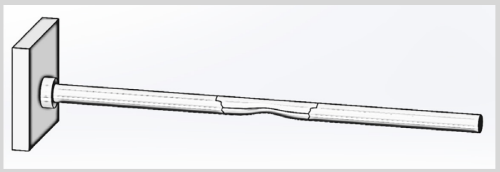
4	2	Tube Fitting	• Allow connection with the rest of the hemodynamic circuit.	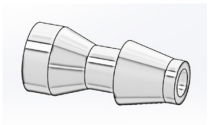
5	2	Anchor	• Merge with the PVA-C. • Hold the Core during the cryo cycle. • Hold the tube fittings during the cryo cycle.	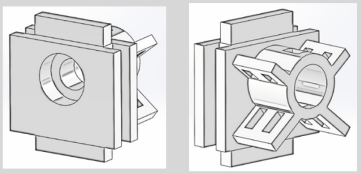

Table 3-1 List of PVA-C Mould Components

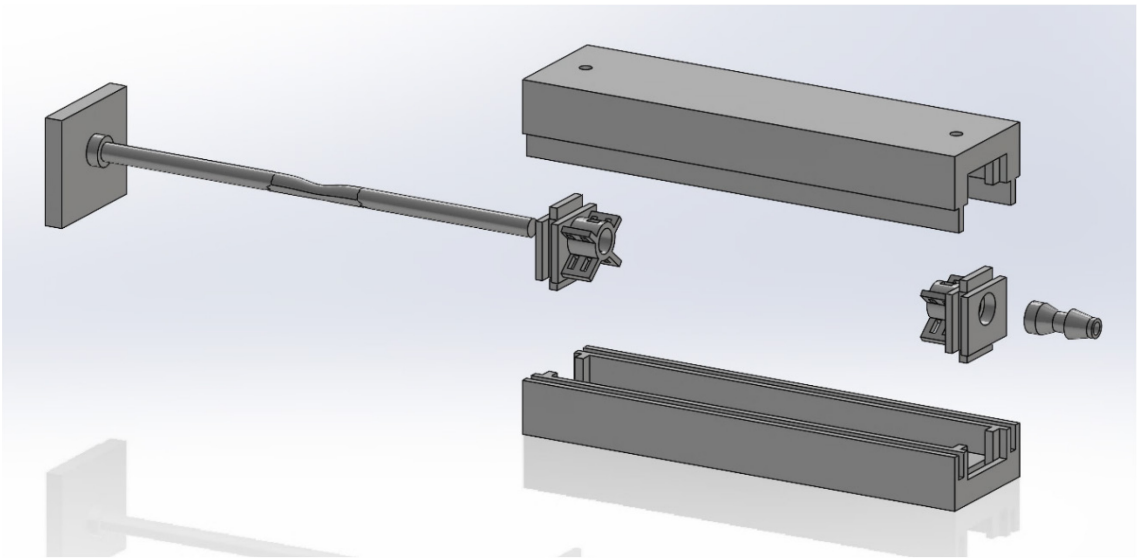

Figure 3-6 PVA-C stenotic coronary artery phantom casting mould final design. exploded view.

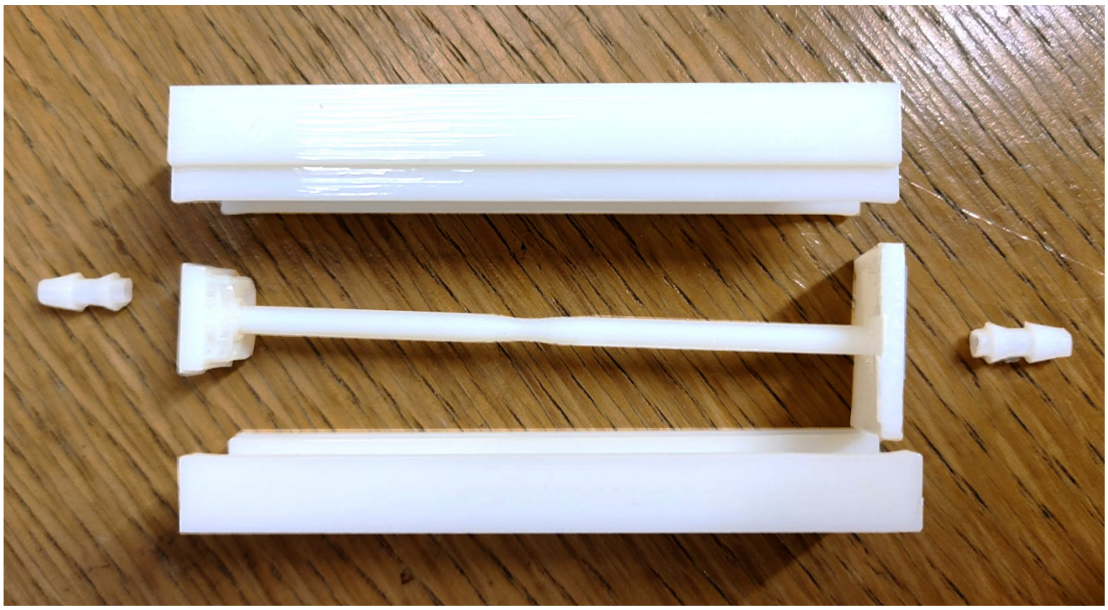

Figure 3-5 PVA-C stenotic coronary artery phantom casting mould. 3D printed with VeroWhite material.

PVA-C Recipe

The appropriate recipe must be followed to achieve properties that resembles those of the walls of human arteries with Polyvinyl Alcohol Cryogel (PVA-C). The PVA-water ratio, the mixing temperature, and the number and duration of the thermal cycles will affect the final PVA-C properties.

The solution used in this research (Table 3-2) was taken from Professor Mongrain's research group, and it has been used widely to mimic artery tissue [20-21], [23-27].

Mix	
Substance A	PVA
Substance B	Distilled Water
PVA Concentration	10%
Mixing Temperature	100°C
Approx. Mixing Time	2 hours

Cryogenic Cycles	
Number of Cyles	6
High Temperature	10°C
Low Temperature	-20°C
Freezing rate	0.333°C/min
Thawing rate	0.111°C/min

Table 3-2 PVA-C Recipe

PVA-C Phantom Fabrication

Fully hydrolyzed and soluble PVA powder was used to prepare the solution to make the phantoms. For this experiment, a concentration of 10% was found to be appropriate to produce phantoms with thin wall thickness [20].

The powder is first dissolved in distilled water at 100°C and continuously stirred until the cloudy mixture becomes a clear solution, approximately 2 hours for a 300ml PVA solution. After being cooled down, it is ready to be injected into the mould and subjected to a cryogenic treatment with varied cycles[21].

The filled mould is then placed on an aluminum block of a programmable Peltier plate and subjected to thermal cycling. The temperature range is from +10°C to -20°C to induce the freezing and thawing cycles. Based on Valerie Pazos's work, this experiment's optimal gel processing parameters were six cryogenic cycles with a freezing rate of 0.333 C/min and a thawing rate of 0.111 C/min [20].

Once the freeze and thaw cycles are complete, the mould can be disassembled. Finally, the tube fittings can be glued to the ends, resulting in the PVA-C Phantom shown in Figure 3-7.

Figure 3-7 PVA-C Stenotic Coronary Artery Phantom

3.1.3 Solid 3D Printed Phantom

One advantage of 3D printing is the greater freedom in design. Also, the rapidity in its process saves time that can be used in carrying out a greater number of iterations in the design, allowing additional optimization.

A 9.5mm X 12mm X 70mm rectangular prism shape was designed for this phantom. Later, the design of the lumen of the previously described stenotic coronary artery was subtracted from it. Finally, tube fittings were added to the ends to allow an appropriate connection with the rest of the hemodynamic circuit (Figure 3-8).

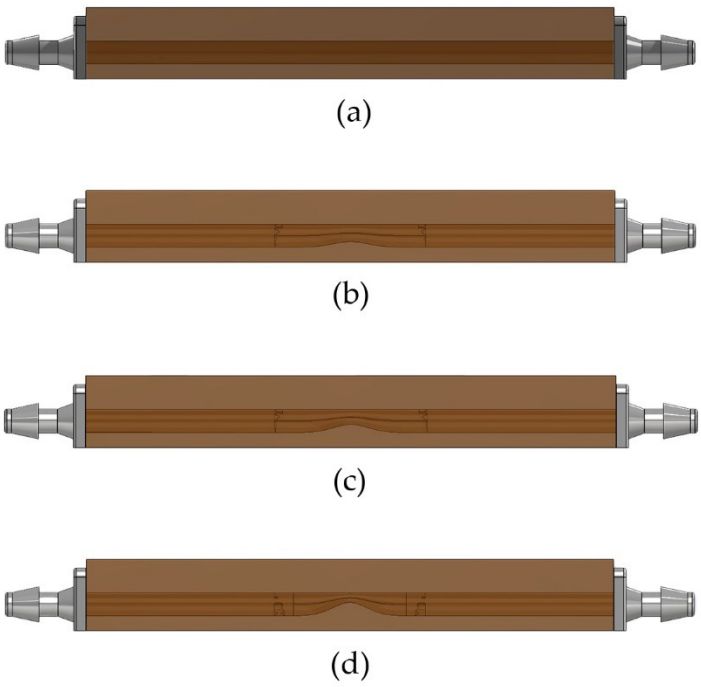

Figure 3-8 Solid TangoPlus 3D Printed Phantom Design, (a) 0% Stenosis, (b) 43% Stenosis, (c) 59% Stenosis, (d) 89% Stenosis.

The rectangular prism shape was printed with TangoPlus material and the connectors with VeroWhite. Because two different materials were used, the design had to be made as separate parts and then united in an assembly that would allow the merge of both materials at the time of printing. This resulted in the export of two STL files, one for each material which would later be printed on the CONNEX3 Object500 (Stratasys, MN, USA). The resulting phantoms are shown in Figure 3-9.

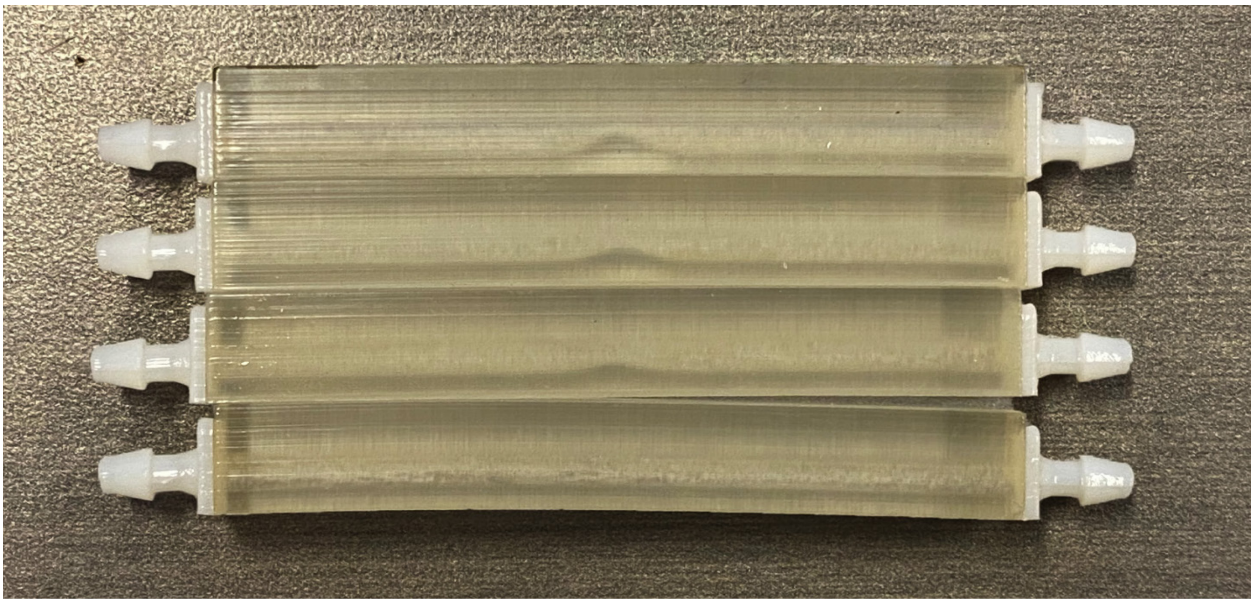

Figure 3-9 Solid TangoPlus 3D Printed Phantoms.

3.1.4 Composite Phantom

In addition to the advantages of 3D printing technology previously discussed, the CONNEX3 Object500 printer (Stratasys, MN, USA) can also print in 3 materials simultaneously. This feature allows the design of a composite phantom. ZhiLin Yang's and Justine Garcia's research uses a multi-material printing technique to control the mechanical properties of the resulting material to mimic artery tissue. This technique consists of embedding sinusoidal waves of a rigid material (VeroWhite) in a matrix of another softer material (TangoPlus)[28, 29].

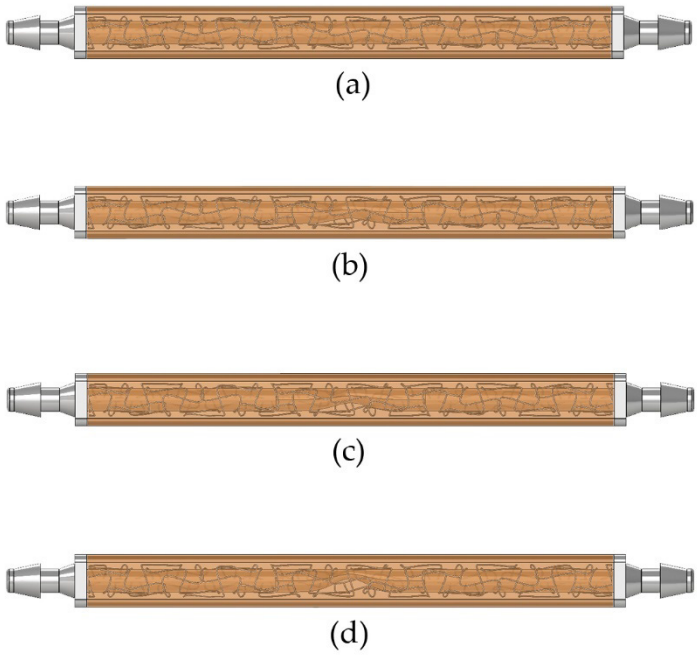

Figure 3-10 Composite 3D Printed Phantom (TangoPlus & VeroWhite), (a) 0% Stenosis, (b) 43% Stenosis, (c) 59% Stenosis, (d) 89% Stenosis.

An additional design was carried out to reduce the number of connections in the circuit. On the original phantoms, the overall length was 70mm, so inside the visualization box, two sections of 1/8" tubing were used to complete the internal length of the box. In the new design shown in Figure 3-11, enough length was added to connect both internal faces of the box. The extension was created only with TangoPlus material. The final extended composite phantoms are shown in Figure 3-12.

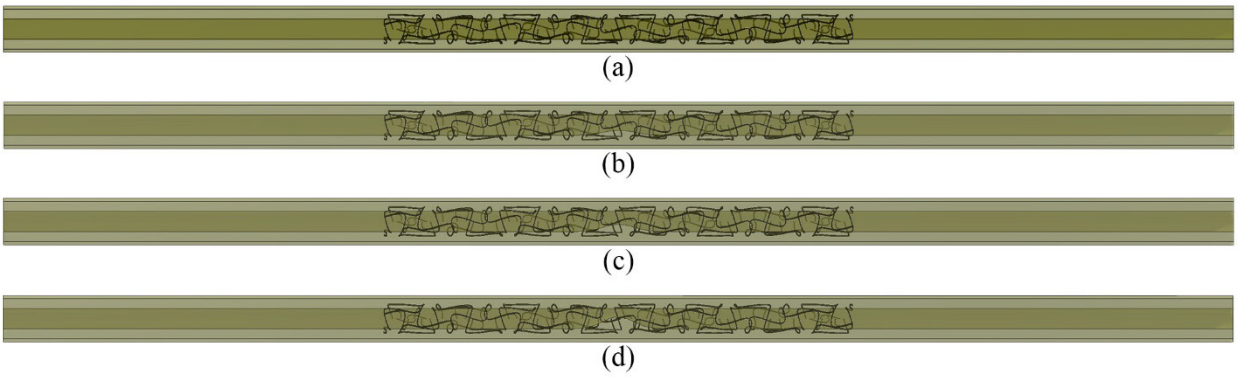

Figure 3-11 XL Composite 3D Printed Phantom (TangoPlus & VeroWhite), (a) 0% Stenosis, (b) 43% Stenosis, (c) 59% Stenosis, (d) 89% Stenosis.

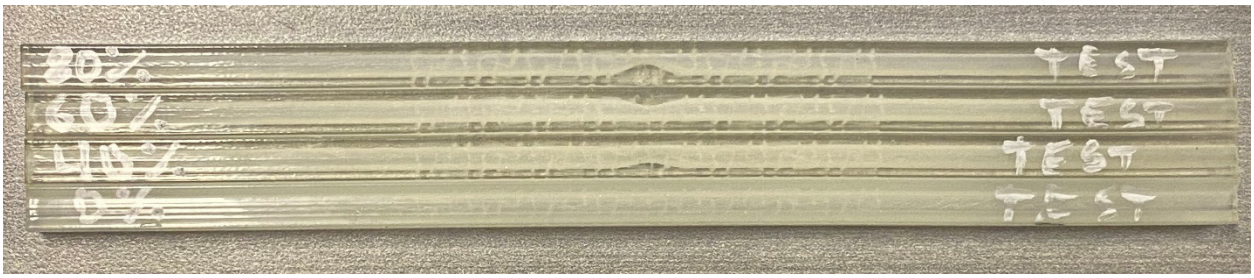

Figure 3-12 XL Composite 3D Printed Phantoms.

3.2 Hemodynamic Circuit

The main objective of the hemodynamic circuit is:

• To provide the stenotic coronary artery phantom with anatomically representative pressure and blood flow.

The desired aortic pressure curve was first selected and then simulated using tubing of different lengths and materials, tube fittings and other components.

The hemodynamic circuit also had to comply with the following additional features:

- To be capable of performing a coronary angiography on the hemodynamic circuit, which implies that it can be subjected to X-Ray imaging, a pressure measuring wire must be able to be introduced to the phantom, a pressure transducer must be able to be added, and the circuit must have an access point to introduce a contrast agent.

- To allow manipulation of the pulsations per minute, the pressure, and the flow in the circuit.

Finally, some considerations taken into account for the circuit are:

- Repeatability: the hemodynamic circuit had to be simple enough to replicate or replace components. All the components in the circuit are standard.

- Versatility: the design must be easy to change and adapt to changes in dimensions or materials so that it can be configured to obtain or modify properties in the pressure curve.

The steps that were undertaken for the development of the hemodynamic circuit are shown in Figure 3-13, where an iterative process was followed until the desired results were reached.

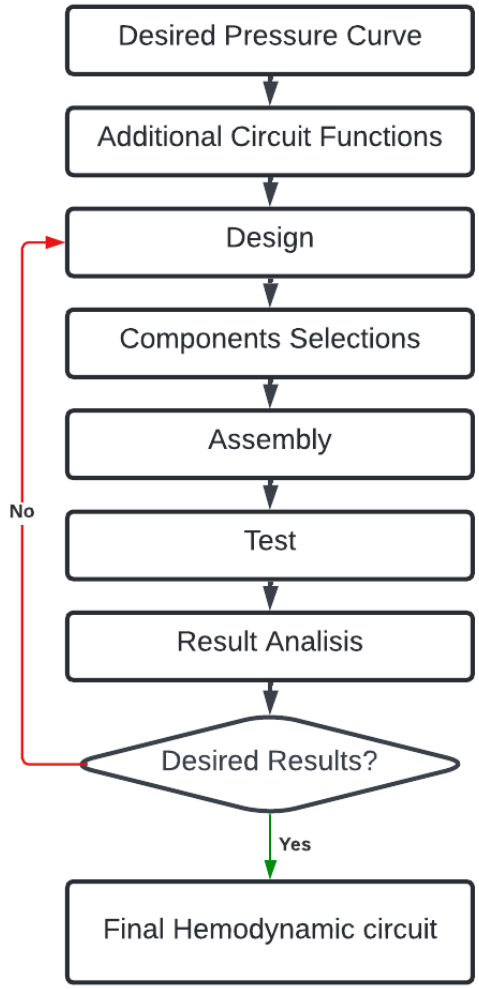

Figure 3-13 Hemodynamic Circuit Workflow

3.2.1 The Desired Curve Profile

The “Wiggers diagram” presented in Figure 3-14 has been a fundamental tool for teaching cardiovascular physiology [30]. It shows the Aortic pressure curve profile, among others. Its pressure range varies from 80 mmHg to 120 mmHg, and it displays a small dicrotic notch, usually attributed to the closure of the aortic valve.

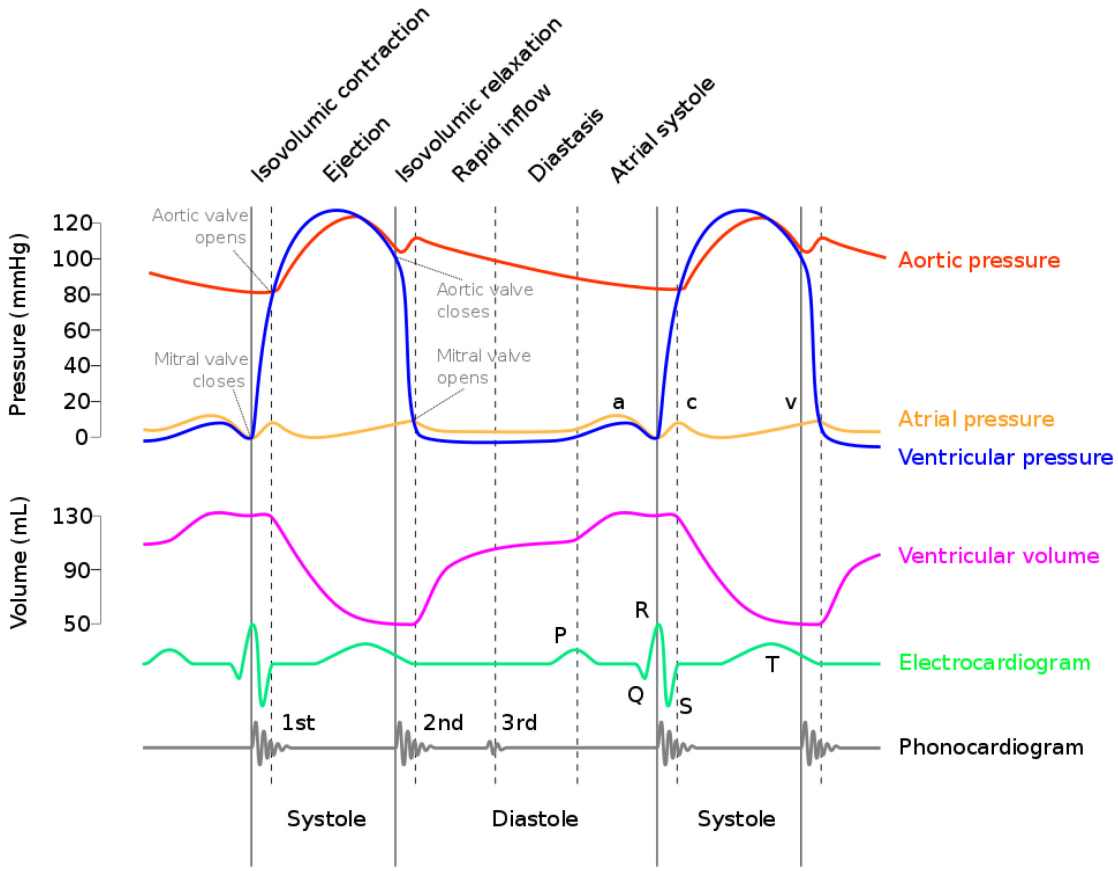

Figure 3-14 A Wiggers diagram, showing the cardiac cycle events occurring in the left ventricle.

3.2.2 Circulatory System Simulation

This section presents the design of the hemodynamic circuit simulating the effects of the circulatory system on a coronary artery. The final design was obtained after conducting several tests with different components, including a semi-lunar aortic valve, a capacitance chamber and other materials plus different lengths of tubes.

Respecting the objectives of repeatability and versatility, the components selected for the circuit are readily commercially available with the complete description and length of tubing (Table 3-3).

No.		Component	Length
1		Pulsatile pump "EDU-P120."	-
2		3/8 – ¼ Quick Connector / Barbed adapter	-
3		Clear Masterkleer Soft PVC Plastic Tubing for Air and Water, ¼" ID, 3/8" OD	15 cm
4		Check Valve, High-Cycling, Nylon Plastic Body for ¼" Tube ID	-
5		Clear Masterkleer Soft PVC Plastic Tubing for Air and Water, ¼" ID, 3/8" OD	10 cm
6		Plastic Barbed Tube Fitting for Air and Water, Easy-View Wye Connector for ¼" Tube ID	-
	6.1	Clear Masterkleer Soft PVC Plastic Tubing for Air and Water, ¼" ID, 3/8" OD	5 cm
	6.2	Plastic Barbed Tube Fitting for Air and Water, Tight-Seal, Reducer, for ½" x ¼" Tube ID	-
	6.3	Super-Soft Latex Rubber Tubing for Air and Water, ½" ID, ¾" OD	15 cm
	6.4	Plastic Barbed Tube Fitting for Air and Water, Tight-Seal, Reducer, for ½" x ¼" Tube ID	-
	6.5	Super-Soft Latex Rubber Tubing for Air and Water, ¼" ID, ½" OD	5 cm

7	Clear Masterkleer Soft PVC Plastic Tubing for Air and Water, ¼” ID, 3/8” OD			5cm
8	Plastic Barbed Tube Fitting for Air and Water, Tight-Seal, Reducer, for ½” x ¼” Tube ID			-
9	Super-Soft Latex Rubber Tubing for Air and Water, ½” ID, ¾” OD			10 cm
10	Plastic Barbed Tube Fitting for Air and Water, Tight-Seal, Reducer, for 1/2" x 1/4" Tube ID			-
11	Clear Masterkleer Soft PVC Plastic Tubing for Air and Water, 1/4" ID, 3/8" OD			5 cm
12	Plastic Barbed Tube Fitting for Air and Water, Easy-View Reducer for 1/4" x 1/8" Tube ID			-
13	Clear Masterkleer Soft PVC Plastic Tubing for Air and Water, 1/8" ID, 1/4" OD			5 cm
14	Dying agent input			-
15	Clear Masterkleer Soft PVC Plastic Tubing for Air and Water, 1/8" ID, 1/4" OD			**2m***
16	Plastic Quick-Disconnect Tube Coupling for Air and Water, Plug and Socket Set, for 1/8" Barbed Tube ID			-
17	Clear Masterkleer Soft PVC Plastic Tubing for Air and Water, 1/8" ID, 1/4" OD			3 m
18	Plastic Quick-Disconnect Tube Coupling for Air and Water, Plug and Socket Set, for 1/8" Barbed Tube ID			-
19	Clear Masterkleer Soft PVC Plastic Tubing for Air and Water, 1/8" ID, 1/4" OD			10 cm
20	Plastic Barbed Tube Fitting for Air and Water, Easy-View Wye Connector for 1/8" Tube ID			-
	20.1	Clear Masterkleer Soft PVC Plastic Tubing for Air and Water, 1/8" ID, 1/4" OD		15 cm
	20.2	Hemostasis Valve		
		20.2.1	Transducer	
		20.2.2	Stopcock (Optowire Input)	
21	Clear Masterkleer Soft PVC Plastic Tubing for Air and Water, 1/8" ID, 1/4" OD			5 cm
22	Visualization box			-
23	**PHANTOM**			-

24	Clear Masterkleer Soft PVC Plastic Tubing for Air and Water, 1/8" ID, 1/4" OD	VARIABLE
25	Plastic Barbed Tube Fitting for Air and Water, Easy-View Reducer for 1/4" x 1/8" Tube ID	-
26	Clear Masterkleer Soft PVC Plastic Tubing for Air and Water, 1/4" ID, 3/8" OD	15 cm
27	3/8 - 1/4 Quick Connector / Barbed adapter	

*For the experiments carried out in this investigation, 2 meters of the tube were used for this section. However, the length can be changed to obtain higher or lower pressures in the pressure curve. Modifications in this length do not affect the measurement of FFR and dPR.

Table 3-3 Hemodynamic Circuit List of Components.

In Figure 3-15**,** the flow path of the liquid is represented by a diagram. The nomenclature of the chart coincides with that used in Table 3-3. These components and its functions are explained in greater depth below.

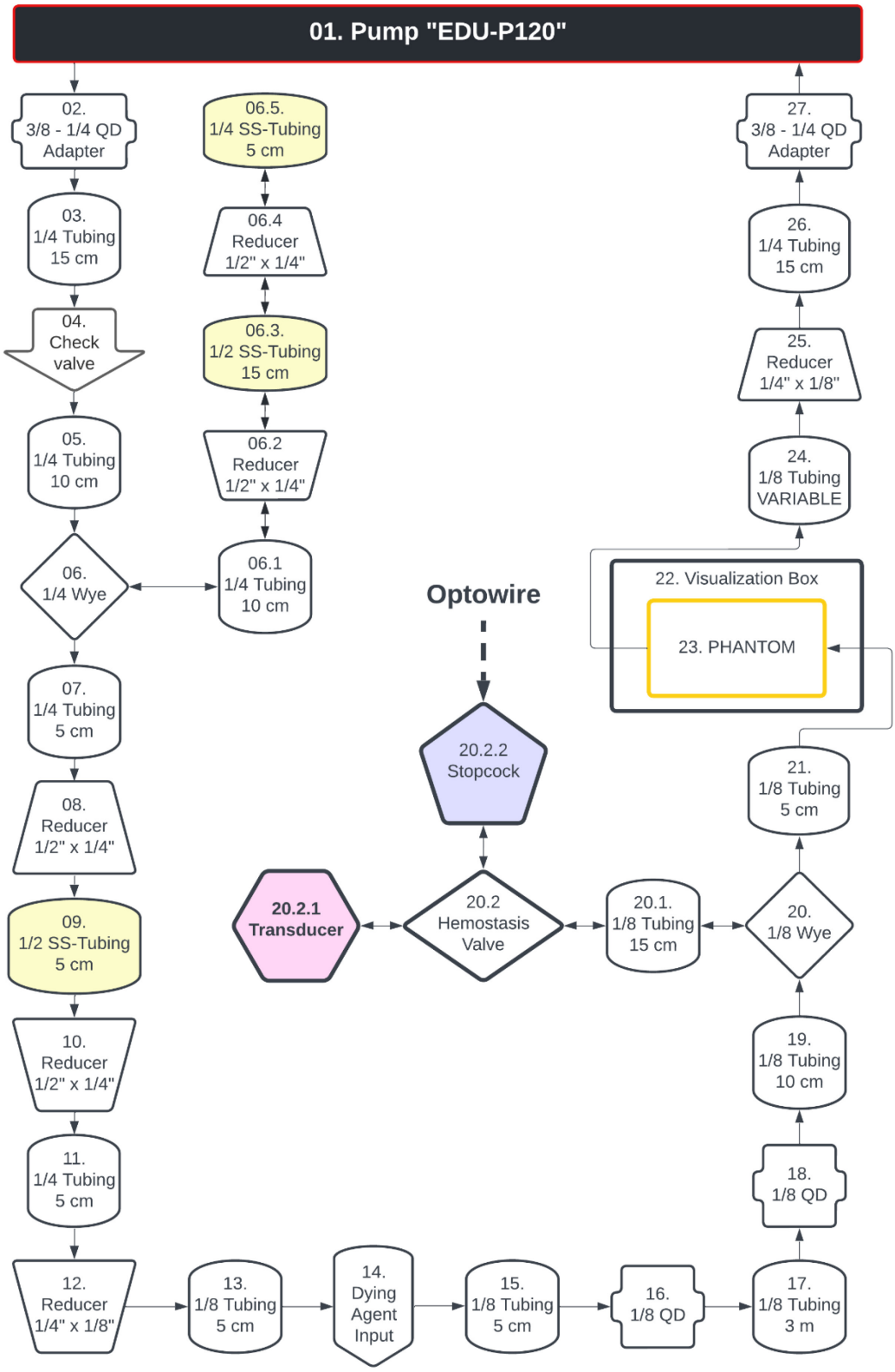

Figure 3-15 Hemodynamic circuit connection diagram

Pulsatile Pump

The mechanical device used to move the system fluids and simulate the work of the human heart is the “EDU-P120” portable pulsatile pump (TRANDOMED, Zhejiang, China), shown in Figure 3-16. This device can produce physiological characteristics such as heart beating frequency, blood pressure, flow rate, simulated blood temperature, and high-pressure duration.

Figure 3-16 Pulsatile Pump EDU-P120

Dicrotic Notch

The dicrotic notch is a critical aspect of the pressure curve to be simulated. This event is represented as a slight increase in pressure just at the beginning of diastole and is usually attributed to the closing of the aortic valve[31], [32]. This section of the circuit intends to generate this notch using a check valve and added compliance by using super soft latex tubing.

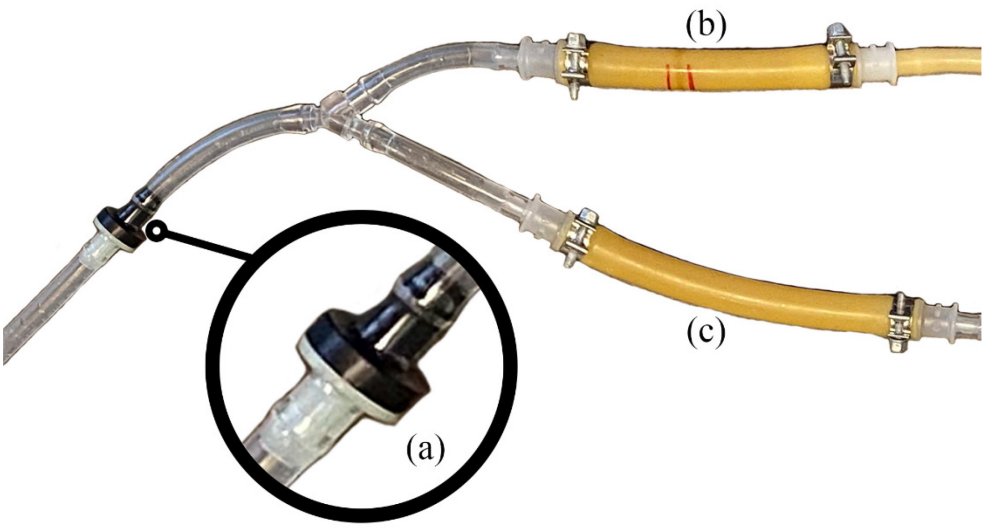

Figure 3-17 Dicrotic notch system. (a) Check valve, (b) Left Super-Soft Tubing (with open end), (c) Right Super-Soft Tubing and continuation of the circuit.

The section of the hemodynamic circuit in charge of generating the dicrotic notch is composed of the following components presented in Figure 3-17:

(a) **Check valve**: The pulsatile pump allows the partial return of the liquid in the circuit, limiting the control over the pressure curve. The primary function of the check valve is to prevent the return of flow, thus controlling the drop in pressure during diastole. The valve requires a minimum of 0.5 psi to open, which means it will close as soon as the

pump boost pressure is less than 25.85 mmHg. Changing this parameter will affect the position of the dicrotic notch on the pressure curve.

(b) **Left Super-soft tubing**: Being a considerably flexible material of shore 40A (similar to a pencil eraser[33]), it can inflate slightly like a balloon when the pressure in the system is high enough. This feature allows limited manipulation of the notch's amplitude and pressure drop duration. Control is achieved by changing the length of super flexible tubing permitted in the system, thus adding or reducing compliance. Clamps are used to close the loop to the desired size. Figure 3-17 shows, with two red lines, the position where the greatest similarity with the desired pressure curve was achieved.

(c) **Right Super-soft tubing**: This component is used to reduce the flow transition to achieve a smooth slope and reduce the steepness after the dicrotic notch. Also, its flexible properties help reduce noise in the pressure curve, but unlike the left one, the flow continues freely through this component without being blocked.

Contrast Agent

Since the hemodynamic circuit will be subjected to X-Ray imaging, an access port is necessary to provide the possibility of introducing a contrast agent.

The position of this access port is critical since it must be located before the area of interest but considering that injecting the contrast agent should not generate a flow disturbance sufficient to alter the measurement.

A 3-way adapter was introduced into the system just after the compliance section. This adapter allows the circuit to be opened, allowing injection of the contrast agent with a syringe.

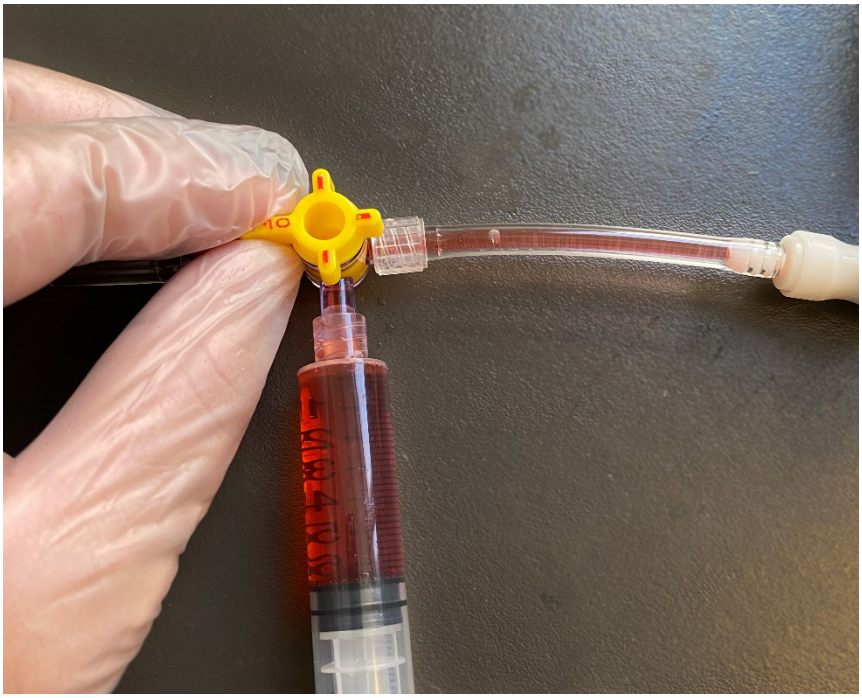

Figure 3-18 Contrast agent injection. Three-way adapter with a syringe attached, injecting the contrast agent.

1/8 Tubing

Given the pump's limitations in pressure control and considering the physical principles of flow in a tube, it was decided to use the tube length of certain sections of the circuit as a controlling factor for resistance to flow. The greater the length, the greater the resistance to be overcome by the flow.

This decision resulted in a 1/8 tubing variable-length section in the circuit. The variable section is located after the visualization box, just before returning to the pump.

This 1/8 tubing variable-length section allows the control of the resistance in the circuit, simulating the resistance compensation that the body generates depending on the level of stenosis. Table 3-4 shows the lengths that performed the best with each stenosis severity.

Stenosis	Length
89%	250 cm
59%	60 cm
43%	15 cm
0%	330 cm

Table 3-4 Variable Tube Length Values for the Stenosis Severity.

There is another section of 1/8 tubing located between the Dicrotic notch and Pressure measuring sections. This section could be used to reduce the pressure in the area of interest, and it does not seem to have any effect on the FFR and dPR measurements.

Transducer and Pressure Wire Access Port

The circuit is divided by a wye connector located after the first variable length tube section and before the area of interest (visualization box).

This access port (Figure 3-19) will allow an access channel for the pressure wire (Optowire). From this point, a column of liquid will be in contact with the transducer to measure the Arterial pressure (Pa) before the stenosis with which the pressure wire will be equalized.

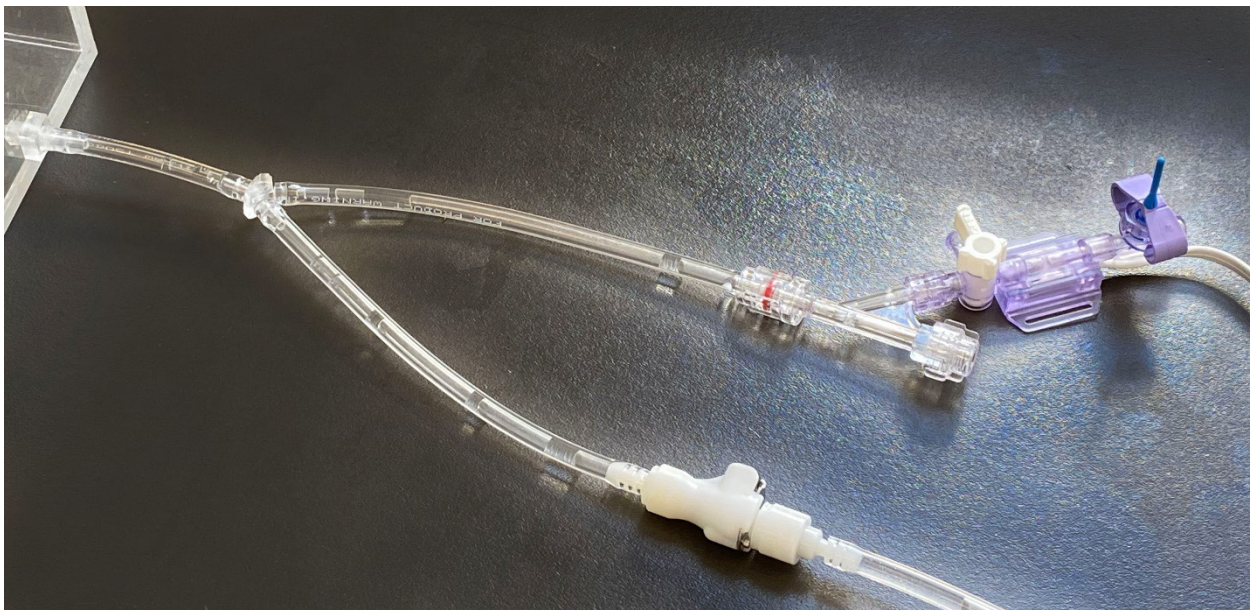

Figure 3-19 Access point. Section of the hemodynamic circuit where the pressure transducer is located and the pressure wire is inserted.

Visualization Box

The primary purpose of the visualization box is to allow the phantom to be immersed in water simulating the rest of the body surrounding the coronary artery during the X-Ray imaging. Water is necessary to absorb part of the X-Ray emitted on the phantom of the coronary artery.

The visualization box is designed using SolidWorks (Figure 3-20), to be manufactured with 5.5 mm thick Plexiglas (Figure 3-21). The lower part of the box has two 5mm drills, one on each side. These holes are filled and sealed with barbed tube fittings to connect with the rest of the hemodynamic circuit and allow the pulsatile flow through the phantom, simulating a human's blood flow.

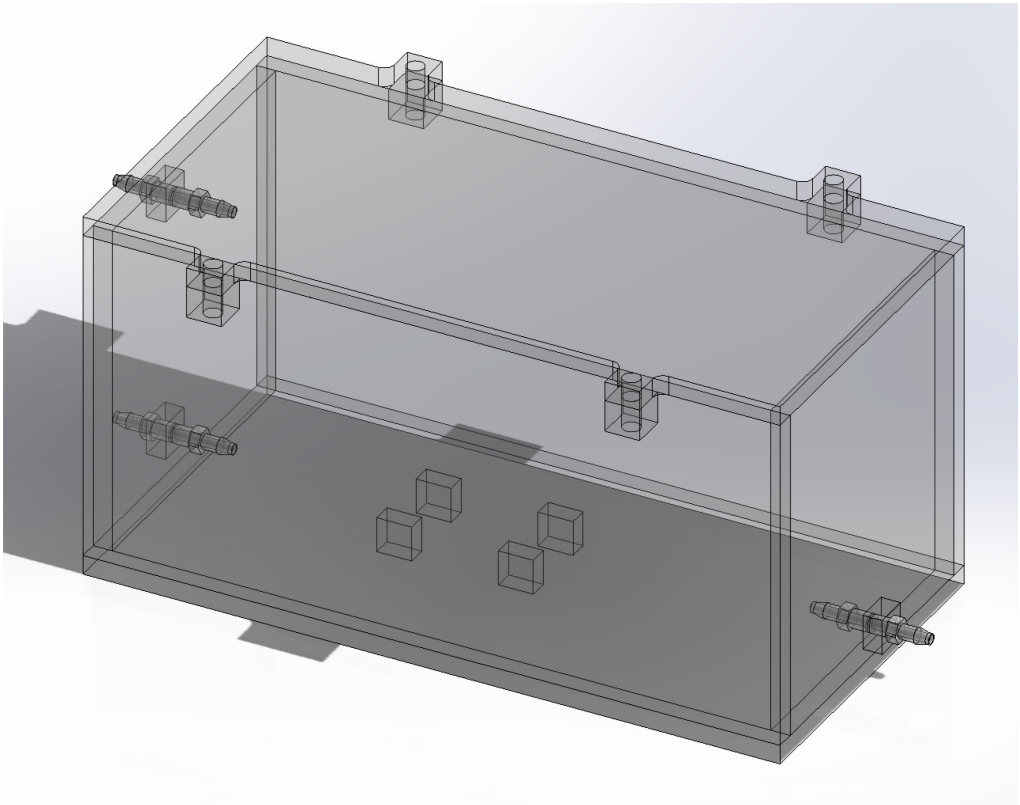

Figure 3-20 Visualization Box (SolidWorks).

One additional 5 mm hole is located on the upper left side of the box. This hole is also filled and sealed with barbed tube fittings. In future research, it will allow control over the air pressure inside the visualization box to mimic the pressure experienced by an artery's exterior walls.

Four 10mm X 10mm X 5.5mm blocks are fixed around the phantom's location to ensure that the phantom remains in place and does not slip off due to the inner pressure of the liquid flowing through.

Finally, a removable lid is designed to perform an airtight closure to allow internal pressure control.

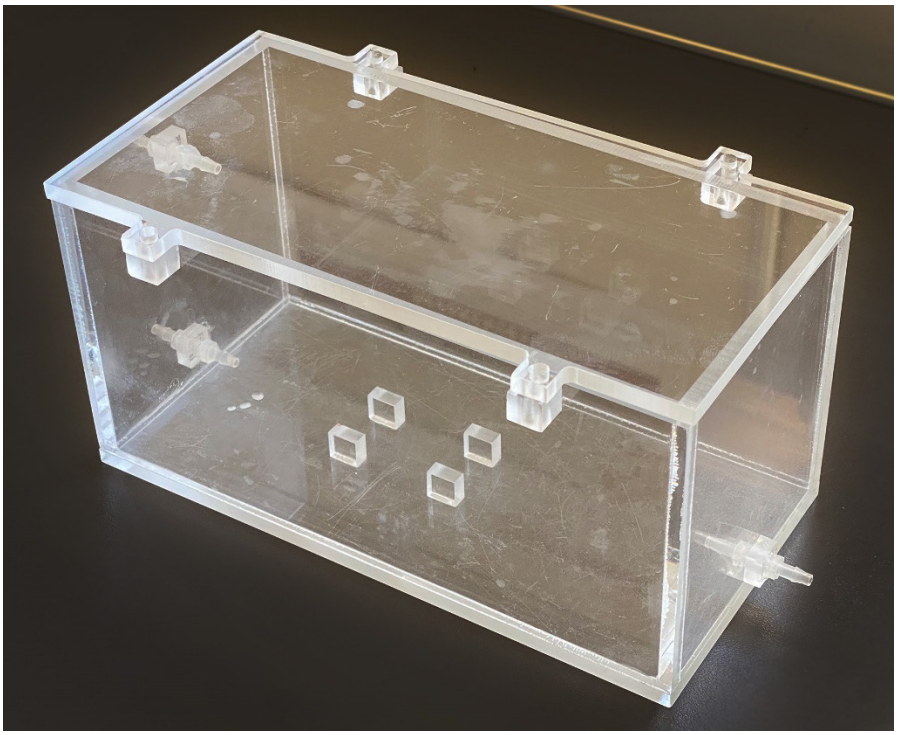

Figure 3-21 Manufactured Visualization Box.

3.2.3 Measurement Equipment

As mentioned before, the purpose of the dynamic coronary artery phantom test system is to be able to perform an FFR reading on a replica of a stenotic coronary artery, for which the use of precise high-tech tools was necessary. For this research, Opsens Medical equipment was employed. Opsens OptoWire: is an innovative pressure guidewire designed explicitly to evaluate stenoses in blood vessels. The nitinol core of the cable allows agile navigation through the blood vessels and, in this case, through the tubing used in the hemodynamic circuit.

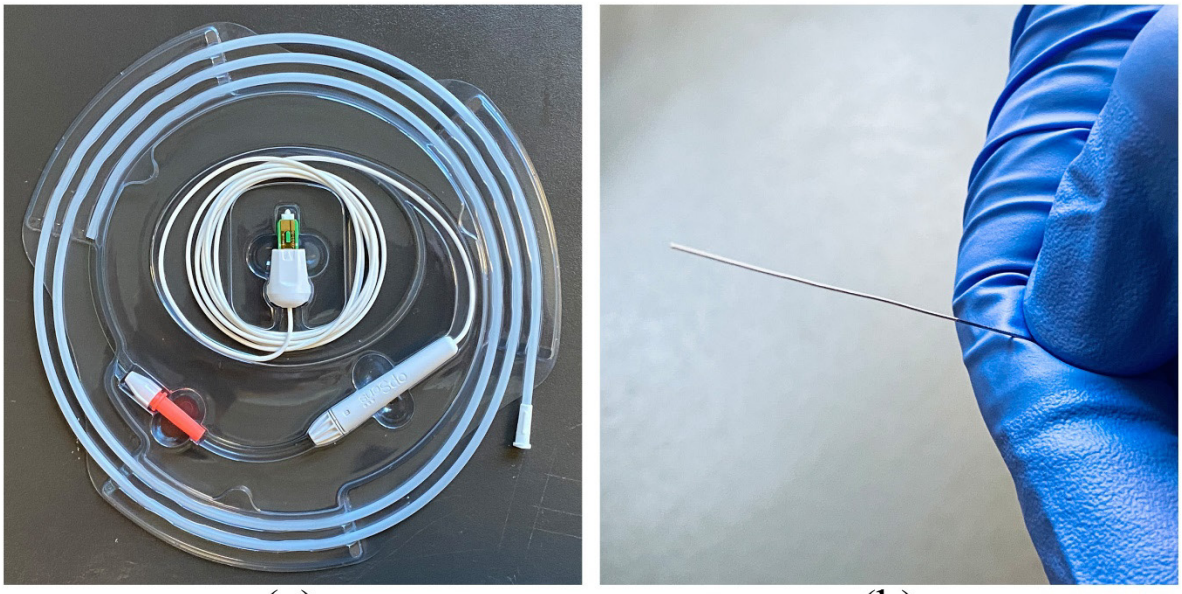

Figure 3-22 Pressure wire (OptoWire) developed and manufactured by OpSens Medical. (a) packaged out of the box, (b) pressure cable tip.

Opsens OptoMonitor: While the OptoWire is a cable that senses pressure, the OptoMonitor is the computer that interprets these readings and allows us to obtain different values such as FFR, Pd/Pa, cFFR and dPR. The device will enable the user to make patient profiles and save the

readings that can later be extracted through a USB memory for subsequent analysis on a personal computer.

Arterial line transducer: finally, in addition to the OptoWire, the Optomonitor also allows reading the measurements of a transducer in charge of monitoring blood pressure. The transducer comes into contact with the circuit's flow through a liquid column inside the tube. The extraction of any bubble in the system must be performed. The transducer reading (Pa) will be used to match the wire's pressure reading before the stenosis, thus achieving an equalization.

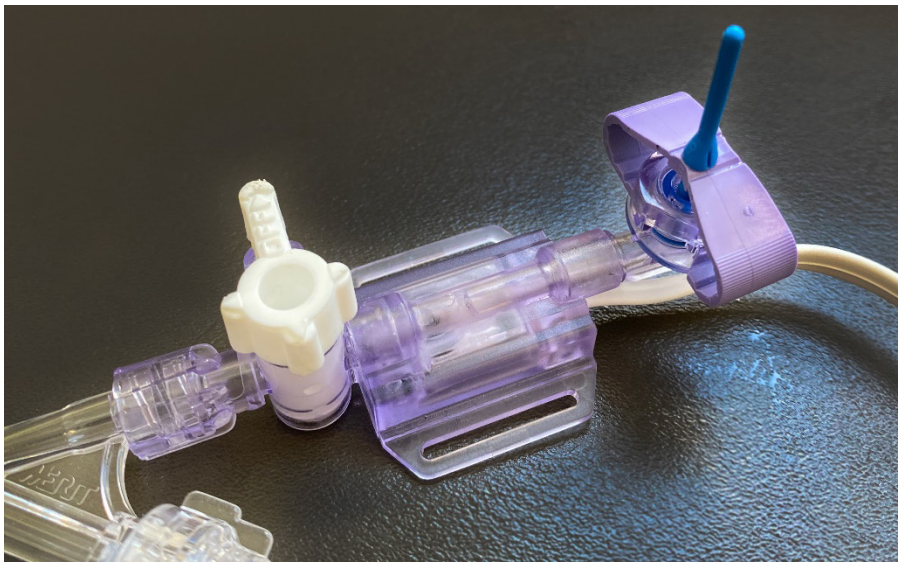

Figure 3-23 In-line pressure transducer. The cable is connected to the OptoMonitor. The 3-way valve is used to perform a zero and to join a pressurized bag of saline solution. The blue valve is used to purge the device since it must expel the air in the circuit.

3.3 Cam System

The objective of the cam system is to accurately represent the movement of the coronary artery caused by the respiratory cycle and by the contraction of the heart itself.

There are four basic considerations that were taking into account for the system:

- Manufacturability: The design must be thought of so that it can be easily manufactured. It will be sought that most of the components are OTS (Off the shelf) and easy to obtain. It is desired that manufactured parts are of minimum complexity.

- Versatility: The design will be as versatile as possible, considering aspects such as variable pump height, the possibility of changing the direction of movement, and the possibility of changing movement patterns.

- Portability: The system should be portable so that it can be used within a Cardiac Catheterization Lab (Cath Lab) to perform an angiogram.

- Usability: Ideally, the system's operation resembles an actual procedure as much as possible. The system must simulate a patient undergoing a coronary angiogram

3.3.1 Desired Movement

For this research, the movements of the coronary artery generated due to respiration and the cardiac cycle itself were considered.

To represent the displacement that the heartbeats cause on the coronary artery, the tracked movement of the mitral valve founded in the work of Toufic Azar et al. was used. Toufic Azar et al.mention that the representative movement occurs in the superior-inferior direction. The movement in other directions is considered negligible[34].

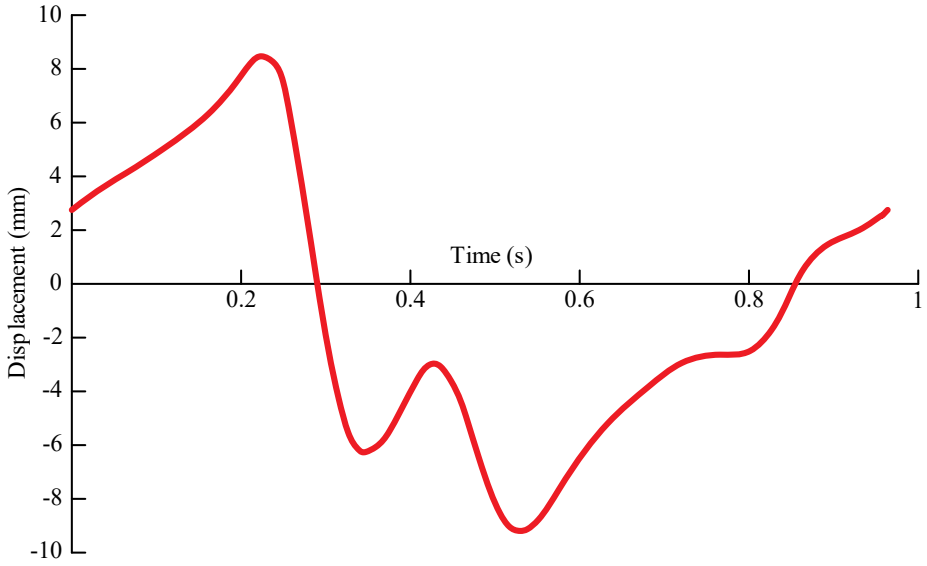

Figure 3-24 Displacement curve at the root of the coronary artery due to the movement of a heartbeat, from [15].

In his work, Toufic Azar uses this movement for a dynamic left atrioventricular phantom test bed emulating mitral valve motion. However, the movement was originally obtained from 3D echocardiography data images in the work of Yuen et al.[35]

After some experiments, it was observed that the displacement curve found in the mitral valve had more aggressive accelerations than the actual displacement found in the coronary artery due to the heart beating, causing to much noise in the FFR and dPR readings. Al-Kwifi et al. performed a characterization of coronary motion in the major coronary arteries and generated its displacement curve during breath-holding[36]. The displacement curve used to represent the displacement that the heartbeats cause on the coronary artery was that experienced by the LAD (Figure 3-25).

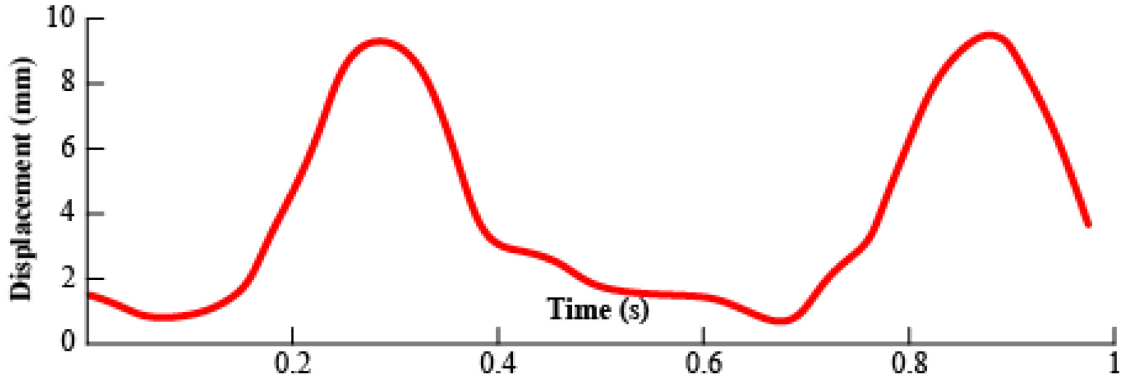

Figure 3-25 Displacement curve at the LAD in a subject during breath-holding from [36]

The movement on the coronary arteries root caused by breathing was obtained from the work of Guy Shechter et al. This movement is mainly due to the movement of the diaphragm during respiration and occurs equally in the superior-inferior direction[37].

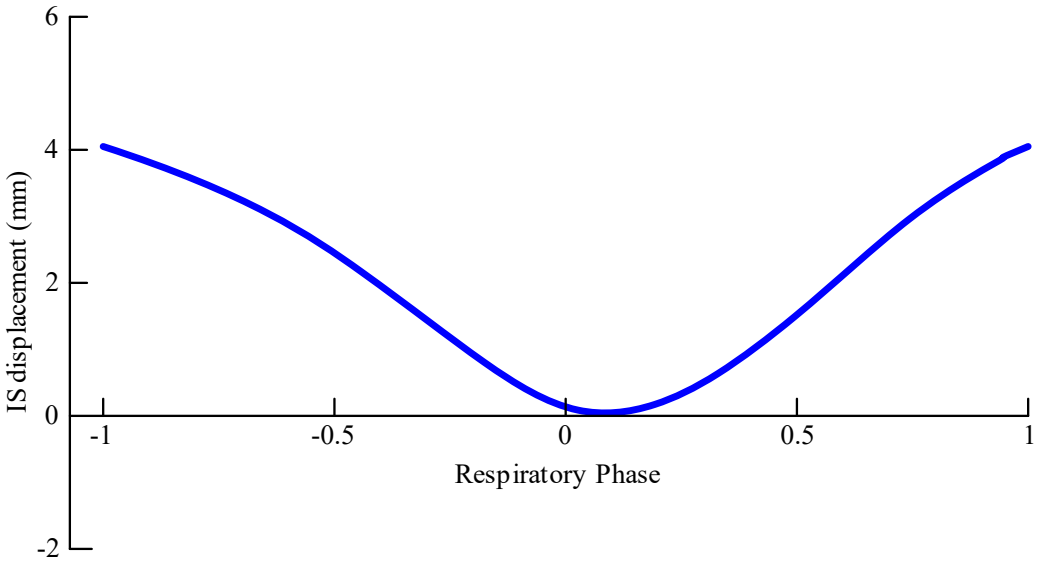

Figure 3-26 Displacement curve at the root of the coronary artery due to respiration, from [17].

Finally, the combined movement of the coronary artery due to breathing and heartbeat simultaneously was also developed. The number of heartbeats of an adult at rest range from 60 to 100 beats per minute. The respiratory rate is between 12 and 20 breaths per minute[38]. A 1:4 ratio of respirations to heartbeats was selected. However, after some experiments and due to the motor's capacity, it was discovered that the 4:1 ratio caused very pronounced curves in the cam plate, causing uncontrolled jumps in the system, so an alternate cam plate with a 2:1 ratio of heartbeats against respiration was designed.

The arithmetic sum of the values of the individual points that make up each wave was made, resulting in the chart shown in Figure 3-27.

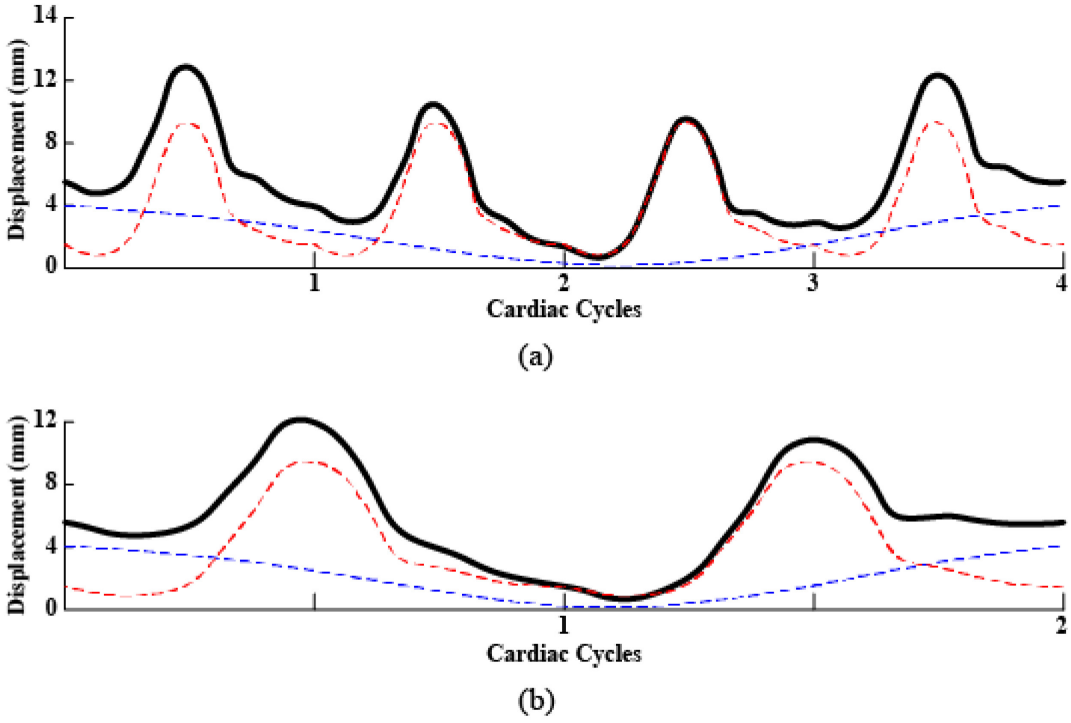

Figure 3-27 Mixed displacement curve at the root of the coronary artery due to respiration and heartbeats. (a) With a ratio of heartbeats to respiration of 4:1 (b) With a ratio of heartbeats to respiration of 2:1.

The literature mentions that the dominant movement is in the superior-inferior direction, that is, from head to toe and vice versa, which is why it was originally thought of as a cam system that would move the phantom vertically. However, the system is so versatile that it was also designed so that with minor alterations. The system can also move the phantom in a horizontal direction, simulating a patient lying on the Cath Lab stretcher.

3.3.2 Structure & Components

This section presents the design and the components selection for the CAM System simulating the anatomical movements affecting the coronary artery. The final design was obtained after evaluating different conceptual ideas and selecting components based on system needs and market availability.

The components selected for the CAM System are readily available and shown in Table 3-5 with the complete item's description.

No.	Qty	Component	Length
1	2	T-Slotted Framing, Single 4-Slot Rail, Silver, 1.5" High x 1.5" Wide, Hollow	3 ft.
2	11	T-Slotted Framing, Single 4-Slot Rail, Silver, 1.5" High x 1.5" Wide, Hollow	1 ft.
3	2	T-Slotted Framing, Single 4-Slot Rail, Silver, 1.5" High x 1.5" Wide, Hollow	10 in.
4	2	T-Slotted Framing, Single 4-Slot Rail, Silver, 1.5" High x 1.5" Wide, Hollow	6 in.
5	6	T-Slotted Framing, Single 4-Slot Rail, Silver, 1.5" High x 1.5" Wide, Hollow	3 in.
6	1	T-Slotted Framing, Single Four Slot Rail, Silver, 1" High x 1" Wide, Solid	1 ft.
7	1	T-Slotted Framing, Single Four Slot Rail, Silver, 1" High x 1" Wide, Solid	10 in.
8	2	T-Slotted Framing, Single Four Slot Rail, Silver, 1" High x 1" Wide, Solid	6 in.
9	4	Silver Corner Bracket, 3" Long for 1-1/2" High Rail T-Slotted Framing	-
10	4	T-Slotted Framing, Silver Bracket, 3" Long for 1-1/2" High Single Rail	-
11	2	T-Slotted Framing, Silver Surface Bracket, 6" Long for 3" High Double/Quad Rail	-
12	2	T-Slotted Framing, Offset Reducer Surface Bracket for Single Rail	-
13	5	Silver Gusset Bracket, 1" Long for 1" High Rail T-Slotted Framing	-
14	10	T-Slotted Framing, Silver Gusset Bracket, 1-1/2" Long for 1-1/2" High Rail	-
15	2	Silver Corner Bracket, 1.5" Long for 1.5" High Rail T-Slotted Framing	-
16	1	Clevis Rod End, 1/4"-20 Thread, 2" Shank Center Length	-

17	1	Water-Resistant Plastic Ball Bearing, Trade Number R4A, for 1/4" Shaft Diameter	-
18	1	Flange-Mount Shaft Collar for 5/8" Diameter, 2024 Aluminum	-
19	1	Parallel Shaft DC Gearmotor, 1/8 hp, 167 rpm at 43 in.-lbs. Torque	-
20	1	Enclosed Single Phase AC to DC Motor Speed Control	-
21	10	T-Slotted Framing, End-Feed Nut with Flanged Head, 5/16"-18 Thread, Steel	-
22	1	18-8 Stainless Steel Right-Angle Weld Studs, 1/4"-20 Thread, 5/8" Long	-
23	1	18-8 Stainless Steel Right-Angle Weld Studs, 5/16"-18 Thread Size, 5/8" Long	-
24	1	Springs with Hook Ends	
25	1	Hook and Loop Cable Tie	
Designed Parts			
26	1	Base (Visualization Box)	-
27	1	Base (Pump)	-
28	1	Cam Plate - Heartbeat	-
29	1	Cam Plate - Respiration	-
30	1	Cam Plate - Combination of heartbeat and respiration	-
31	1	Visualization Box	-
32	2	Slider	-
8		Pulley Wheels 625zz	-
8		Hex Drive Flat Socket Cap Screw M5-0.8 x 40mm	-
8		Hex Lock Nuts M5 x 0.8mm	-

Table 3-5 Cam System List of Components.

T-Slotted Framing Rails & Structural Brackets

For the structure of the cam system, a design based on T-Slotted framing rails and structural Brackets was used due to its accessibility, easy assembly and versatility that allows future modifications.

Cam Plates and Follower

The cam plates were developed with the movement curves attributed to heartbeats and breaths in the distance-time charts discussed in section 3.3.1. The steps for the designs are shown in Figure 3-28 .

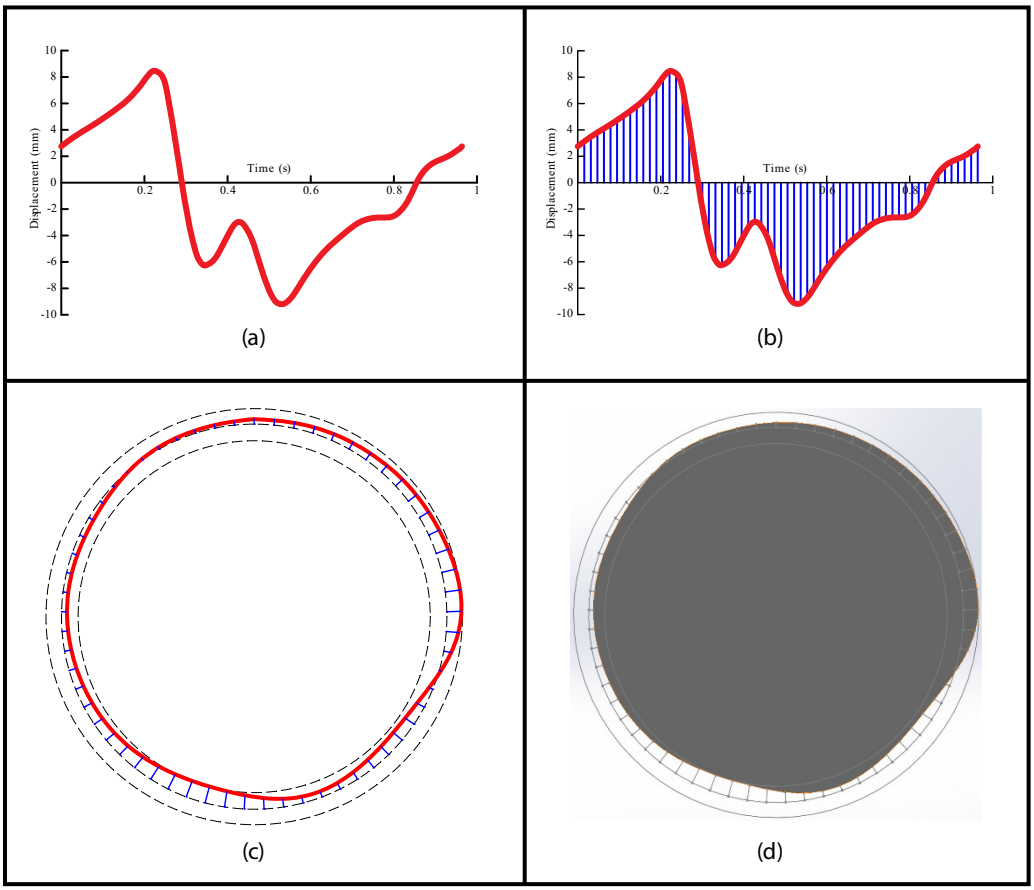

Figure 3-28 Cam Plates Design Process. (a) Heartbeat displacement curve. (b) Heartbeat displacement curve, segmented into 62 lines of independent magnitude. (c) 62 lines distributed equally in one revolution with a controlled maximum diameter and matching dimensions to (b). (d) Extrusion of the resulting curve.

Once the designs were completed, they were manufactured on an Original Prusa i3 MK3S+ (Prusa Research a.s., Prague, Czechia) 3D printer using PLA as material. Additionally, the

manufacture of an aluminum cam plate was carried out using a waterjet machine. The perimeter that contacts the cam follower was polished by hand with sandpaper. The manufacturing time for each cam plate in 3D printing was around 16 hours. The aluminum cam plate manufacturing in waterjet only took about 1 hour.

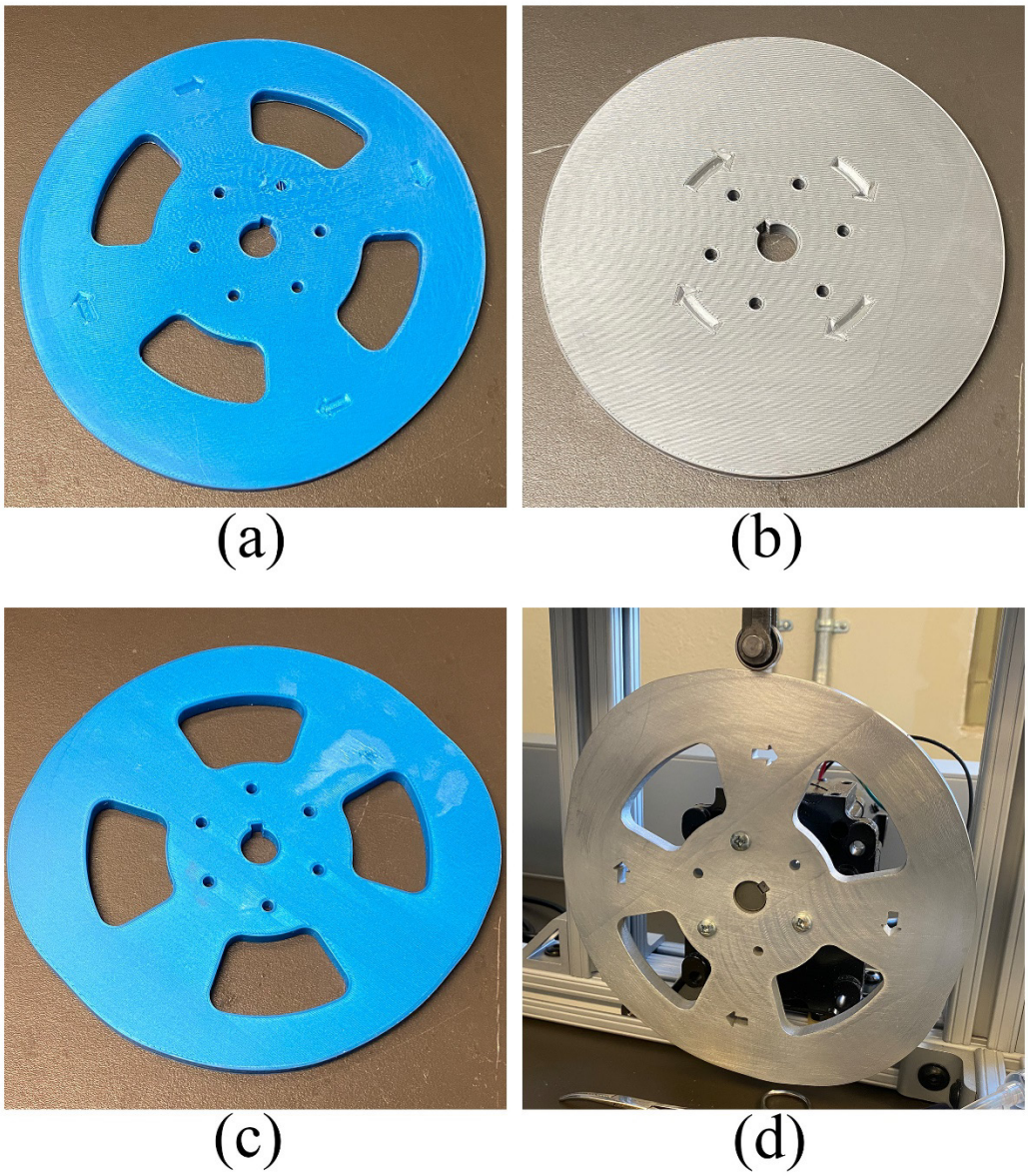

Figure 3-29 Cam Plates. (a) one Heartbeat per revolution, (b) one respiration per revolution, (c) a combination of four heartbeats to one respiration per revolution, (d) a combination of two heartbeats to one respiration per revolution.

Sliders

There are sliders on the market designed to work with the aluminum profiles used. However, some tests showed that these generated much friction and caused jams in the system when used in vertical movement.

A custom slider design was developed. It would work with bearings and V-shaped wheels that ride on the channel in the center of each side of the T-Slotted Framing Rails. The exterior of the slider was designed to be easy to anchor and align to the aluminum profiles. With the final design ready, the slider body was manufactured with the Original Prusa i3 MK3S+ (Prusa Research a.s., Prague, Czechia) 3D printer, and the wheels and bolts were purchased.

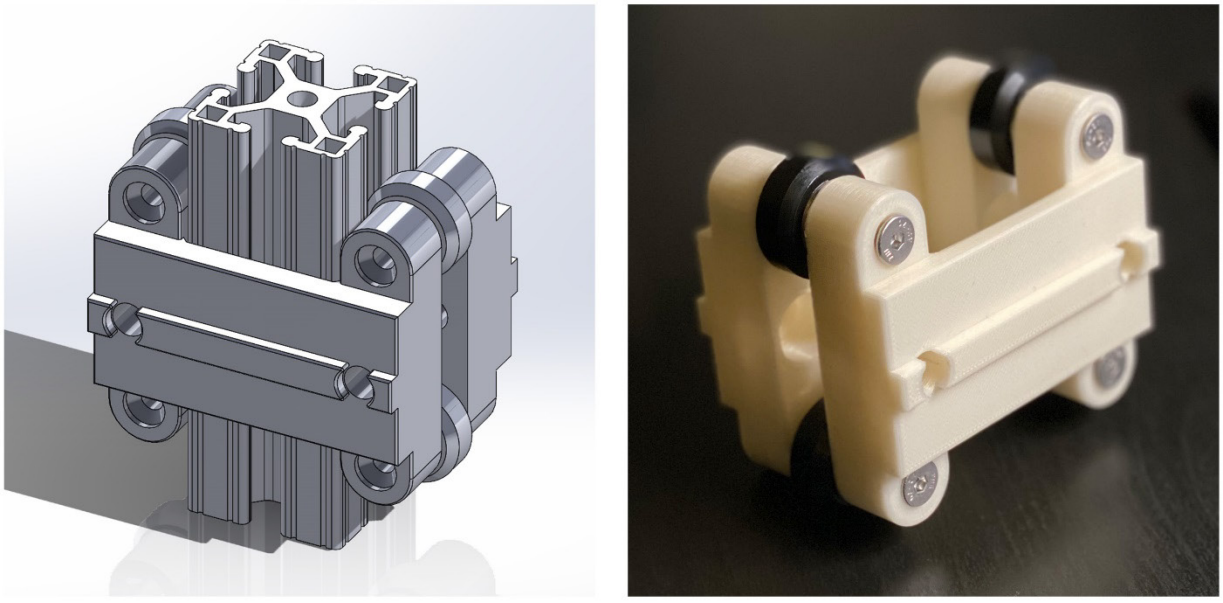

Figure 3-30 Slider. Two 3D printed components, designed to operate on a 1.5" x 1.5" T-Slotted framing aluminum profile, joined by four bolts and nuts and four pulley wheels.

Motor & Controller

The motor was chosen based on the needs of the cam system listed below:

- Speed: the average heartbeat per minute of an adult can vary from 60 to 100 beats per minute, and the design of the cam plate represents one beat per revolution. An engine with a maximum speed of at least 100 revolutions per minute (rpm) was considered.

- Torque: to know the necessary torque, the design of the dynamic section of the cam system moved by the motor was carried out in SolidWorks, and using its "motion Analysis" library, a simulation was performed, resulting in the torque versus time curve (Figure 3-31). Once this curve was obtained, it was decided to select a motor with at least twice the torque to counteract possible details in the assembly that were not considered in the simulation.

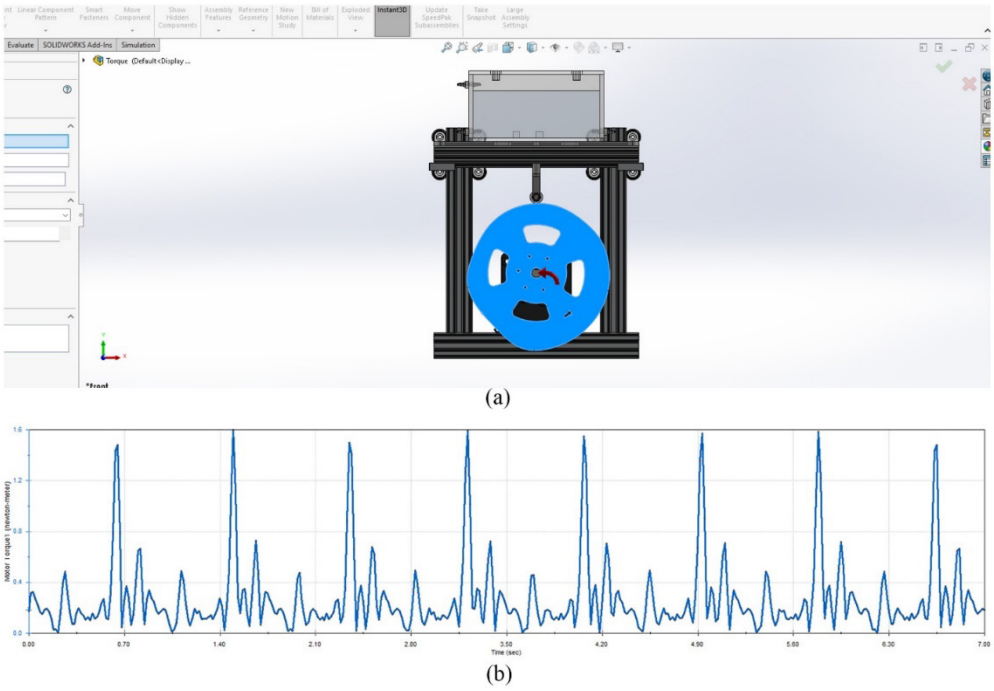

Figure 3-31 Estimation of the torque needed to operate the cam system. The study was carried out in SolidWorks's "Motion Analysis" library. Result: maximum peaks of 1.6 newton-meter.

Figure 3-32 (a) Selected motor: Parallel Shaft DC Gearmotor 1/8 hp, 167 rpm At 43 in.-lbs. (4.85 Nm) Torque. Mounted on the shaft is a Flange-Mount Shaft Collar, where the cam plates will be attached. (b) Selected speed controller: Enclosed Single-Phase AC to DC Motor Speed Control. It is recommended that once connected to the power outlet (110V), the knob is positioned at speed 0 before activating the power switch. Once the switch is activated, the knob is gradually turned until the desired speed is reached.

3.3.3 Assembly

Once the components were selected, the assembly of the cam system was carried out. A CAD (computer-aided design) version with two configurations was designed. The first configuration (Figure 3-33) is used to generate the desired movement in a vertical direction, that is, in a superior-inferior direction in a patient in an upright position.

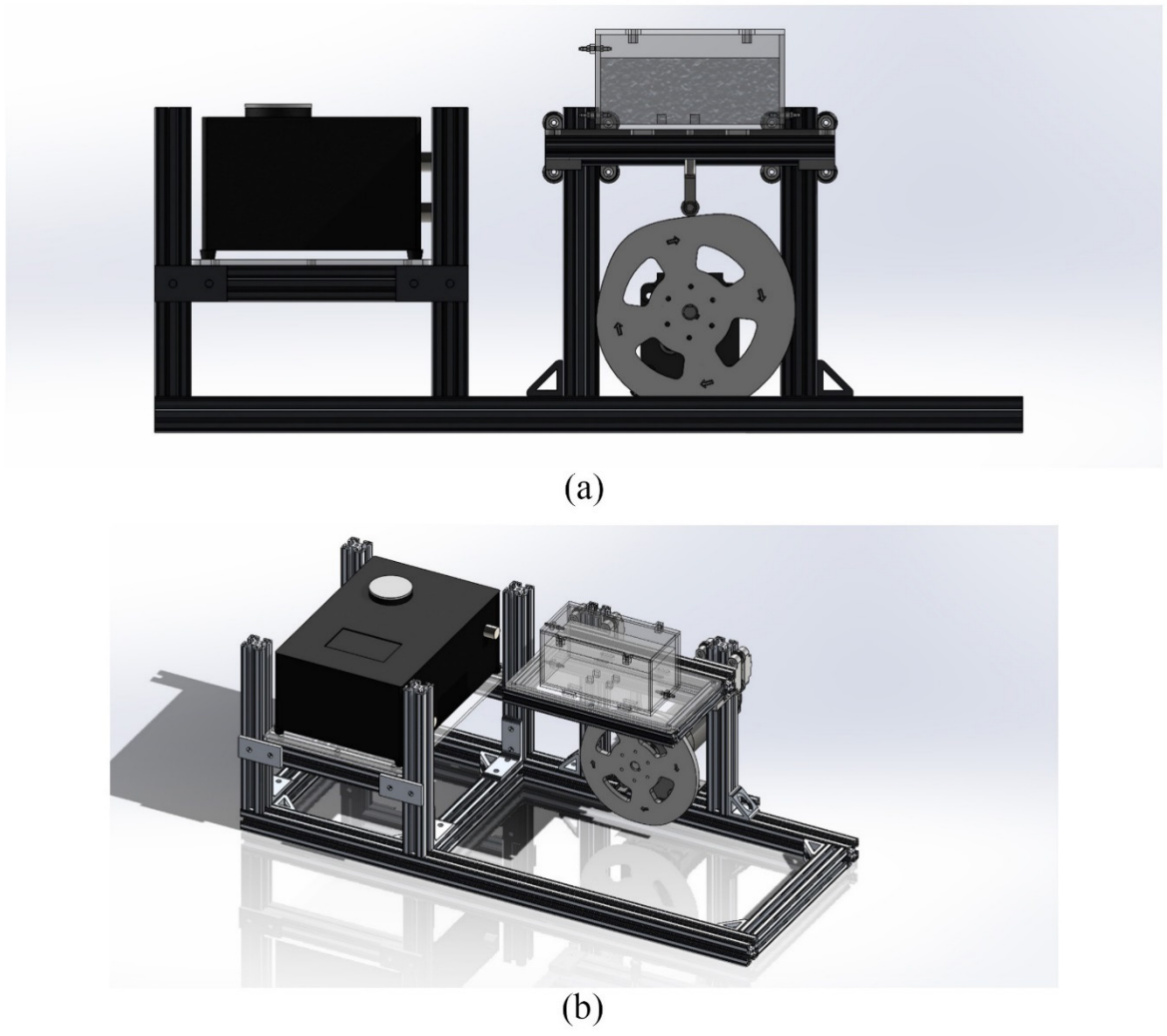

Figure 3-33 Cam system modelled with SolidWorks.(a) Frontal and (b) isometric view. Configuration for vertical movement.

The second configuration designed in CAD (Figure 3-34) could be used to generate the desired movement in a horizontal direction, that is, in a superior-inferior direction in a patient in a supine position.

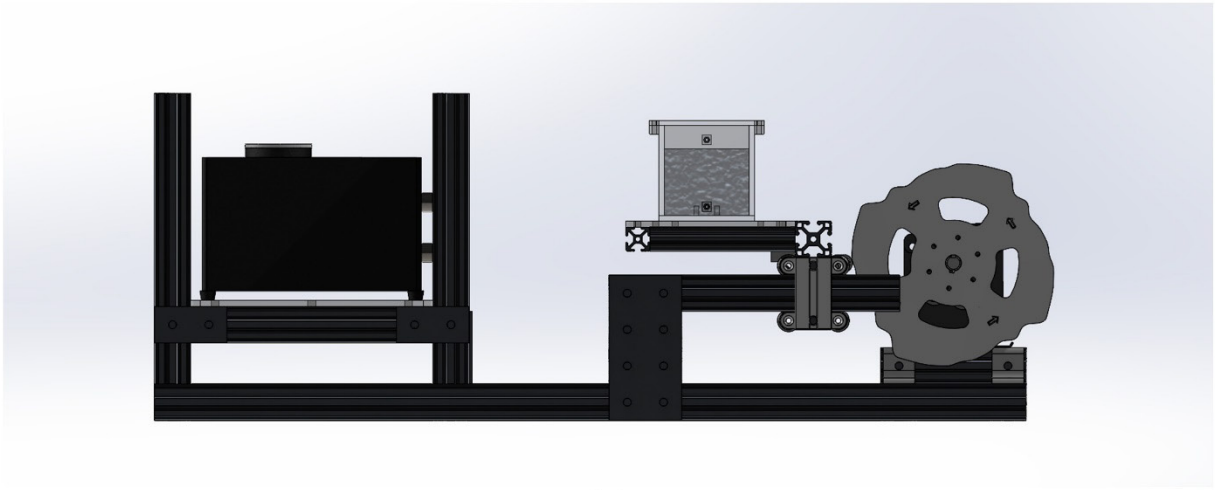

(a)

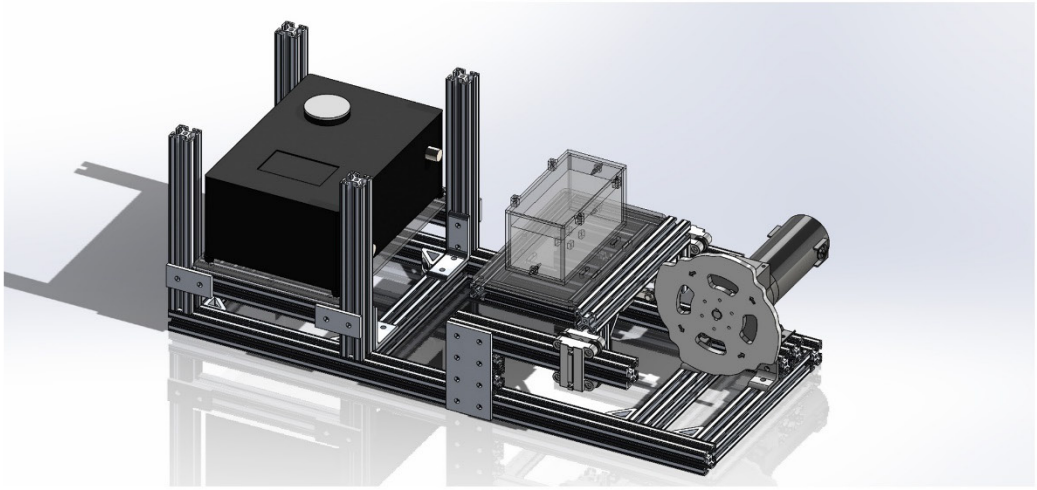

(b)

Figure 3-34 Cam system modelled with SolidWorks.(a) Frontal and (b) isometric view. Configuration for horizontal movement.

McMaster, the OTS (off the shelf) components supplier, offers the 3D design of most of their products within their catalogue. This option simplified the CAD assembly. The OTS

components were downloaded from the supplier's webpage and added to the assembly. The slider, visualization box, and acrylic bases that would support the pump and visualization box were all designed, fabricated and added to the assembly. Finally, the pulsatile pump was also drawn in 3D for illustrative purposes.

With the final CAD assembly, the components were purchased and manufactured. The assembly of the cam system was carried out (Figure 3-35). It can move the visualization box with the phantom of the stenotic coronary artery in a vertical direction, with three different cam plates that will allow emulation of the movement caused by breathing, the heartbeat and a combination of the two. Additionally, it was designed in such a way that with minimal alterations, it can also generate movements in a horizontal direction.

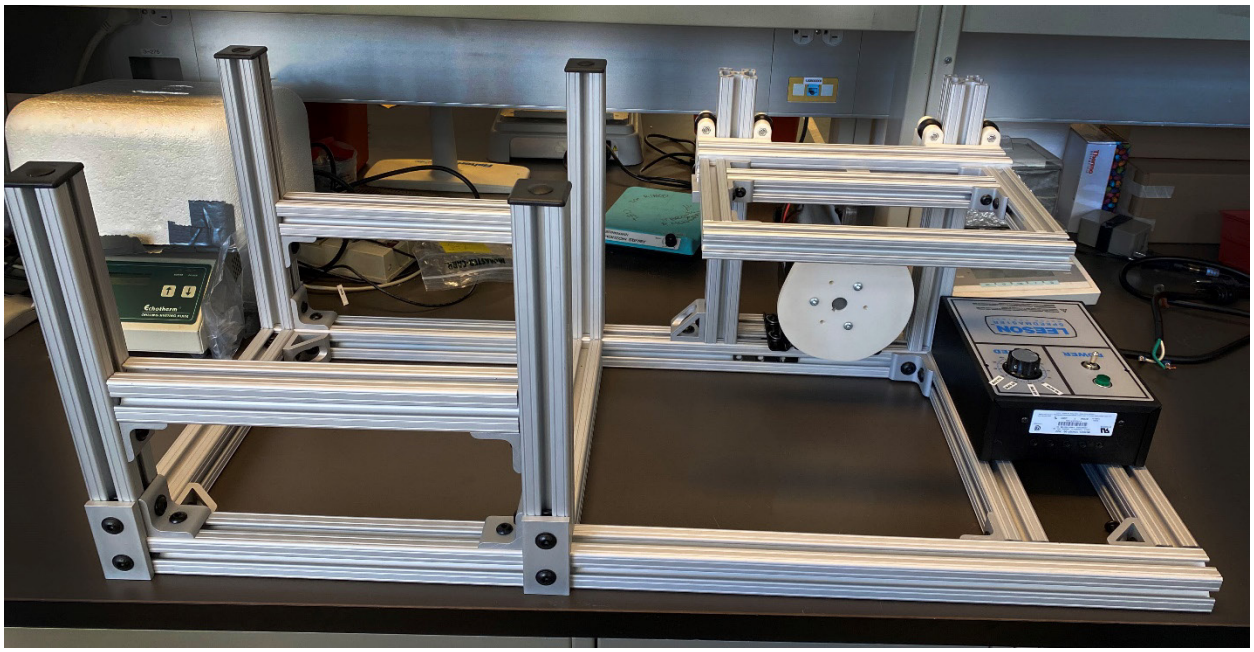

Figure 3-35 Assembled cam mechanism, showing the aluminum profile structure assembled, the moving table attached to the sliders, the motor velocity controller and one of the cam plates attached to the motor.

3.4 Testing

This section shows the methodologies developed for adequately using the dynamic coronary artery phantom test system, from setup to FFR and dPR readings.

3.4.1 Hemodynamic System (Testing)

Once the hemodynamic circuit discussed in section 3.2 was assembled, the FFR and dPR readings were performed. The tests required training on the equipment used to diagnose coronary diseases. The equipment used for these readings is developed and manufactured by the company OpSens. The protocol used for the readings was the following:

1. **Baseline assembly:**

The pump must first be positioned on a flat, levelled surface. The dicrotic notch section (Check valve, extra-soft rubber tubing) is connected to the pump's "Outlet." At the end of the right ultra-soft tubing, the access to the contrast agent will be connected and, after, the first section of the 1/8 in. variable tube (2 meters). Then the measurement section is connected where access to the transducer and the pressure guidewire will be allowed. The other end is connected to the visualization box. On the pump's "inlet," a 1/4 in. tubing section is connected. At the end of this section is an adapter for a 1/8 in. tubing.

Free space is left between the visualization box and this tube section, where the second variable 1/8" tube section will be connected. The length of this section depends on the severity of

the stenosis to be evaluated. Finally, the transducer is attached to the hemostatic valve to complete the baseline assembly of the hemodynamic circuit.

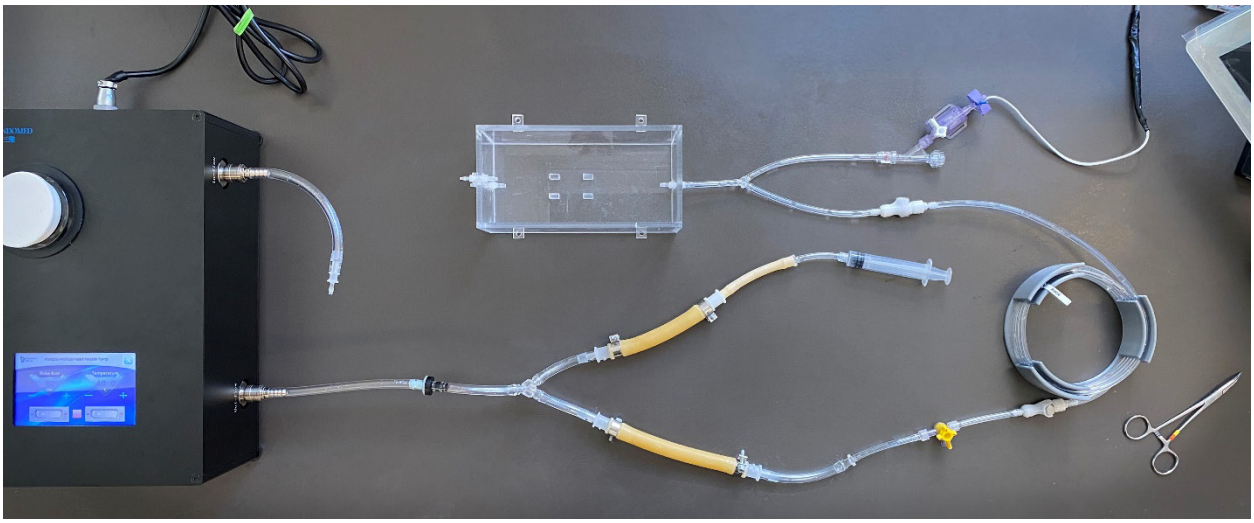

Figure 3-36 Hemodynamic circuit's baseline connection.

2. Stenotic coronary artery phantom selection:

The corresponding phantom is connected inside the visualization box depending on the selected severity. Likewise, the corresponding 1/8 tubing section is connected to the outlet of the display box and the end of the circuit.

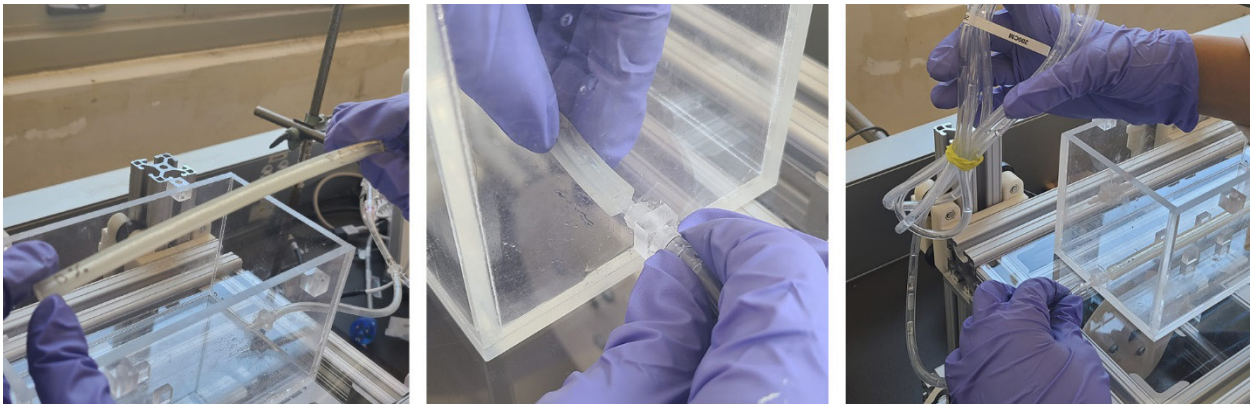

Figure 3-37 (a) Stenotic coronary artery phantom severity selection. (b) Phantom connection inside the visualization box. (c) Variable 1/8 tubing connection with the length corresponding to the selected phantom.

3. Closed hemodynamic circuit:

At this point, the circuit should be closed. First, a syringe must be attached to the endpoint of the Left Super-soft tubing. The syringe functions as an end cap and is used to remove air in the tubing. Also, to help prevent leaking, a pair of pliers are clamped to the super-soft tubing. The 3-way adapter in the circuit used to inject the contrast agent should also be closed. Finally, on the Hemostasis Valve, the transducer should be securely attached and with its valve closed. Furthermore, the Stopcock should also be closed.

(a) (b) (c)

Figure 3-38 Possible leak points: (a) left super soft tubing, closed by a pair of pliers clamped to the tubing, (b) contrast agent three-way adapter, (c) transducer three-way adapter and stopcock.

4. Pulsatile pump preparation:

A solution composed of 40% glycerol and 60% water is poured into the pump's tank, mimicking the density and viscosity of human blood. Then, the pump is connected to the power outlet (110V), and finally, it is turned on with the only physical button on it located next to the power inlet.

Figure 3-39 (a) Filling the pump's chamber with a mixture of 40% glycerine and 60% Water to represent blood viscosity. (b) Connect the power cable to the power outlet (110v). (c) Connect the cable to the pump's power inlet and screw the connector to secure it.

5. Pump activation and air removal:

The first time the pump is activated after being turned on, it will conduct the liquid flush that will try to remove the bubbles from the system for the time selected in the "air-out" parameter. Once the "air-out" time is over, the remaining air inside the circuit is manually extracted.

First, the syringe at the end of the Left Super-soft tubing can be removed to liberate the trapped air. Once the air has been removed, the syringe is attached back, and the scissor clamps are also attached on the Left Super-soft tubing to generate the dicrotic notch. Also, the Stopcock can be opened on the hemostasis valve for just enough time to expel all the air in this section.

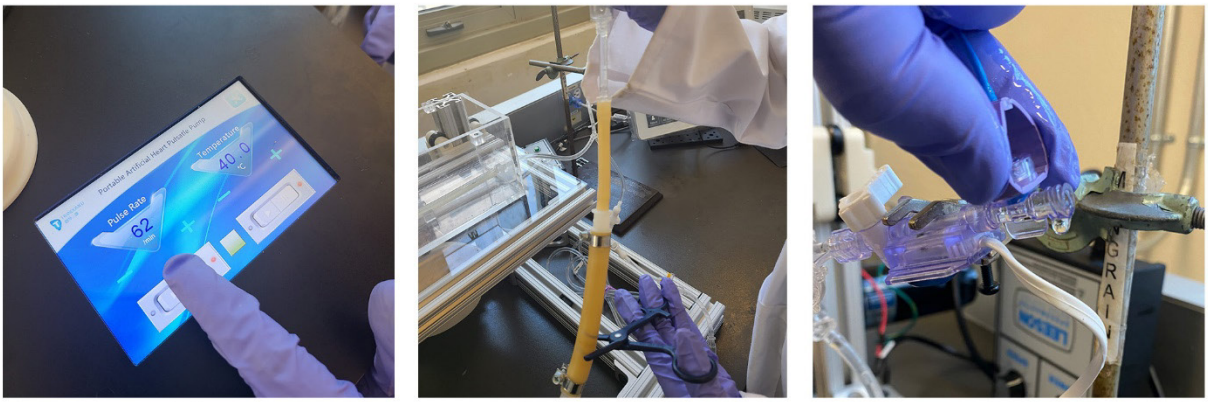

Figure 3-40 (a) Activation of the pump's pulsations. (b) Carefully removing the pliers to allow the liquid to expel the air occupying its space. (c) Purging the transducer allows a fluid column between the sensor and liquid flow in the hemodynamic circuit.

6. Measuring equipment setup:

The first step to start the measurement equipment setup is to turn on the OptoMonitor. The OptoMonitor will turn on when connected to the power outlet (110V). After a few seconds, the system is initialized. The transducer connected to the Optomonitor automatically performs a zero process and begins to display its reading on the screen.

The pressure sensor must be positioned at the phantom's height. Once the pressure sensor is positioned, it is connected to the Optomonitor. The system automatically performs a zero on the pressure sensor at that level.

Subsequently, with the pump inactive, the Stopcock on the hemostasis valve is opened, and the pressure sensor is inserted into the desired position. After several readings, the optimal position was obtained and marked on the phantoms (Figure 3-41).

Once the pressure sensor is positioned, the Stopcock should be closed, and the pump can be activated to start the measurements.

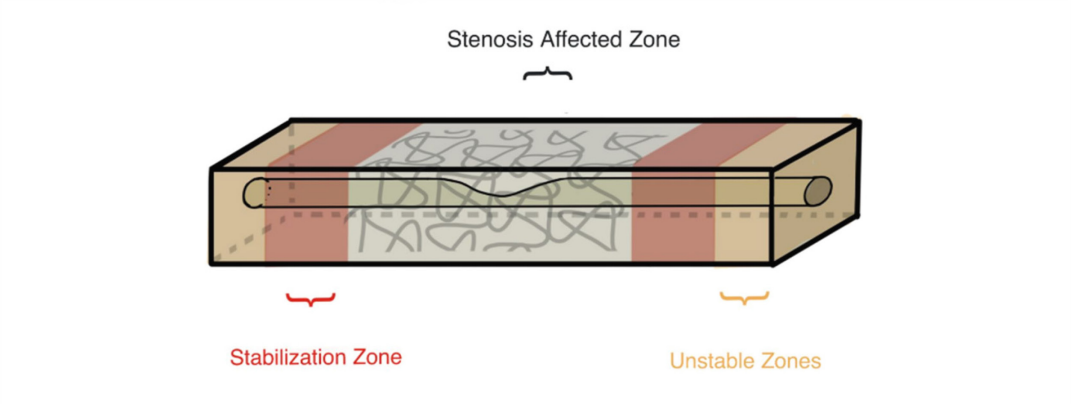

Figure 3-41 Schematic indicating in red the stable pressure zones where it is recommended to perform the equalization of the measurement system and the FFR and dPR readings.

3.4.2 Hemodynamic System with Vertical & Horizontal Movement (Testing)

With the system assembled for vertical or horizontal movement, as shown in section 3.3.3, the following should be considered for accurate FFR and dPR readings:

1. The pulsatile pump is positioned on the acrylic pump's base. The base's height is variable, and it is recommended that it be positioned so that the pump's "inlet" is located below or at the same level as the base of the phantom in its lowest position.

2. The visualization box is positioned on the moving acrylic base of the system. It is recommended to secure it with the hook and loop cable tie.

3. Finally, the hemodynamic circuit is connected. The connection follows the same steps followed in section 3.4.1.

Start movement

Once the hemodynamic circuit is connected and mounted on the cam system, it is ready to start moving. First, the AC to DC motor speed controller is connected to the power outlet (110V). Then, the position of the variable knob at its lowest speed is confirmed, and the power switch can be turned on, energizing the motor. Finally, the variable knob is turned clockwise until achieving the desired speed.

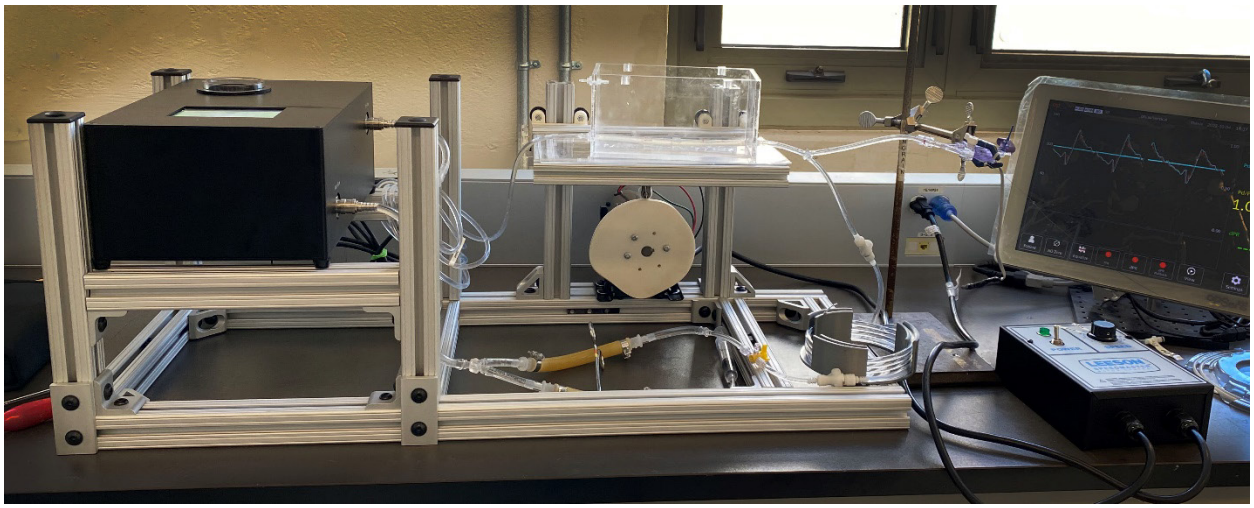

Figure 3-42 Assembled dynamic coronary artery phantom test system. Cam mechanism with the hemodynamic circuit.

Chapter 4: Results

4.1 FFR & dPR Readings

Distal (Pd) and proximal (Pa) pressure were measured using the pressure guidewire (OpSens). The data displayed on the OptoMonitor (OpSens), represents the ratio between the pressures to produce the FFR and dPR measurements. The results are then compared to the expected results based on previous literature. Stenotic coronary artery phantoms with four different levels of severities: 0%, 40%, 60%, and 80%, were tested on the hemodynamic circuit. Then, the same readings were done, adding three types of movement: generated by heartbeats, by breathing, and by a combination of heartbeats and breathing.

4.1.1 Expected Results

Relation between FFR measurement and % stenosis

Two main methods are used when measuring stenosis severity: the percentage of cross-sectional area reduction and the percentage of diameter reduction. The phantoms used in this experiment were modelled using the percentage of area reduction. To validate the results, the expected FFR values must be calculated for proper comparison.

Joo Myung Lee's research was composed of a sample size of one hundred and fifteen patients suffering from left anterior descending artery stenosis, all of which had a single lesion [39]. Figure 4-1 demonstrates the relationship between percent diameter stenosis and their FFR value.

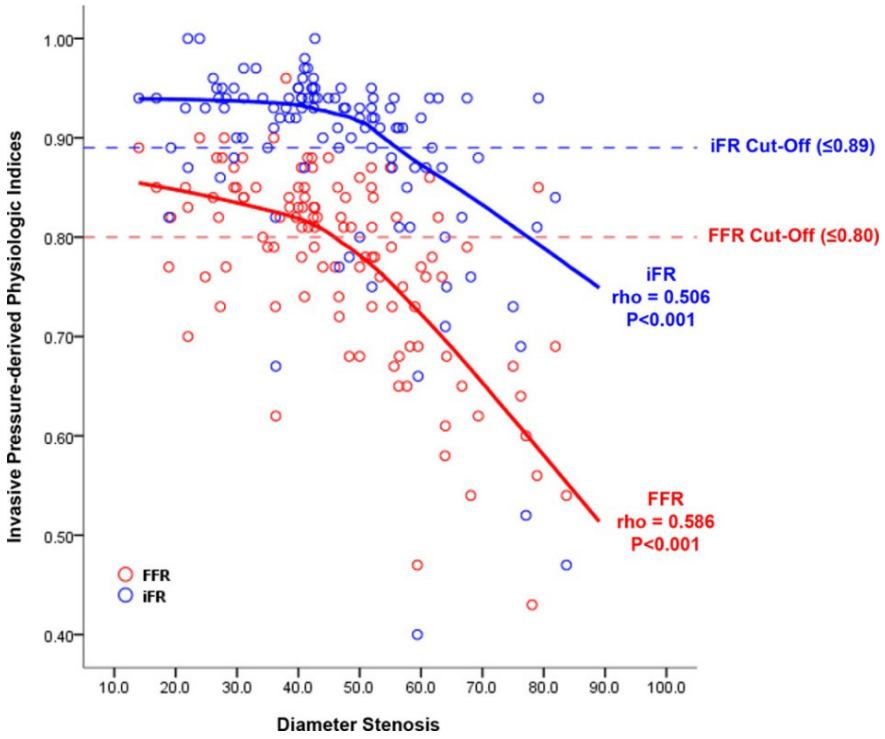

Figure 4-1 Comparison Between % Diameter Stenoses and FFR Values

Correlation between % diameter reduction and % cross-sectional area reduction

The specification of whether the percent stenosis is measured by reduction in diameter or cross-sectional area is needed as they differ from one another. To enable an appropriate comparison, a relationship between percent diameter reduction and percent area reduction must be established.

The percentage of diameter stenosis is determined by using the following formula [40],

$$\%\ stenosis = \left(1 - \frac{L}{R}\right) * 100 \qquad 4\text{-}1$$

Where L is the area or diameter of the lesion and R is the area or diameter of the non-affected reference site.

A study by Hideki Ota et al., determined a correlation between the two types of percent reductions using ultrasonography [40]. The results are shown in Figure 4-2 below.

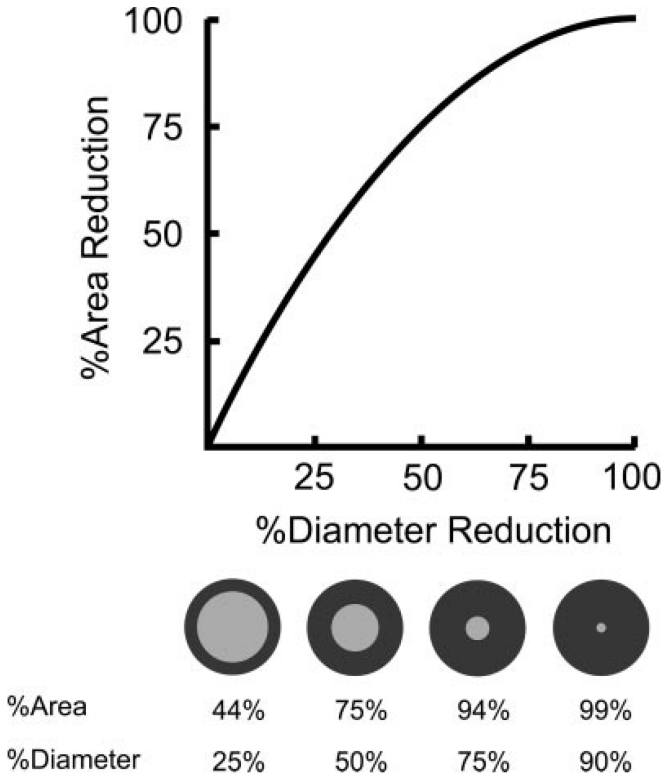

Figure 4-2 Graph (top) illustrates the relationship between area reduction and diameter reduction in a completely concentric stenosis. Drawings at bottom illustrate cross-sectional views of lumina at various percentages of area and diameter stenosis. Reproduced with the permission of The Radiological Society of North America (RSNA®).

From this, the following relation was derived between the percent reductions,

$$A = D * \left(2 - \left[\frac{D}{100}\right]\right) \qquad 4\text{-}2$$

Where A is the percentage of area reduction, and D is the percentage of diameter reduction.

Converting the severity of stenoses from our samples from percent area stenosis to percent diameter stenosis is shown in Table 4-1.

% Area Stenosis	% Diameter Stenosis
0%	0%
40%	23%
60%	37%
80%	55%

Table 4-1 Conversion from Area Stenosis to Diameter Stenosis

Expected FFR

Using the conversion from percent area to percent diameter stenosis done in Table 4-1 in combination with the relation between percent diameter stenosis and FFR value done in Figure 4-1, the expected results, based on previous literature, were obtained. These expected FFR measurements are shown in Table 4-2 below.

% Area Stenosis	% Diameter Stenosis	Expected FFR
0%	0%	1
40%	23%	0.85
60%	37%	0.83
80%	55%	0.78

Table 4-2 Expected FFR Measurement in Relation to the Stenosis Severity.

4.1.2 Hemodynamic Circuit (Measurements)

This section presents the results obtained from the FFR and dPR readings of the hemodynamic circuit subjected to no motion. The summarized results are shown in Table 4-3. Figure 4-3 and Figure 4-4 show the screenshots obtained from the Optomonitor of the FFR and dPR measurements, respectively.

% Area Stenosis	Variable Tubing Length	Expected Result	FFR	% Error	dPR	%Error
0%	330 cm	1	0.97	03%	0.98	02%
40%	15 cm	0.85	0.84	01%	0.85	00%
60%	60 cm	0.83	0.83	00%	0.83	00%
80%	250 cm	0.78	0.78	00%	0.78	00%

Table 4-3 FFR and dPR Result Readings on the Hemodynamic Circuit with No-Motion.

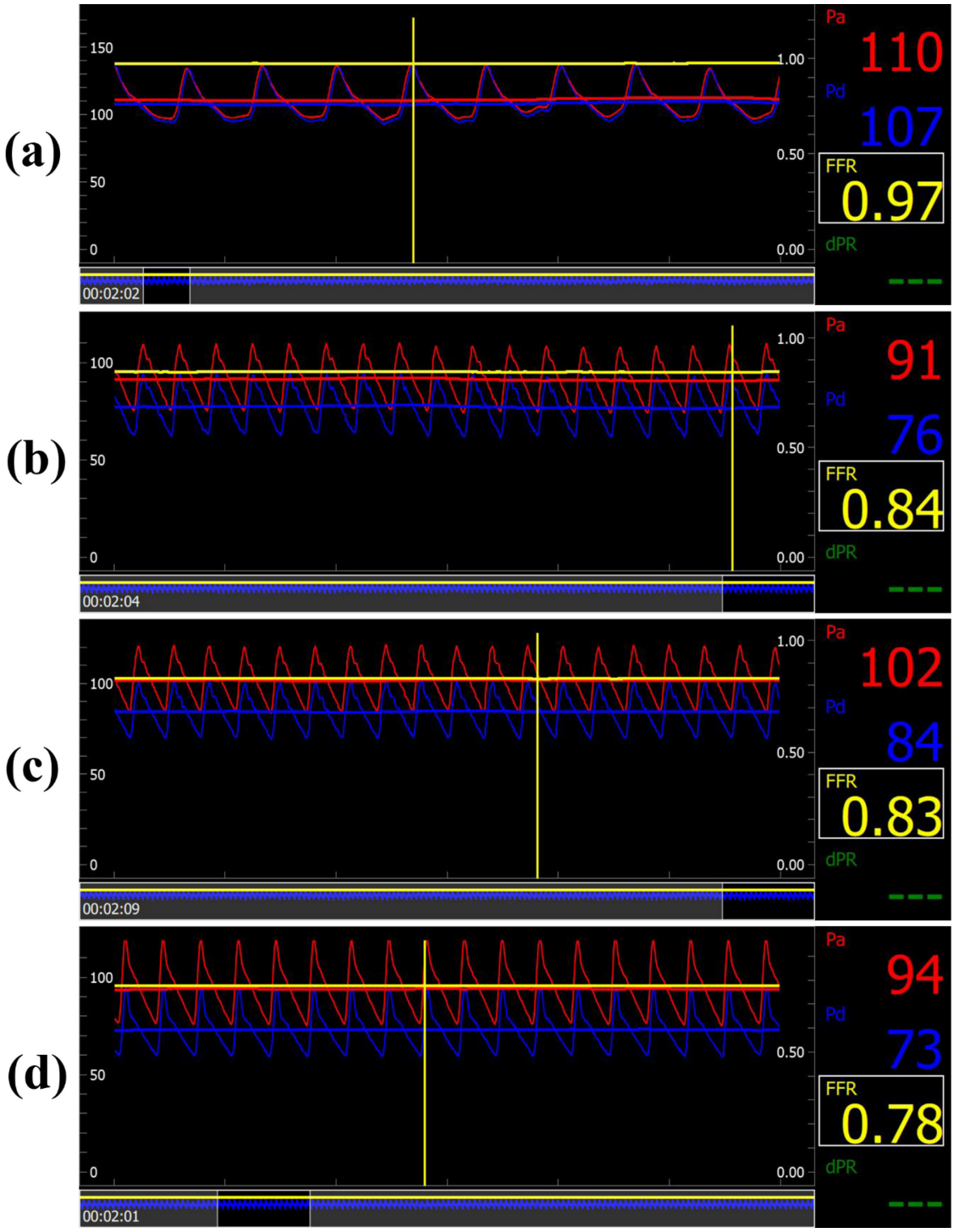

Figure 4-3 Screenshots of the FFR readings performed with the Optomonitor in the non-motion hemodynamic circuit using the phantoms of the stenotic coronary artery with different severities: (a) 0%, (b) 40%, (c) 60% and (d) 80%. The figures show the anatomically representative pressure curves obtained.

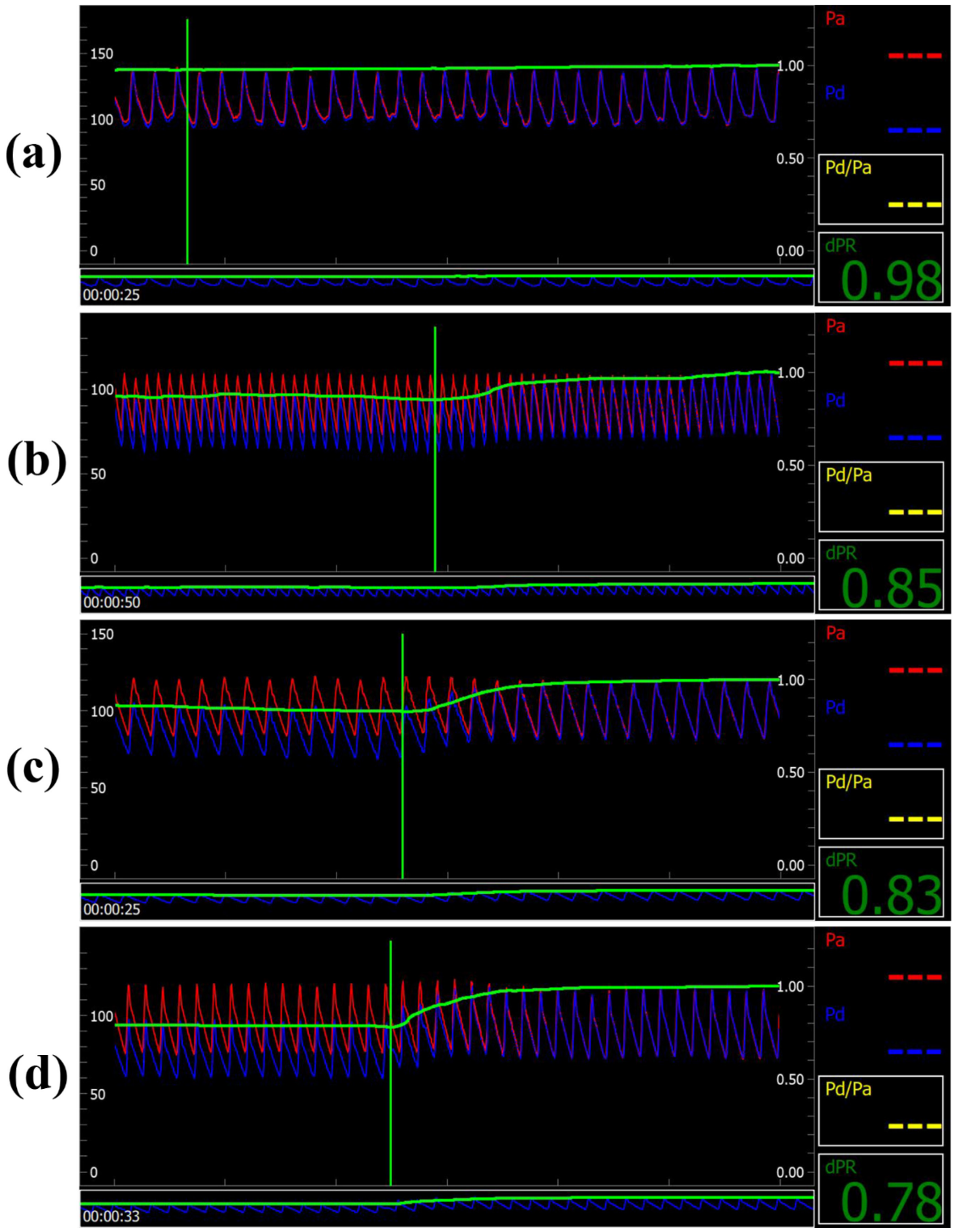

Figure 4-4 Screenshots of the dPR readings performed with the Optomonitor in the non-motion hemodynamic circuit using the phantoms of the stenotic coronary artery with different severities: (a) 0%, (b) 40%, (c) 60% and (d) 80%.

4.1.3 Hemodynamic Circuit with Vertical Heartbeat Movement

This section presents the results obtained from the FFR and dPR readings of the hemodynamic circuit subjected to vertical movement mimicking the displacement found in the LAD due to heartbeats and during breath-holding. The summarized results are shown in Table 4-4. Figure 4-5 and Figure 4-6 show the screenshots obtained from the Optomonitor of the FFR and dPR measurements, respectively.

% Area Stenosis	Variable Tubing Length	Expected Result	FFR	% Error	dPR	%Error
0%	330 cm	1	0.98	02%	0.98	02%
40%	15 cm	0.85	0.85	00%	0.83	02%
60%	60 cm	0.83	0.82	01%	0.83	00%
80%	250 cm	0.78	0.78	00%	0.78	00%

Table 4-4 FFR and dPR Result Readings on the Hemodynamic Circuit Subjected to the Movement Caused in the LAP by the Heartbeat.

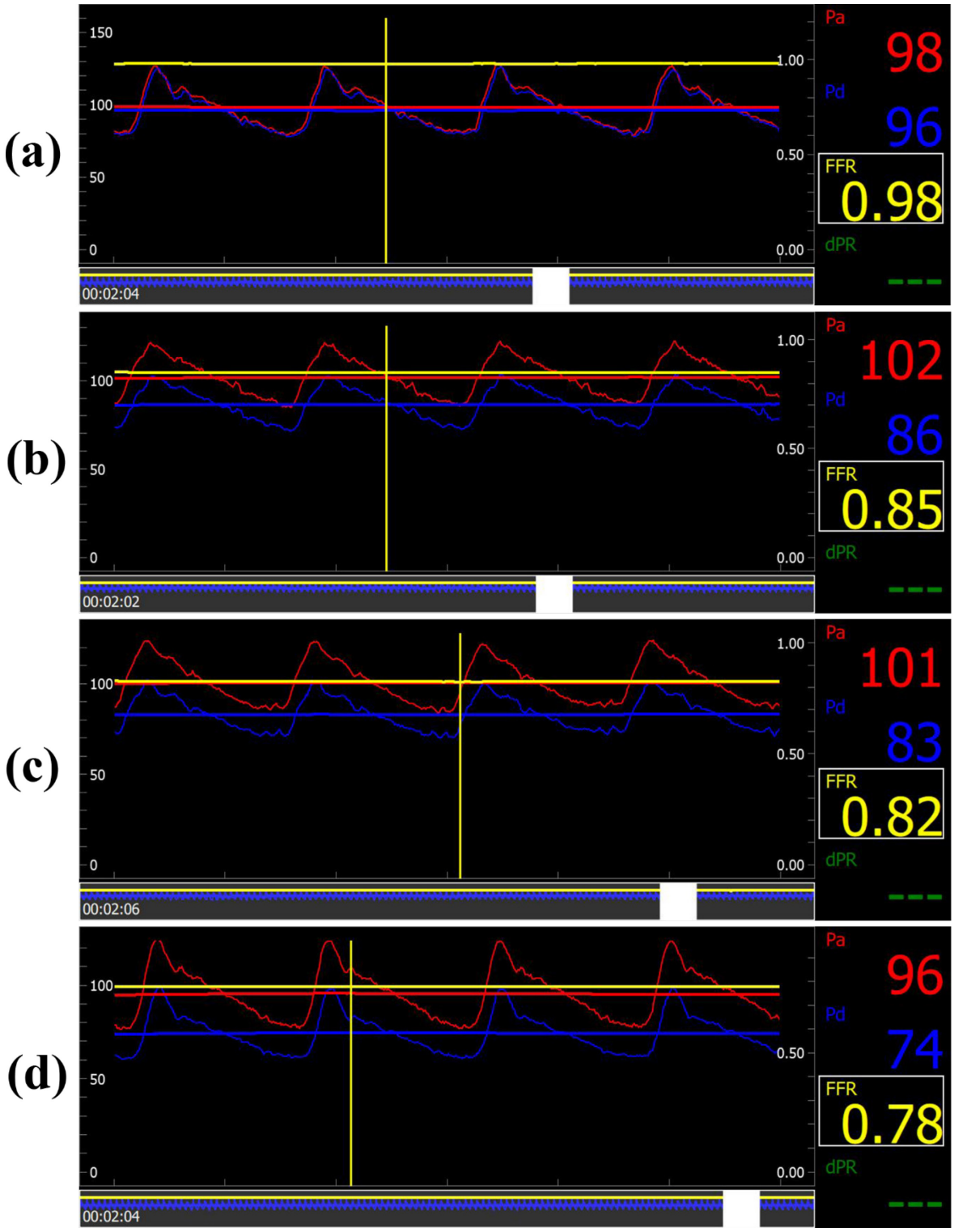

Figure 4-5 Screenshots of the FFR readings performed with the Optomonitor in the hemodynamic circuit subjected to the movement caused in the LAP by the heartbeat and using the phantoms of the stenotic coronary artery with different severities: (a) 0%, (b) 40%, (c) 60% and (d) 80%. The figures show the anatomically representative pressure curves obtained.

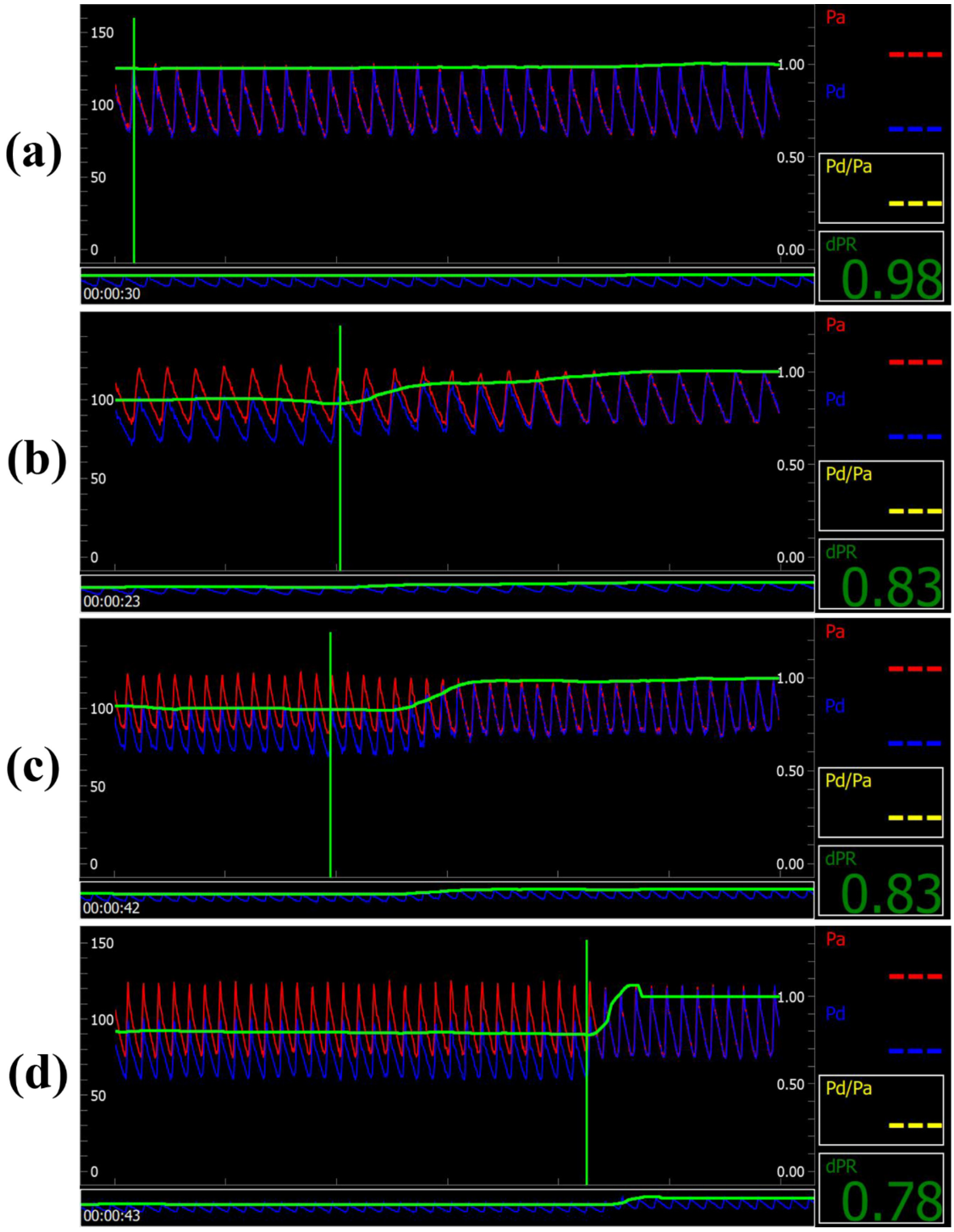

Figure 4-6 Screenshots of the dPR readings performed with the Optomonitor in the hemodynamic circuit subjected to the movement caused in the LAP by the heartbeat and using the phantoms of the stenotic coronary artery with different severities: (a) 0%, (b) 40%, (c) 60% and (d) 80%.

4.1.4 Hemodynamic Circuit with Vertical Respiration Movement

This section presents the results obtained from the FFR and dPR readings of the hemodynamic circuit subjected to vertical movement mimicking the displacement found in the coronary artery due to breathing. The summarized results are shown in Table 4-5. Figure 4-7 and Figure 4-8 show the screenshots obtained from the Optomonitor of the FFR and dPR measurements, respectively.

% Area Stenosis	Variable Tubing Length	Expected Result	FFR	% Error	dPR	%Error
0%	330 cm	1	0.97	03%	0.98	02%
40%	15 cm	0.85	0.85	00%	0.85	00%
60%	60 cm	0.83	0.83	00%	0.83	00%
80%	250 cm	0.78	0.78	00%	0.77	01%

Table 4-5 FFR and dPR Result Readings on the Hemodynamic Circuit Subjected to the Movement Caused in Coronary Artery by Breathing.

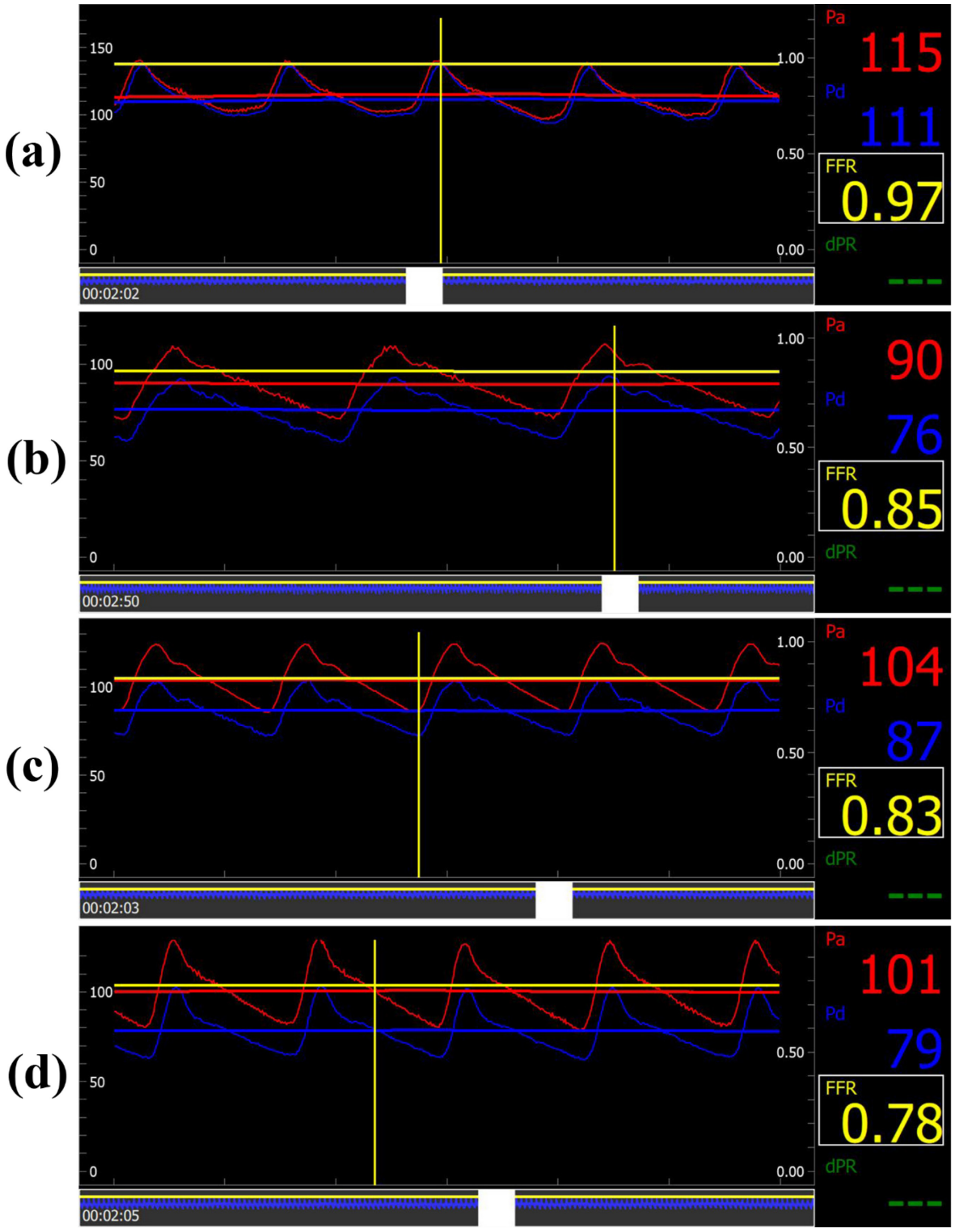

Figure 4-7 Screenshots of the FFR readings performed with the Optomonitor in the hemodynamic circuit subjected to the movement caused in the coronary artery by breathing and using the phantoms of the stenotic coronary artery with different severities: (a) 0%, (b) 40%, (c) 60% and (d) 80%. The figures show the anatomically representative pressure curves obtained.

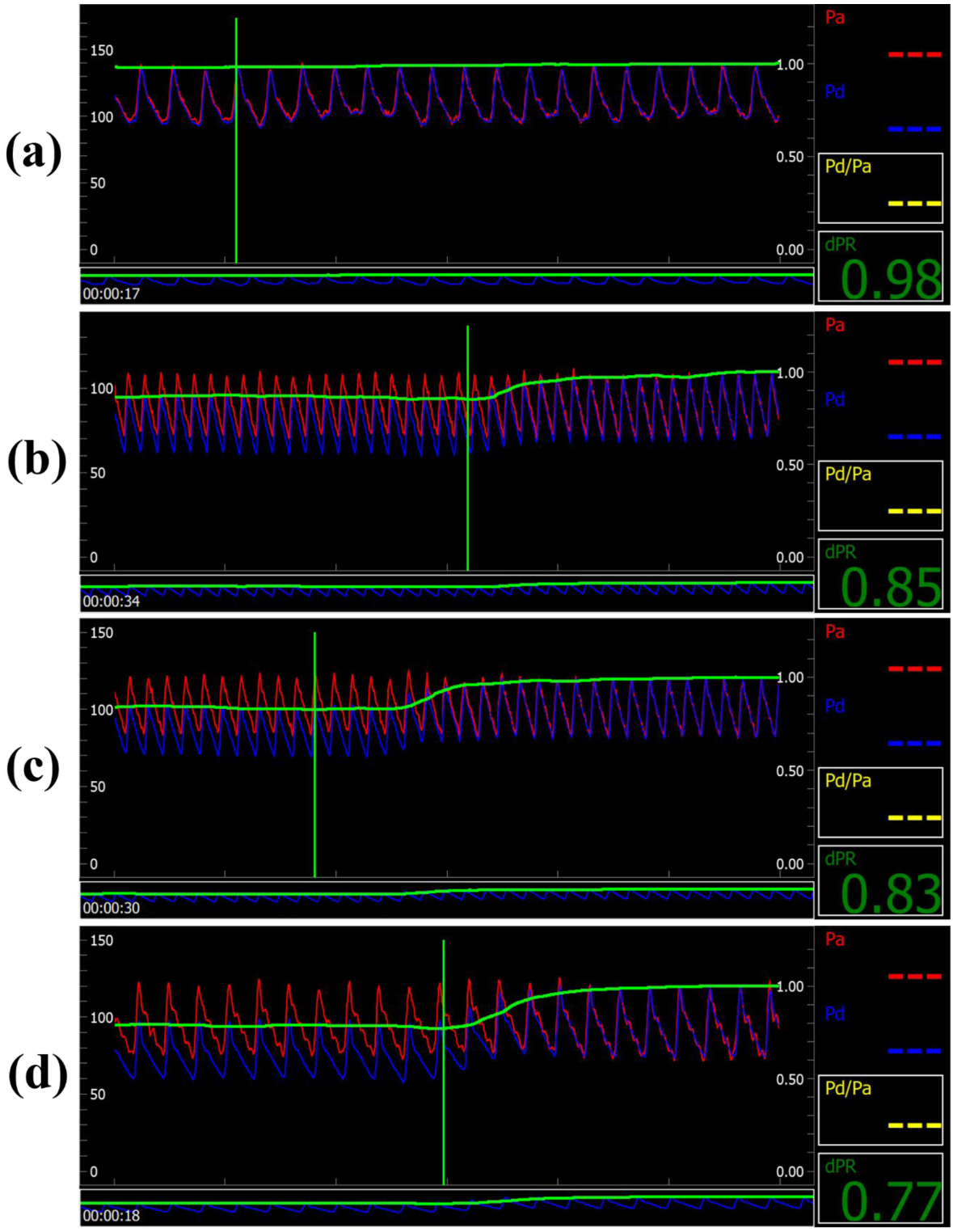

Figure 4-8 Screenshots of the dPR readings performed with the Optomonitor in the hemodynamic circuit subjected to the movement caused in the coronary artery by breathing and using the phantoms of the stenotic coronary artery with different severities: (a) 0%, (b) 40%, (c) 60% and (d) 80%.

4.1.5 Hemodynamic Circuit with Vertical Mix Movement

This section presents the results obtained from the FFR and dPR readings of the hemodynamic circuit subjected to vertical movement mimicking the displacement found in the coronary artery due to breathing and heart beating. The summarized results are shown in Table 4-6. Figure 4-9 and Figure 4-10 show the screenshots obtained from the Optomonitor of the FFR and dPR measurements, respectively.

% Area Stenosis	Variable Tubing Length	Expected Result	FFR	% Error	dPR	%Error
0%	330 cm	1	0.99	01%	0.97	03%
40%	15 cm	0.85	0.85	00%	0.83	02%
60%	60 cm	0.83	0.82	01%	0.82	01%
80%	250 cm	0.78	0.78	00%	0.78	02%

Table 4-6 FFR and dPR Result Readings on the Hemodynamic Circuit Subjected to the Movement Caused in Coronary Artery by Breathing and Heart Beating.

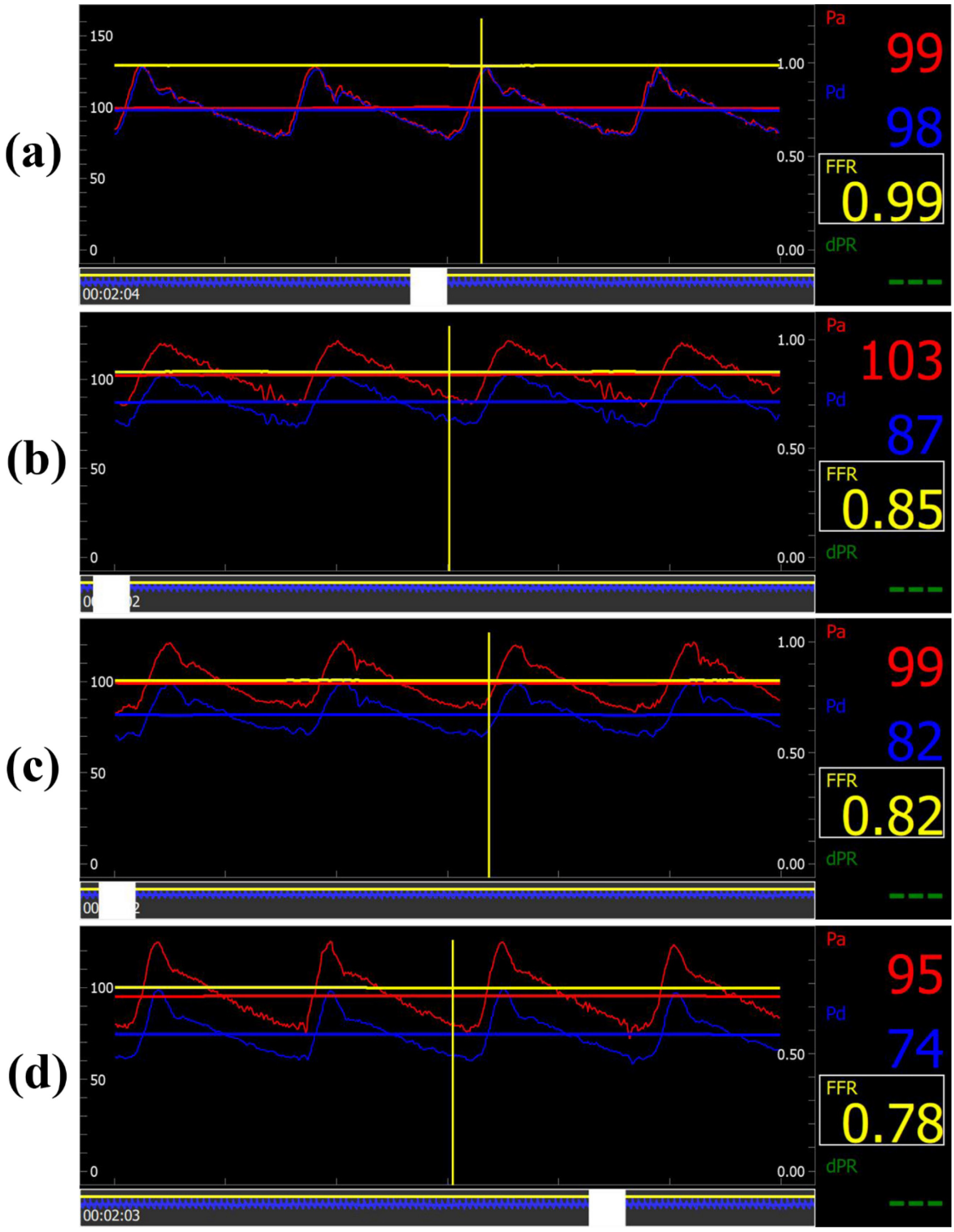

Figure 4-9 Screenshots of the FFR readings performed with the Optomonitor in the hemodynamic circuit subjected to the movement caused in the coronary artery by breathing and heart beating. Using the phantoms of the stenotic coronary artery with different severities: (a) 0%, (b) 40%, (c) 60% and (d) 80%. The figures show the anatomically representative pressure curves obtained.

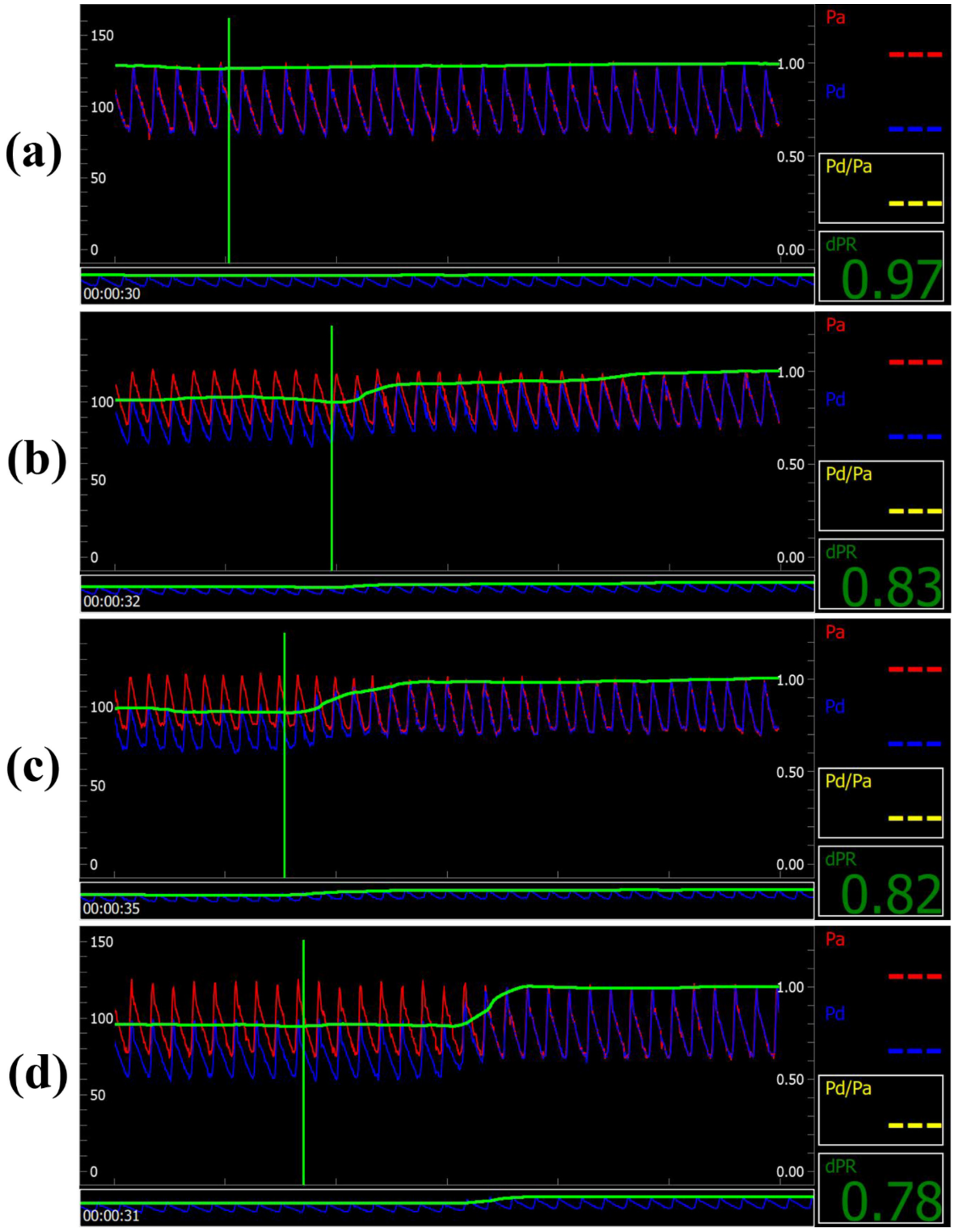

Figure 4-10 Screenshots of the dPR readings performed with the Optomonitor in the hemodynamic circuit subjected to the movement caused in the coronary artery by breathing and heart beating. Using the phantoms of the stenotic coronary artery with different severities: (a) 0%, (b) 40%, (c) 60% and (d) 80%.

Chapter 5: Discussion

Phantom Material

PVA-C is a material that meets the mechanical properties found in blood vessel tissue. However, two main aspects were found that complicate the use of this material. Firstly, although the PVA material is considered not expensive, its cryogenic treatment requires expensive freezing equipment capable of reproducing the temperature-time curves of the freezing and thawing cycles for curing PVA-C. As this equipment was unavailable, curing was carried out in a commercial refrigerator and freezer. The lack of control over the cycles and the differences in the temperature marked in the literature [20] resulted in phantoms with a homogeneous but extremely porous cure.

Adapters were designed and 3D-printed so the phantom could communicate with the rest of the system. The adapters were designed with channels through which the liquid PVA could enter and anchor once cured. However, the properties of PVA-C, and the problem mentioned with curing in a conventional refrigerator, prevented an airtight union. Shortly after several uses, the phantoms tended to leak at the adapter's junction.

During the unmolding process of the phantoms, another problem arose: bubbles formation. Bubbles were formed during the injection of the PVA into the mould. These bubbles affected the mechanical properties of the phantom and would quickly collapse. To solve this issue, a syringe's needle was used to slowly stir the solution around the inner side of the mould to push the bubbles to the surface and eliminate as many as possible before commencing the freezing cycle.

Another inconvenient with the PVA-C phantoms was the lack of long-term stability due to the mechanical properties varying in time caused by decomposition and drying out of the material. Because of this, the phantom's shelf-life is expected from a few days up to four months, depending on usage and how they are preserved [21]. During this research, the phantoms were preserved in water at ambient temperature until testing to prevent dehydration, evaporation, or disfiguration [25].

The complex manufacturing and maintenance process, especially in small-sized phantoms such as those of coronary arteries, led to the search for other technologies such as 3D printing.

It was found that there are no 3D-printed materials that perfectly meet the mechanical properties of blood vessels. However, the possibility of printing two or more materials simultaneously in a single part allows us to develop printing strategies to customize the mechanical properties of a composite material, as shown in ZhiLin Yang's research.

The complexity in developing phantom composites remains in designing the desired structure to meet the desired mechanical properties. However, once the design is ready, the phantom can be printed as often as necessary.

After carrying out test measurements, it was found that the results of the FFR and dPR readings in phantoms made of PVA-C material and composite phantoms did not differ significantly, so for this research, it was decided to continue only with composite phantoms.

Hemodynamic Circuit

During the construction of the hemodynamic circuit, it was found that slight alterations completely changed the pressure curve and the FFR and dPR readings.

An artificial aortic valve was used to generate the dicrotic notch. However, it did not work as expected. It is believed that it is because the pressure at the outlet was not high enough to close the valve. Changes in the position of the valve and pipe diameters did not solve the problem, so a nylon plastic, high-cycling check valve was chosen.

For noise control in the circuit, a capacitance chamber was used. However, after experimenting with it, it was found that it was not controllable nor repeatable due to the highly variable amount of liquid it can store. Another adverse effect of the dome was over-attenuating the curve, eliminating the dicrotic notch. It was decided not to use the chamber, and the noise was reduced by adding super-soft rubber tubing to the circuit.

The combination of the check valve and super-soft rubber tubing allowed for obtaining a notch in the curve with an appearance similar to that found in arterial pressure curves. The appearance and position of the notch can be altered by manipulating the position of the pliers, i.e. changing the length of the left super soft rubber tubing.

After experimenting with different components as previously described, it was found that the components before the phantom significantly impacted the pressure curve but not the FFR and dPR readings. The variable that has the most significant impact on the FFR and dPR readings is the length of the 1/8 tubing at the outlet of the visualization box, that is, the outlet resistance of the hemodynamic circuit.

Medical Expert Assessement

With the final selection of components of the hemodynamic circuit and achieved the desired results in the tests performed. A qualified physician tested the circuit.

According to the feedback provided by the physician, the results were satisfactory. The DPR Pullback readings were very similar to reality. The lesions were idealized but representative of human physiology. Thanks to the pump used, it was possible to have better control over the bubbles in the circuit, one of the most common problems in this type of simulation according to the physician. Finally, due to the materials used and the design of the circuit, it is possible to obtain X-ray images of excellent quality (Appendix C).

System Movement

The results from the tests carried out in the static hemodynamic circuit against the ones with the system in vertical movement show that movement affects the pressure curve. The magnitude of the effect is related to the generated movement's intensity, that is, the acceleration of the movement. However, the movement did not cause any significant effect on the measurement of FFR and dPR.

The mechanism turned out to be very versatile. It can be adapted to generate vertical or horizontal movement. The development of different cam plates, as shown in this investigation, is a relatively simple process that will allow the generation of different motion profiles.

One drawback the system showed is that the motor generates vibrations that alter the pressure curve. Also, after making experiments with the mitral valve displacement curve cam plate, the readings showed noise generated on the curves when the movement was activated, since this movement profile shows a rapid fall that can be translated into a high acceleration. Due to this drop or high acceleration, it is considered that the movement obtained when tracking the mitral valve may be too high compared to that seen in the coronary artery. Therefore, a new cam plate

was generated considering the displacement at the LAD reducing noise considerably. Vibrations were also reduced by using soft gaskets between the motor joints and the rest of the frame.

During the experiments, it was observed that some noise in the pressure curve was due to vibrations acting on the system's tubing. Therefore, separating the tube from the ground could help to undermine vibrations and noise in the curve.

Added Value

Although this testing bed was developed with the objective of testing and fine-tuning medical measurement equipment, it is considered that it can also be very helpful for educational purposes and medical training. The attributes of this testing station can generate more realistic scenarios that nurture the experience of a future physician.

Chapter 6: Summary and Conclusions

This research presented the development of an anatomical and biomechanically correct test station capable of replicating different motion profiles triggered by respiration and heartbeat on a stenotic coronary artery phantom with different severities, capable of perfusion under controlled and repeatable conditions.

A 3D printed composite phantom was developed, composed of TangoPlus and VeroWhite material, with a configuration that allows obtaining mechanical properties similar to those found in the tissue of arteries.

A hemodynamic circuit was built to simulate an anatomically correct blood pressure curve, on which angiograms and FFR and dPR readings can be performed with a pressure guidewire.

Finally, the testing bed was complemented by adding motion to the stenotic coronary artery phantom. The movement is achieved with a cam mechanism which works with cam plates that can be interchanged to achieve different movement profiles (heartbeat, respiration and combined).

This dynamic coronary artery phantom test system emulating cardiac and respiratory motion has shown potential for use in testing and tuning new medical equipment and in medical education and training.

6.1 Future Work

- Tracking the movement of different points along the coronary artery during a heartbeat to develop different cam plates simulating different movements.

- Achieve communication between the pulsatile pump and the motor, optimizing the synchrony between the beats generated by the pump and the heartbeats movement.

- Optimize coronary artery movement by adding a perfused ventricle phantom whose expansion moves the stenotic coronary artery phantom attached to it in a radial way.

Bibliography

[1] M. A. Khan, M. J. Hashim, H. Mustafa, M. Y. Baniyas, S. K. B. M. Al Suwaidi, R. AlKatheeri, F. M. K. Alblooshi, M. E. A. H. Almatrooshi, M. E. H. Alzaabi, R. S. Al Darmaki, and S. N. A. H. Lootah, "Global Epidemiology of Ischemic Heart Disease: Results from the Global Burden of Disease Study," *Cureus*, Jul. 2020, doi: 10.7759/cureus.9349.

[2] "Global health estimates: Leading causes of death." https://www.who.int/data/maternal-newborn-child-adolescent-ageing/advisory-groups/gama/gama-related-resources/gho (accessed Mar. 03, 2022).

[3] J.-E. Kim and B.-K. Koo, "Fractional Flow Reserve: The Past, Present and Future," *Korean Circulation Journal*, vol. 42, no. 7, p. 441, 2012, doi: 10.4070/kcj.2012.42.7.441.

[4] D. E. Mohrman and L. J. Heller, *Cardiovascular Physiology*, 9th edition. New York: McGraw-Hill, Education/Medical, 2018.

[5] A. Saxton, R. Chaudhry, and B. Manna, "Anatomy, Thorax, Heart Right Coronary Arteries," in *StatPearls*, Treasure Island (FL): StatPearls Publishing, 2022. Accessed: Oct. 17, 2022. [Online]. Available: http://www.ncbi.nlm.nih.gov/books/NBK537357/

[6] J. P. Kannam, J. M. Aroesty, and B. J. Gersh, "Chronic coronary syndrome: Overview of care," p. 14, Sep. 2022.

[7] J. G. Betts, P. Desaix, E. Johnson, J. E. Johnson, O. Korol, D. Kruse, B. Poe, J. A. Wise, M. Womble, and K. A. Young, *Anatomy & Physiology*. openstax, 2013.

[8] N. H. J. Pijls, B. de Bruyne, K. Peels, P. H. van der Voort, H. J. R. M. Bonnier, J. Bartunek, and J. J. Koolen, "Measurement of Fractional Flow Reserve to Assess the Functional Severity of Coronary-Artery Stenoses," *N Engl J Med*, vol. 334, no. 26, pp. 1703–1708, Jun. 1996, doi: 10.1056/NEJM199606273342604.

[9] K. L. Gould, K. Lipscomb, and G. W. Hamilton, "Physiologic basis for assessing critical coronary stenosis," *The American Journal of Cardiology*, vol. 33, no. 1, pp. 87–94, Jan. 1974, doi: 10.1016/0002-9149(74)90743-7.

[10] K. L. Gould and K. Lipscomb, "Effects of coronary stenoses on coronary flow reserve and resistance," *The American Journal of Cardiology*, vol. 34, no. 1, pp. 48–55, Jul. 1974, doi: 10.1016/0002-9149(74)90092-7.

[11] N. H. Pijls, J. A. van Son, R. L. Kirkeeide, B. De Bruyne, and K. L. Gould, "Experimental basis of determining maximum coronary, myocardial, and collateral blood flow by pressure measurements for assessing functional stenosis severity before and after percutaneous transluminal coronary angioplasty.," *Circulation*, vol. 87, no. 4, pp. 1354–1367, Apr. 1993, doi: 10.1161/01.CIR.87.4.1354.

[12] B. De Bruyne and J. Sarma, "Fractional Flow Reserve: a Review," *Heart*, vol. 94, no. 7, pp. 949–959, Jul. 2008, doi: 10.1136/hrt.2007.122838.

[13] Developed with the special contribution of the European Association for Percutaneous Cardiovascular Interventions (EAPCI), Authors/Task Force Members, W. Wijns, P. Kolh, N. Danchin, C. Di Mario, V. Falk, T. Folliguet, S. Garg, K. Huber, S. James, J. Knuuti, J. Lopez-Sendon, J. Marco, L. Menicanti, M. Ostojic, M. F. Piepoli, C. Pirlet, J. L. Pomar, N. Reifart, F. L. Ribichini, M. J. Schalij, P. Sergeant, P. W. Serruys, S. Silber, M. Sousa Uva, D. Taggart, ESC Committee for Practice Guidelines, A. Vahanian, A. Auricchio, J. Bax, C.

Ceconi, V. Dean, G. Filippatos, C. Funck-Brentano, R. Hobbs, P. Kearney, T. McDonagh, B. A. Popescu, Z. Reiner, U. Sechtem, P. A. Sirnes, M. Tendera, P. E. Vardas, P. Widimsky, EACTS Clinical Guidelines Committee, P. Kolh, O. Alfieri, J. Dunning, S. Elia, P. Kappetein, U. Lockowandt, G. Sarris, P. Vouhe, Document Reviewers, P. Kearney, L. von Segesser, S. Agewall, A. Aladashvili, D. Alexopoulos, M. J. Antunes, E. Atalar, A. Brutel de la Riviere, A. Doganov, J. Eha, J. Fajadet, R. Ferreira, J. Garot, J. Halcox, Y. Hasin, S. Janssens, K. Kervinen, G. Laufer, V. Legrand, S. A. M. Nashef, F.-J. Neumann, K. Niemela, P. Nihoyannopoulos, M. Noc, J. J. Piek, J. Pirk, Y. Rozenman, M. Sabate, R. Starc, M. Thielmann, D. J. Wheatley, S. Windecker, and M. Zembala, "Guidelines on Myocardial Revascularization: The Task Force on Myocardial Revascularization of the European Society of Cardiology (ESC) and the European Association for Cardio-Thoracic Surgery (EACTS)," *European Heart Journal*, vol. 31, no. 20, pp. 2501–2555, Oct. 2010, doi: 10.1093/eurheartj/ehq277.

[14] T. F. Whayne, M. J. Sousa, and A. Abdel-Latif, "Use and Value of Fractional Flow Reserve in Coronary Arteriography," *Angiology*, vol. 71, no. 1, pp. 5–9, Jan. 2020, doi: 10.1177/0003319719848559.

[15] Y. Gong, Y. Feng, T. Yi, F. Yang, Y. Li, L. Zhang, B. Zheng, T. Hong, Z. Liu, Y. Huo, J. Li, and Y. Huo, "Coronary Angiography-Derived Diastolic Pressure Ratio," *Front. Bioeng. Biotechnol.*, vol. 8, p. 596401, Oct. 2020, doi: 10.3389/fbioe.2020.596401.

[16] M. J. Kern and A. H. Seto, "dPR, Another Diastolic Resting Pressure Ratio: Refinements and Nuances With Identical Results," *Circ: Cardiovascular Interventions*, vol. 11, no. 12, p. e007540, Dec. 2018, doi: 10.1161/CIRCINTERVENTIONS.118.007540.

[17] N. P. Johnson, W. Li, X. Chen, B. Hennigan, S. Watkins, C. Berry, W. F. Fearon, and K. G. Oldroyd, "Diastolic pressure ratio: new approach and validation vs. the instantaneous wave-free ratio," *European Heart Journal*, vol. 40, no. 31, pp. 2585–2594, Aug. 2019, doi: 10.1093/eurheartj/ehz230.

[18] "Cam," *Merriam-Webster.com Dictionary, s.v.* Accessed: Sep. 05, 2022. [Online]. Available: https://www.merriam-webster.com/dictionary/cam.

[19] H. A. Rothbart, Ed., *Cam design handbook*. New York: McGraw-Hill, 2004.

[20] V. Pazos, R. Mongrain, and J.-C. Tardif, "Mechanical characterization of atherosclerotic arteries using finite-element modeling: Feasibility study on mock arteries," *IEEE Trans. Biomed. Eng.*, vol. 57, no. 6, pp. 1520–1528, Jun. 2010, doi: 10.1109/TBME.2010.2041001.

[21] Z. He, R. Mongrain, S. Lessard, B. Chayer, G. Cloutier, and G. Soulez, "Anthropomorphic and biomechanical mockup for abdominal aortic aneurysm," *Medical Engineering and Physics*, vol. 77, pp. 60–68, Mar. 2020, doi: 10.1016/j.medengphy.2019.12.005.

[22] R. Galaz, C. Pagiatakis, E. Gaillard, and R. Mongrain, "A parameterized analysis of the mechanical stress for co-ronary plaque fibrous caps," *Journal of Biomedical Science and Engineering*, vol. 06, no. 12, pp. 38–46, 2013, doi: 10.4236/jbise.2013.612a006.

[23] V. Pazos, R. Mongrain, and J. C. Tardif, "Polyvinyl alcohol cryogel: Optimizing the parameters of cryogenic treatment using hyperelastic models," *Journal of the Mechanical Behavior of Biomedical Materials*, vol. 2, no. 5, pp. 542–549, Oct. 2009, doi: 10.1016/j.jmbbm.2009.01.003.

[24] V. Pazos, R. Mongrain, and J. C. Tardif, "Deformable mock stenotic artery with a lipid pool," *Journal of Biomechanical Engineering*, vol. 132, no. 3, Mar. 2010, doi: 10.1115/1.4000937.

[25] T. Jaramillo, “Human Heart Phantom for Catheter Navigation Assessment,” 2019.
[26] Z. He, “Role of Abdominal Aortic Aneurysm Wall Biomechanics in Endovascular Repair Assessment,” 2020.
[27] P. Mahbeer, “Experimental assessment of mock calcifications in abdominal aortic aneurysm phantoms,” 2021.
[28] Z. Yang, “Development of 3D Printed Patient Specific Ascending Aortic Training Models for Cardiac Surgery,” McGill University, 2015.
[29] J. Garcia, “Patient specific surgical simulation of the ascending thoracic aorta,” 2019.
[30] J. R. Mitchell and J.-J. Wang, “Expanding application of the Wiggers diagram to teach cardiovascular physiology,” *Advances in Physiology Education*, vol. 38, no. 2, pp. 170–175, Jun. 2014, doi: 10.1152/advan.00123.2013.
[31] M. A. Gamrah, J. Xu, A. El Sawy, H. Aguib, M. Yacoub, and K. H. Parker, “Mechanics of the dicrotic notch: An acceleration hypothesis,” *Proc Inst Mech Eng H*, vol. 234, no. 11, pp. 1253–1259, Nov. 2020, doi: 10.1177/0954411920921628.
[32] J. Balmer, R. Smith, C. G. Pretty, T. Desaive, G. M. Shaw, and J. G. Chase, “Accurate end systole detection in dicrotic notch-less arterial pressure waveforms,” *J Clin Monit Comput*, vol. 35, no. 1, pp. 79–88, Feb. 2021, doi: 10.1007/s10877-020-00473-3.
[33] “Rubber Hardness Chart, Rubber Durometer Scale – Mykin Inc.” https://mykin.com/rubber-hardness-chart (accessed Sep. 15, 2022).
[34] T. Azar, S. McLennan, M. Walsh, J. Angeles, J. Kövecses, T. Jaramillo, R. Mongrain, and R. Cecere, “Dynamic Left Atrioventricular Phantom Test Bed Emulating Mitral Valve Motion,” *Journal of Medical Devices, Transactions of the ASME*, vol. 14, no. 3, Sep. 2020, doi: 10.1115/1.4046862.
[35] S. G. Yuen, D. T. Kettler, P. M. Novotny, R. D. Plowes, and R. D. Howe, “Robotic motion compensation for beating heart intracardiac surgery,” *International Journal of Robotics Research*, vol. 28, no. 10, pp. 1355–1372, 2009, doi: 10.1177/0278364909104065.
[36] O. Al-Kwifi, J. Stainsby, W. D. Foltz, M. S. Sussman, Y. Huang, and G. A. Wright, “Characterizing Coronary Motion and its Effect on MR Coronary Angiography—Initial Experience,” *J. Magn. Reson. Imaging*, vol. 24, no. 4, pp. 842–850, Oct. 2006, doi: 10.1002/jmri.20697.
[37] G. Shechter, “Respiratory Motion of the Heart: Implications for Magnetic Resonance Coronary Angiography,” 2004.
[38] J. (Jane W.) Ball, J. E. Dains, J. A. (Physician) Flynn, B. S. Solomon, R. W. Stewart, and H. M. Seidel, “Vital Signs and Pain Assessment,” in *Seidel’s guide to physical examination*, Tenth edition., 1 online resource : illustrations (some color) vols., St. Louis, Missouri: Elsevier, 2023, pp. 79–92. [Online]. Available: https://www.clinicalkey.com/dura/browse/bookChapter/3-s2.0-C20180051506
[39] J. M. Lee, D. Hwang, J. Park, J. Zhang, Y. Tong, C. H. Kim, J.-I. Bang, M. Suh, J. C. Paeng, G. J. Cheon, and B.-K. Koo, “Exploring Coronary Circulatory Response to Stenosis and Its Association With Invasive Physiologic Indexes Using Absolute Myocardial Blood Flow and Coronary Pressure,” *Circulation*, vol. 136, no. 19, pp. 1798–1808, Nov. 2017, doi: 10.1161/CIRCULATIONAHA.117.029911.
[40] H. Ota, K. Takase, H. Rikimaru, M. Tsuboi, T. Yamada, A. Sato, S. Higano, T. Ishibashi, and S. Takahashi, “Quantitative Vascular Measurements in Arterial Occlusive Disease,” *RadioGraphics*, vol. 25, no. 5, pp. 1141–1158, Sep. 2005, doi: 10.1148/rg.255055014.

Appendix A – Copyright Documentation

All images referenced in this page ar from public domain or licensed for reuse under Creative Commons license. Please se below for full citation and attribution information.

Figure 2-1 "Diagram of the human heart", by Wapcaplet in Sodipodi. Cropped by Yaddah to remove white space. Licensed under the Creative Commons Attribution-Share Alike 3.0 Unported license.
Link: https://commons.wikimedia.org/wiki/File:Diagram_of_the_human_heart_(cropped).svg

Figure 2-2 "Coronary arteries", by Patrick J. Lynch (medical illustrator), derivative work: Fred the Oyster, adaption and further labeling: Mikael Häggström M.D. Licensed under the Creative Commons Attribution-Share Alike 3.0 Unported license.
Link: https://commons.wikimedia.org/wiki/File:Coronary_arteries.svg

Figure 2-3 "Structure of an Artery Wall" by Blausen.com staff (2014). "Medical gallery of Blausen Medical 2014". WikiJournal of Medicine 1 (2).
DOI:10.15347/wjm/2014.010. ISSN 2002-4436. This file is licensed under the Creative Commons Attribution 3.0 Unported license.
Link: https://commons.wikimedia.org/wiki/File:Blausen_0055_ArteryWallStructure.png

Figure 2-4 "Atherosclerosis" by OpenStax College. Licensed under a Creative Commons Attribution License.
Book URL: https://openstax.org/books/anatomy-and-physiology/pages/1-introduction
Section URL: https://openstax.org/books/anatomy-and-physiology/pages/20-2-blood-flow-blood-pressure-and-resistance

Figure 2-5 "Coronary Angiography" by BruceBlaus. Licensed under the Creative Commons Attribution-Share Alike 4.0 International license.
Link: https://commons.wikimedia.org/wiki/File:Coronary_Angiography.png

Figure 2-6 "Concept of fractional flow reserve (FFR)" Reproduced from; "Fractional flow reserve: a review", B De Bruyne. J Sarma, Volume: 94, License date: Oct 27,2022, License Number: 5417311058170, with permission from BMJ Publishing Group Ltd..

Figure 2-7 “FFR procedure” by StatPearls Publishing LLC contributed by St. Jude Medical. Licensed under a Creative Commons Attribution 4.0 International License.
Book URL: https://www.ncbi.nlm.nih.gov/books/NBK482324/
Figure URL: https://www.ncbi.nlm.nih.gov/books/NBK482324/figure/article-37744.image.f1/?report=objectonly

Figure 3-14 “Wiggers diagram” by adh30 revised work by DanielChangMD who revised original work of DestinyQx; Redrawn as SVG by xavax. Licensed under the Creative Commons Attribution-Share Alike 4.0 International license.
Link: https://commons.wikimedia.org/wiki/File:Wiggers_Diagram_2.svg

Figure 4-1 “Association between stenosis severity and invasive pressure-derived physiological indexes.” Reproduced from; “Exploring Coronary Circulatory Response to Stenosis and Its Association With Invasive Physiologic Indexes Using Absolute Myocardial Blood Flow and Coronary Pressure”, Joo Myung Lee, Doyeon Hwang, Jonghanne Park, et al , Volume: 136, License date: Nov 08,2022, License Number: 5424361258291 , with permission from Wolters Kluwer Health, Inc.

Figure 4-2 “Relationship between area reduction and diameter reduction in a completely concentric stenosis.” Reproduced from; “Quantitative Vascular Measurements in Arterial Occlusive Disease”, Hideki Ota, et al., Volume:, License date:, with permission from The Radiological Society of North America (RSNA®)

Appendix B - Pump's Operation

When the pump is turned on, the startup interface will be displayed on the screen, as shown in Figure 3-17.

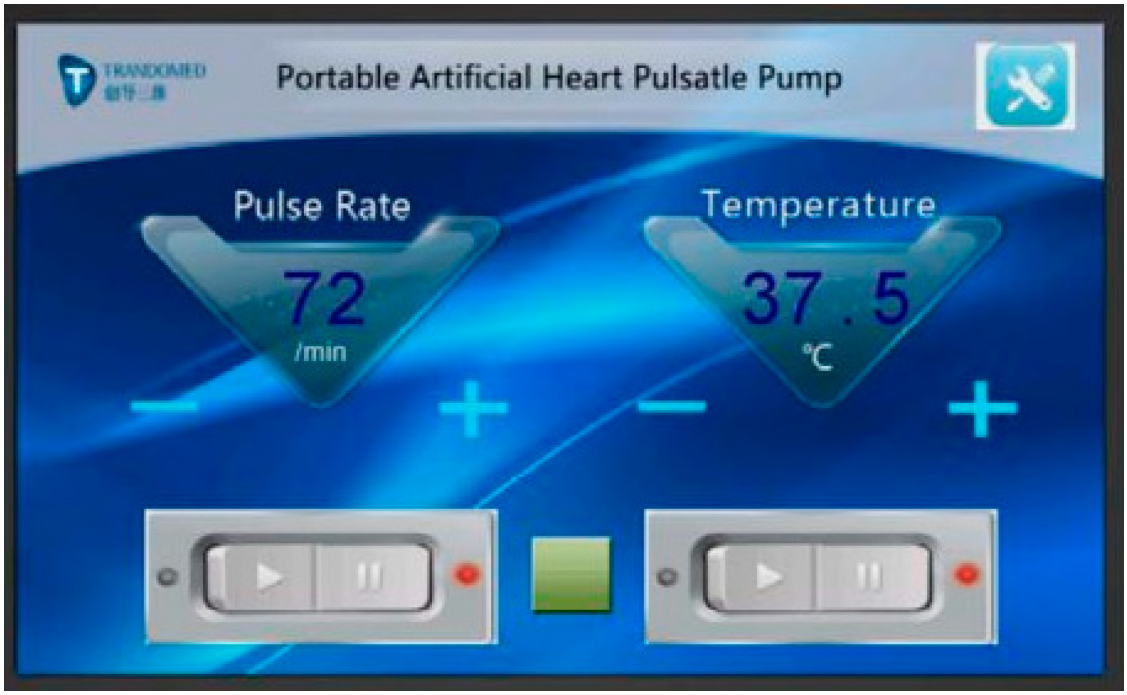

Figure B-0-1 Schematic diagram of startup interface of portable pump.

In this startup interface, the following actions can be performed:

Pulse rate: This module allows to increase and decrease the number of beats per minute generated by the pump. The value can be manipulated in two ways. First, through the "+" and "-" buttons below the module. Second, pressing directly on the module, cause the appearance of a keypad where a specific value can be entered. The pulsation range supported by the "Pulsatile Pump EDU-P120" is 10 – 200 bpm.

Temperature: This permits to increase and decrease the temperature of the liquid inside the pump. The heater can be manipulated similarly to the pulse rate module. The temperature setting range supported by the “Pulsatile Pump EDU-P120” is 25°C - 45°C.

The operation control button controls the pulsations start or pause. When turning on the pump, this button is idle by default, which could be seen through a red indicator to the right of the button. When a click on the area is performed, the pump would go into its active state, showing the green indicator on the left of the button and starting the pulsations in the system.

Heating control button: This button is used to start or pause the heating function of the device. This button works the same way as the operation control button.

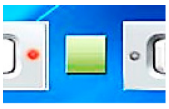

This indicator situated between the two buttons is a liquid level indicator used to know that the level of the liquid inside the pump was sufficient to operate correctly If it is not enough liquid, the display will be red.

This button at the top right of the startup interface switch to the settings interface of detailed function parameters introduced below.

In the configuration interface shown in Figure 3-18, the following actions could be performed:

Flow: This module controls the flow from the pump. The flow could be managed between 10% - 100%. According to the pump manual, these percentages correspond to 1 - 5 L/min. As this

parameter was increased, the amplitude of the curve decreased. This was because this pump uses a limit to control the flow and pressure; that is, if the pressure range is defined as 50%, it means

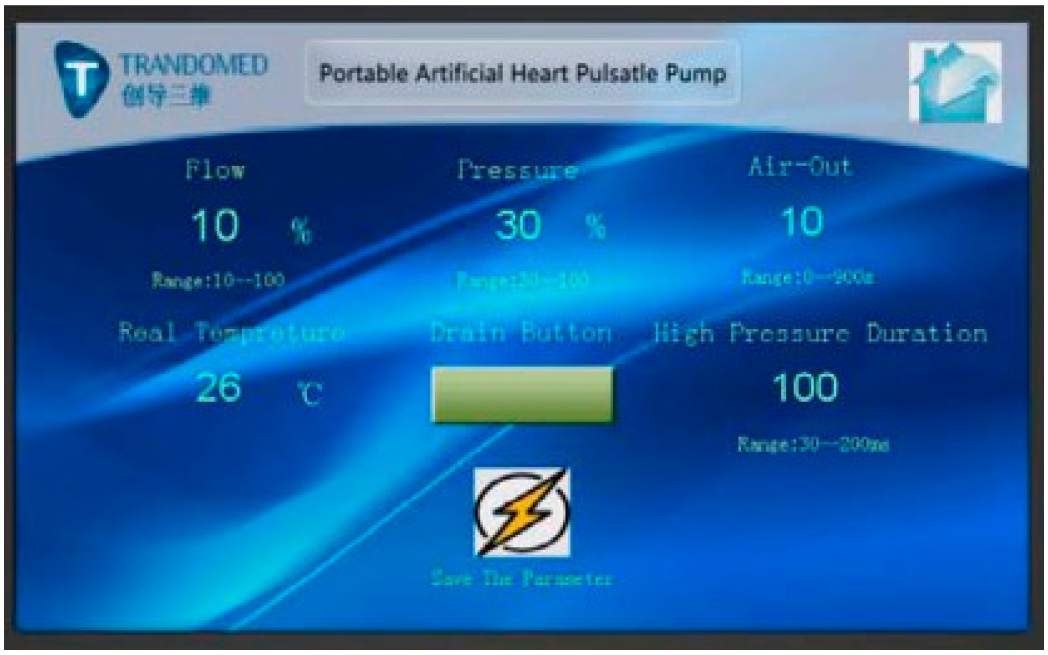

Figure B-0-2 Schematic Diagram of Setting Interface of Detailed Function Parameters.

that the pump will allow a maximum of 50% of its capacity (≈2.75 L/min), and this will give us pressure in the circuit that will vary depending on the circuit built. Since the pressure is limited to a specific value, increasing the flow would cause the lower peak of the pressure curve to increase, thereby decreasing the amplitude.

Pressure: This module controls the pressure of the fluid coming out of the pump. The pressure can be handled in the range of 30% - 100% (20 – 350 mmHg). As the pressure increased, the elevation and amplitude of the wave also increased.

Air-Out: When starting the pulsations of the pump for the first time after completely turning off the equipment, the pump begins a cycle of expelling air from the circuit. The duration of this cycle can vary from 30 – 200 ms. and be controlled with this module.

High-pressure duration: This parameter represents the time that the pump's turbine is active during a pulsation. The manipulation of this module affected the wavelength. As it increased, the wavelength would become wider, and the amplitude would increase.

Appendix C - Physician Survey

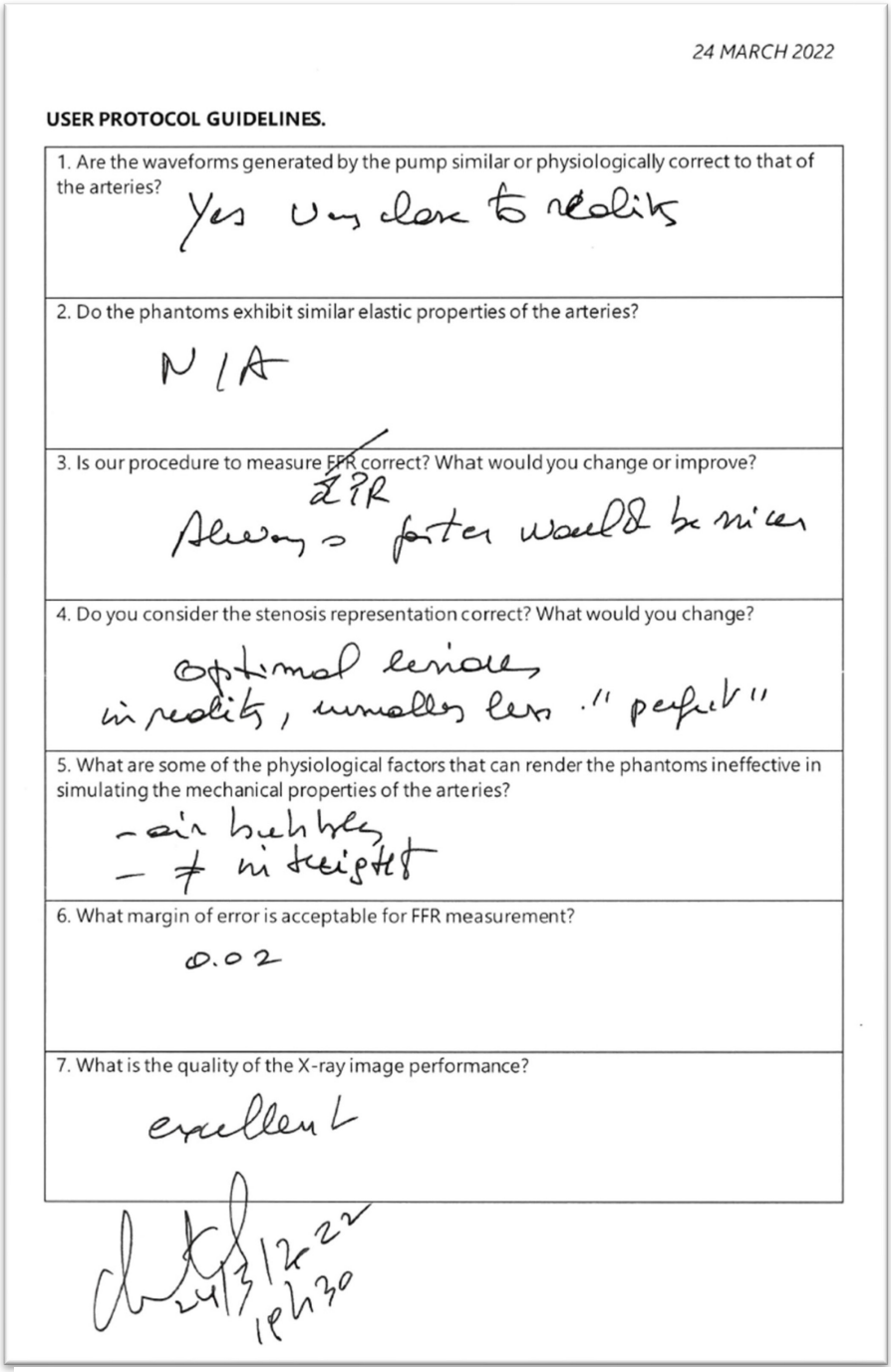

24 MARCH 2022

USER PROTOCOL GUIDELINES.

1. Are the waveforms generated by the pump similar or physiologically correct to that of the arteries?
Yes very close to reality

2. Do the phantoms exhibit similar elastic properties of the arteries?
N/A

3. Is our procedure to measure ~~FFR~~ dPR correct? What would you change or improve?
Always faster would be nicer

4. Do you consider the stenosis representation correct? What would you change?
Optimal lesions
in reality, usually less "perfect"

5. What are some of the physiological factors that can render the phantoms ineffective in simulating the mechanical properties of the arteries?
- air bubbles
- ≠ in height

6. What margin of error is acceptable for FFR measurement?
0.02

7. What is the quality of the X-ray image performance?
excellent

24/3/22 12:20

Yes, very close to reality

N/A

Always faster would be nicer

Optimal lesion, in reality, usually less "Perfect"

-Air bubles
-Not equal in height

0.02

excellent

Figure C-0-1 Survey of the physician who performed the angiography tests and FFR and dPR readings in the hemodynamic circuit.

Appendix D – Multiple dPR Results

dPR results

	No Motion				Heartbeat Vertical Motion				Respiration Vertical Motion				Mix Vertical Motion			
%Sev.	0%	40%	60%	80%	0%	40%	60%	80%	0%	40%	60%	80%	0%	40%	60%	80%
	dPR	dPR	dPR	dPR	dPR	dPR	dPR	dPR	dPR	dPR	dPR	dPR	dPR	dPR	dPR	dPR
1	0.98	0.85	0.82	0.77	0.98	0.85	0.82	0.77	0.98	0.86	0.83	0.77	0.99	0.84	0.81	0.79
2	0.98	0.87	0.81	0.78	0.98	0.85	0.83	0.78	0.98	0.85	0.82	0.77	0.98	0.86	0.82	0.79
3	0.98	0.86	0.81	0.78	0.98	0.85	0.83	0.76	0.98	0.85	0.81	0.77	0.98	0.86	0.83	0.78
4	0.98	0.86	0.82	0.77	0.97	0.85	0.84	0.77	0.98	0.86	0.83	0.77	0.98	0.86	0.82	0.78
5	0.98	0.85	0.82	0.78	0.98	0.86	0.82	0.77	0.98	0.85	0.82	0.77	0.98	0.86	0.83	0.78
6	0.98	0.85	0.83	0.78	0.97	0.86	0.83	0.78	0.98	0.86	0.82	0.77	0.98	0.84	0.82	0.78
7	0.98	0.87	0.82	0.78	0.98	0.86	0.82	0.78	0.98	0.85	0.83	0.78	0.98	0.85	0.82	0.78
8	0.97	0.86	0.82	0.78	0.98	0.85	0.82	0.78	0.98	0.85	0.82	0.77	0.98	0.88	0.82	0.78
9	0.98	0.86	0.83	0.77	0.98	0.86	0.82	0.77	0.98	0.86	0.82	0.78	0.99	0.87	0.81	0.78
10	0.98	0.86	0.82	0.77	0.98	0.86	0.81	0.78	0.98	0.85	0.83	0.78	0.98	0.85	0.82	0.77
Average	**0.979**	**0.859**	**0.82**	**0.776**	**0.978**	**0.855**	**0.824**	**0.774**	**0.98**	**0.854**	**0.823**	**0.773**	**0.982**	**0.857**	**0.82**	**0.781**

Figure D-0-1 Since the dPR can have variations in the reading depending on how the measurement is performed, the measurements were made ten times for each of the stenosis severities and each of the movement profiles, resulting in an dPR average reading.